Spectral linewidth and coherence

Johanne Lein

Thesis submitted for the degree of

Master of Science

Department of Physics

Faculty of Natural Sciences

University of Oslo

2010

Abstract

Our aim has been to give a contribution to the study of the nature and wave-particle duality of light through an analysis of the concept of optical coherence. We have carried out a numerical study of a pulse model of light, and experimentally determined the temporal coherence length of the spectral line of wavelength 692 nm in neon. The experimental setup proved to be less accurate than expected, but the measurements indicate a coherence length in the order of 30 mm. The numerical simulations suggest the possibility of using the auto-correlation function to determine the temporal size of pulses of electromagnetic radiation.

Acknowledgments

A lady I know lives and works in a community of people with strong mental handicaps. Part of her work is to teach them gardening. She told me: *Weeding is hard work, and even more so when you not only have to pull the weed, but also the person weeding.* Over the past two years, I have often pictured myself as the person being pulled, clinging to my thesis while the *real* work was being done by those around me. I therefore would like to direct my thanks to...

...my supervisor, *Arnt Inge Vistnes* for his dedication to the work of his students.

...*Borys Jagielski*, PhD student and my senior in the lab by one year, both of which made him an infallible source of Matlab tips, oscilloscope s.o.s, and general wisdom.

...*Efim Brondz*, our very easy-to-ask engineer.

...*Erik Alfsen, Joakim Bergli, Håkon Brox, Simen Kvaal*, and *Sølve Selstø* for our discussions.

...*Håkon Bjørgen, Torbjørn Næss, and Mikkjel Thorsrud* who, challenging their (strongly) theoretical disposition, helped me with lab work, pressing the button of the oscilloscope when time didn't allow me to fight with the trigger, and *Kyrre Ness Sjøbæk*, for his help with the numerical part of the work.

...*The students in the MEF/MENA program and on the group of theoretical physics*, these five years would have been much less fun if you weren't there.

...My *uncle Peter Luitjens* who proofread my thesis.

...*My family*, for being very easy to impress, and *my friends outside the department of physics* who from time to time forced me out of my dark lab and the bubble of Matlab simulations into the real world.

...The sisters of *Abbaye de Sainte Marie de Maumont* and *Sta. Katarinahjemmet* for all their help, ranging from moral support and prayers to supplying LaTeXcode.

Contents

Introduction

> *"We are convinced that our present problems, our methods, our scientific concepts are, at least partly, the results of a scientific tradition which accompanies or leads the way of science through the centuries. It is therefore natural to ask to what extent our present work is determined or influenced by tradition. Are the problems in which we are engaged freely chosen according to our interest or inclination, or are they given to us by an historical process? To what extent can we select our scientific methods according to the purpose, to what extent do we again follow a given tradition? And finally how free are we in choosing the concepts for formulating our questions? Any scientific work can only be defined by formulating the questions which we want to answer. But in order to formulate the questions we need concepts by which we hope to get hold of the phenomena. These concepts usually are taken from the past history of science; they suggest already a possible picture of the phenomena. But if we are going to enter into a new realm of phenomena, these concepts may act as a collection of prejudices, which hamper progress rather than foster it"* (Werner Heisenberg in [21]).

In every subject there comes a point when one has to accept some facts. To be able to build one needs to be on solid ground. If not, one will find oneself floundering awkwardly about in a confusing vacuum. Science will never advance if every scientist were to do everything from scratch. If we know more than our predecessors, it is because of what they gave us. Every physicist should recognize themselves in what sir Isaac Newton famously wrote: *"If I have seen further, it is by standing on the shoulders of giants"* [31].

However, as Heisenberg argues in the opening quote, the scientific tradition is always in danger of being a collection of prejudices. Every once in a while, one needs to critically examine the giants. They, also, need *our* support and approval to remain standing. The work that is being performed at Oslo Quantum-optic Laboratory has the expressed goal of examining one of these giants, namely that of the duality of the nature of light.

As the title suggests, the work that has been done has centered around the concept of coherence time and length. A passable definition of the term *coherence time* is

the time τ one may predict the state of the system if one knows its current state. Coherence length of light is the length covered by the light in that time: $l_{coh} = c\tau$, where c is the speed of light. The above definition will be closer analysed and specified in the course of the work. Our aim has been to obtain a greater understanding of the concept of optical coherence through experimental measurements on light emitted from gasses consisting of a single chemical element.

While working on the thesis, the author has collaborated with Borys Jagielski and Arnt Inge Vistnes on a numerical analysis of various methods of determining temporal coherence length for different models of light. It should be mentioned that much of what is being discussed in the thesis is, directly or indirectly, a fruit of that collaboration.

Some authors have indirectly suggested that the coherence time of light is a measure of the temporal size of a photon [2], [25]. As we will see, this is plausible if one examines a *single photon* depicted as a wave-packet of electromagnetic radiation. It may, however, become problematic if the signal to be examined is a collection of many such wave-packets. It has been said about the electron that *"We experience it as a causal tie or link between two events, its "birth" in the electron source and its death (or transmutation) in the interaction with the detector"* [19]. It seems that this could equally well have been uttered about particles of light, but, in that case, must that link always be a one-to-one relation between its emission from the source and its absorption in our detectors?

The somewhat sloppy definition of coherence time as being linked to the predictability of a system also seems to suggest a picture of coherence length of being due to more or less random fluctuations in the system. Is it possible that the coherence time and length of a light source is an indication of the average time between the fluctuations in the source? During our work, we will keep this picture in mind.

We begin in chapter one by introducing the model of light that will serve to give us the mental pictures needed in the continuation. In chapter two, we will briefly describe the phenomenon of interference, before introducing the main topic of the thesis, coherence of light. The predictions made in this chapter will form the basis of numerical simulations, the results of which will be presented in chapter three. We will also discuss the concept of the photon, and show how its size may be understood in relation to the coherence length found in the simulations. In chapter four and five, the experimental setup and methods are described in some detail. The experimental results will be presented and discussed in chapter six, and we will round off in chapter seven with a summary and some concluding remarks. In addition, a brief, conceptional review of Fourier transforms, the experimental data, and the program used in simulations have been included in appendices.

It should be mentioned that much time has been spent doing the seemingly trivial work of building up and testing the experimental setup. In quantum optics, doing

an experiment in general means spending hours of choosing the right pieces of equipment, aligning and adjusting, and *re*-aligning and *re*-adjusting them. The author is only the second student to obtain a master's degree at the laboratory, and the first whose work has been completely centered around experiment[1]. Part of the goal has therefore been to take part in choosing and purchasing experimental equipment, to gain competence and learn about its behaviour in practical application, to test and develop methods for our specific use, and to describe it all to allow future students to avoid the mistakes, improve that which has potential for improvement, and, maybe, repeat that which was successful.

The theory that is presented has also been chosen with an experimental rather than theoretical goal in mind. The author has tried to give a simple and pragmatic presentation of background information and concepts, while keeping the question *"why and how does it work?"* in mind. As a result, a person more theoretically minded will possibly find that some details are excessively elaborated, while other interesting relations are omitted. Hopefully, future students may also here benefit from the choices made.

Let us in closing include a few words on the notation used. Some figures are made up of several sub-figures. These will, starting from the top left, be denoted (a), (b), and so on. Since we are only working with relative quantities, most constants of normalisation have been excluded. In particular, the intensity is said to be the absolute square of the electric field, $I = |E|^2$, omitting the constant $\epsilon_0 c/2$. Also, the symbols λ and c are taken to be the wavelength and speed of the light in a medium. To denote the wavelength and speed of light in vacuum, we will write λ_{vac} and c_{vac}. As described in appendix A, if F and G are Fourier pairs, we will write $F \rightleftharpoons G$.

[1]The first student was Borys Jagielski, whose thesis also included experimental work. The main focus, however, was theoretical.

Chapter 1

Models of light

Often in the natural sciences, many models that describe the same phenomenon exist side by side. The different models may emphasize different aspects of the physical reality that they aim to describe. Although a model rarely or never can claim to capture the whole truth of the phenomenon in question, several models taken together may offer a more complete picture.

In the physics of optics, various models often fit into one of two main categories: The particle and the wave description of light. In the particle description light is perceived as a collection of indivisible quanta. At the present moment perceiving light as particles or quanta seems to offer the best explanation of the results of coincidence experiment, where light is sent through a beam splitter and into detectors on the two outgoing sides. If the intensity of the light is very low, the detectors do not respond at the same time, and this is interpreted as a proof that light is indeed made up of indivisible entities [16].

The wave description builds on Maxwell's equations, and in it, light is perceived as continuous, propagating electromagnetic fields. As we will see, the model allows for describing interference and diffraction phenomena of light with a rather simple mathematical formalism, and for intuitive conceptional analogies to other wave-phenomena in nature.

It is difficult to conceive a phenomenon *both* as a continuous field *and* as indivisible particles. Efforts have been made to force light to reveal the interference pattern without *actually* interacting with it, to be able to experimentally see examples of wave and particle behaviour at the same time [2], but there is not full consensus of the validity of the conclusions from such experiments [14], [46].

A thorough discussion of historical and experimental aspects of the wave-particle duality of light is given in [22].

In section 1.2, we will introduce the beam model that will serve as our reference in the continuation. As an hors d'oeuvre, we have included a description of a

geometrical ray model. This ray model will not, or very little, be referred to in the continuation, but has been included since it with some simple geometrical arguments allows us to find a formula for the propagation of light through an optical system that, once derived in the ray model, may easily be transferred to and justified in the beam model.We have not meant to give an exhaustive description of either of the two model, but a pragmatic introduction of concepts that will become useful in describing the experimental work.

1.1 Ray optics

Among the many models that are used to describe light, one of the simplest is a ray description. This model sees light as collections of infinitely thin rays, and is only concerned with the location and direction of these rays. The propagation of the rays is described using a set of geometric rules, and ray optics is therefore sometimes referred to as geometrical optics. The model's use is limited to situations where light propagates through and around objects much larger that the wavelength of the light. Then the effects of the wave nature of light can often be neglected.

We will begin by describing the laws or principles governing the propagation of the rays. We will then use those laws to find a matrix representation of calculating the propagation of the rays through a system of optical components. As an example, we will derive the matrix that describes the propagation through a thin lens.

Two laws govern the propagation of light rays:

1. **The law of reflection**

   "The reflected ray lies in the plane of incidence; the angle of reflection equals the angle of incidence" [44].

2. **The law of refraction**

   "The refracted ray lies in the plane of incidence; the angle of refraction is related to the angle of incidence by Snell's law :

$$n_r \sin\theta_r = n_i \sin\theta_i \text{ [44]}''. \tag{1.1}$$

The n's in the above equation are defined as $n = c_{vac}/c$. The indices r and i denote the reflected and incoming rays respectively.

A third law is also often mentioned with these two: *In a homogeneous medium, light rays travel in straight lines.* However, this can be deduced by using the law of refraction with $n_r = n_i$.

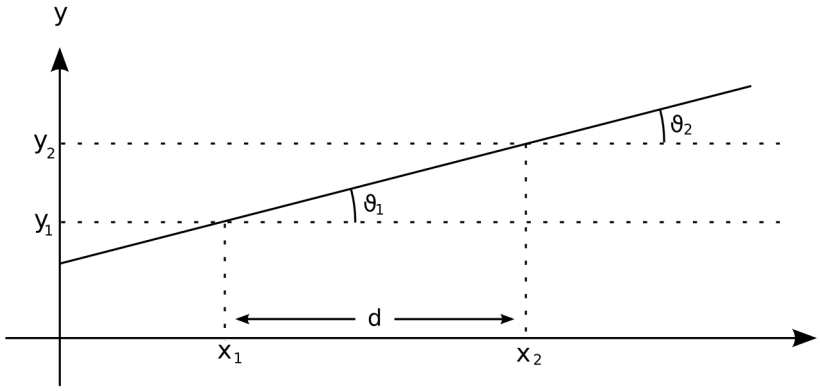

Figure 1.1: Light ray propagating a distance d through homogeneous medium

ABCD-matrix in ray optics

As mentioned above, ray optics is only concerned with the position and direction of a ray of light. If we assume that the ray is propagating in the (x, y)-plane, the ray will be unambigously determined if we know its y-position for some x, and the angle θ it makes with the x-axis. Examining figure 1.1, one finds that for a ray propagating a distance whose x-component is d, in a homogeneous medium, one finds that y_2 and θ_2 at the point x_2 are

$$\begin{aligned} y_2 &= 1 \times y_1 + d \times \tan\theta_1 \\ \tan\theta_2 &= 0 \times y_1 + 1 \times \tan\theta_1, \end{aligned}$$

where y_1, θ_1 are the y-position and angle with the $x-$axis when $x = x_1$.

In the paraxial approximation, with all θ_i being small so that $\tan\theta_i \approx \sin\theta_i \approx \theta_i$, this can be written:

$$\begin{pmatrix} y_2 \\ \theta_2 \end{pmatrix} = \begin{pmatrix} 1 & d \\ 0 & 1 \end{pmatrix} \begin{pmatrix} y_1 \\ \theta_1 \end{pmatrix}.$$

In general, any optical system can in the paraxial approximation be written in the form

$$\begin{pmatrix} y_2 \\ \theta_2 \end{pmatrix} = M \begin{pmatrix} y_1 \\ \theta_1 \end{pmatrix}, \quad \text{with } M = \begin{pmatrix} A & B \\ C & D \end{pmatrix}.$$

If the optical system consists of i components, each with ABCD-matrix

$$m_i = \begin{pmatrix} a_i & b_i \\ c_i & d_i \end{pmatrix},$$

the final matrix M is just the product of the separate matrices. The outcome of the system of optical components is uniquely determined by the final matrix

$M = \prod_i m_i$. Two systems of different optical components with matrices m_i that multiply to the same matrix M will have the same effect on the propagation of the light, as illustradet with the "black box" in figure 1.2. When finding the total matrix M of a system of optical components, the *far left matrix* will correspond to the *last* optical component, since it will be the last matrix to operate on the vector $\begin{pmatrix} y \\ \theta \end{pmatrix}$.

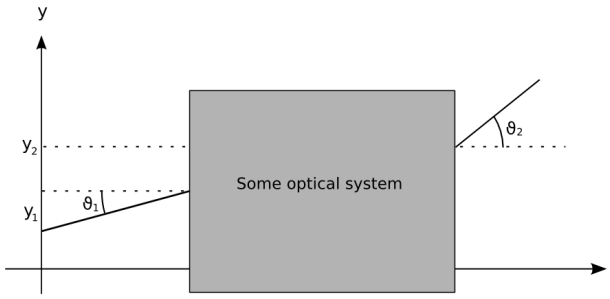

Figure 1.2: Propagation of a light ray through some optical system is uniquely determined by the ABCD-matrix of the total system. The matrix of the system is the product of the matrices of its components.

ABCD-matrix for propagation through a thin lens

To make even clearer the concept of the ABCD-method, and since it will be relevant in the experimental setup, let us find the matrix for propagation of a ray through a thin lens.

When the ray crosses a boundary of refraction, the y-parameter will, because of continuity, remain the same, $y = y_2 = y_1$, where y_1 and y_2 are the distances to the axis of propagation as the ray hits and leaves the boundary respectively.

From figure 1.3, Snell's law for refraction through a curved surface gives

$$n_1 \sin(\alpha + \theta_1) = n_2 \sin(\alpha - \theta_2).$$

Assuming that α, θ_1 and θ_2 are small[1] this is

$$\begin{aligned} & n_1(\alpha + \theta_1) = n_2(\alpha - \theta_2) \\ \Rightarrow \theta_2 = & \frac{n_2\alpha - n_1(\alpha + \theta_1)}{n_2} = \frac{n_2 - n_1}{n_2 R} y_1 - \frac{n_1}{n_2}\theta_1 \end{aligned}$$

[1] the θ's are small by the assumption that we work in the paraxial approximation, the α is small since we are looking at a thin lens. Using a thin lens, the y-position of the ray will always be much smaller than the radius of curvature of the lens, and α can therefore be assumed to be small.

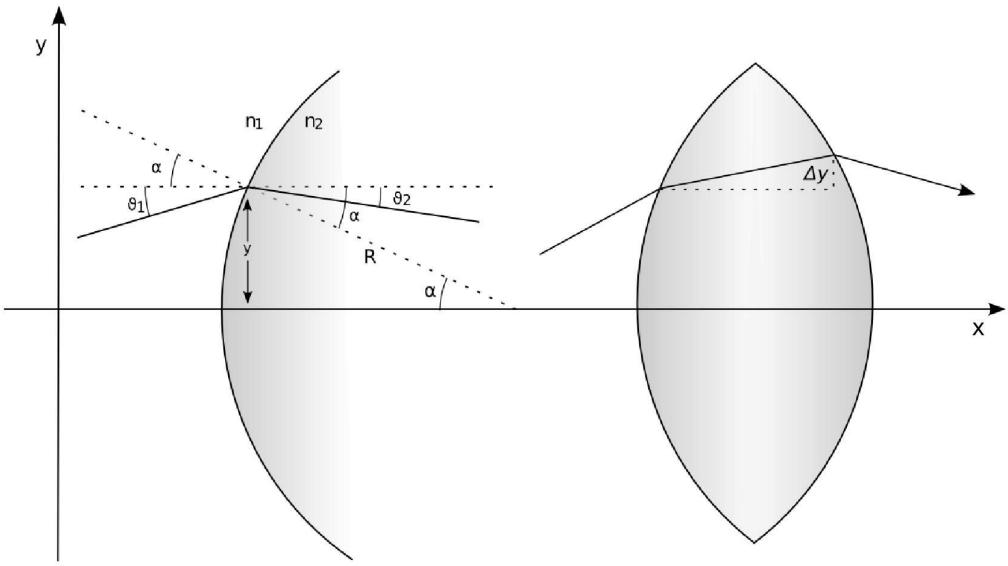

Figure 1.3: If the lens is thin, the difference in position, Δy, can be neglected, and the matrix for a ray through the lens equals the product of the matrices of two curved surfaces

where in the last line we have used the identity

$$\alpha \approx \sin\alpha = y/R,$$

which can be verified by studying figure 1.3. Thus, the matrix of refraction through a curved surface is:

$$\begin{pmatrix} 1 & 0 \\ \frac{n_2-n_1}{n_2 R} & -\frac{n_1}{n_2} \end{pmatrix}. \tag{1.2}$$

Now, the matrix for diffraction through a lens is the product of three matrices: That of propagation through a homogeneous media wedged between the matrices of refraction through two curved surfaces[2]. Since we are assuming the lens to be thin, the matrix of propagation will be almost equal to the identity matrix, so the total matrix of the lens will be the product of the matrices of two surfaces with radii R_1 and R_2:

$$\begin{pmatrix} 1 & 0 \\ \frac{n_1-n_2}{n_1 R_1} & -\frac{n_2}{n_1} \end{pmatrix} \begin{pmatrix} 1 & 0 \\ \frac{n_2-n_1}{n_2 R_2} & -\frac{n_1}{n_2} \end{pmatrix} = \begin{pmatrix} 1 & 0 \\ \frac{n_1-n_2}{n_1}(\frac{1}{R_1}+\frac{1}{R_2}) & 1 \end{pmatrix} \equiv \begin{pmatrix} 1 & 0 \\ -\frac{1}{f} & 1 \end{pmatrix}. \tag{1.3}$$

The f in the above equation is called the focal length of the lens and is perhaps the most important parameter of the lens.

[2]Note that in the second surface (the leftmost matrix) n_2 will be the refractive index at the incoming surface, and n_1 at the outgoing, opposite to that of equation (1.2). Note also that the definition of the sing of the radius of a boundry, and therefore the C-parameter of the third matrix in (1.3) may look slightly different in different texts.

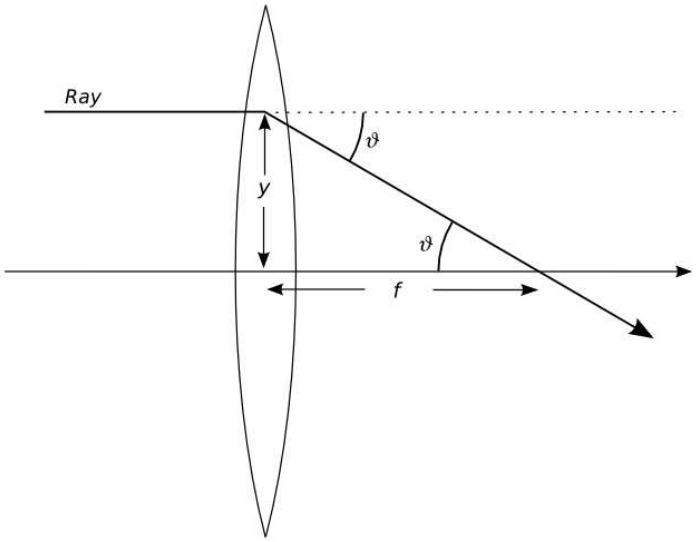

Figure 1.4: Rays that enter the lens parallel to the z-axis will be focused a distance f from the lens.

A ray entering the lens parallel to the z-axis may be described with the vector

$$\begin{pmatrix} y \\ 0 \end{pmatrix}.$$

After having propagated through a thin lens, this becomes:

$$\begin{pmatrix} 1 & 0 \\ -\frac{1}{f} & 1 \end{pmatrix} \begin{pmatrix} y \\ 0 \end{pmatrix} = \begin{pmatrix} y \\ -\frac{y}{f} \end{pmatrix}.$$

From figure 1.4 we see that when working with a thin lens and therefore with small angles so that $\theta \approx \tan\theta = y/f$, rays that enter the lens parallel to the z-axis will be focused one focal distance f from the lens.

The definition of the mathematical expression for the focal length in equation (1.3):

$$\frac{1}{f} = \frac{n_2 - n_1}{n_1}(\frac{1}{R_1} + \frac{1}{R_2})$$

is known as *the lensmakers' equation*. More generally, it may be shown that the inverse of the focal length is equal to the inverse of the distance from an object to the lens, plus the inverse of the distance to the image of that object created by the lens [35].

In table 1.1, we have included the ABCD-matrices of some of the most used optical components. Note that the matrix for a curved mirror with radius of curvature R_m is equal to the matrix of a thin lens of focal length $-f$.

Table 1.1: Some ABCD-matrices (Convention of [44]).

Component	*Matrix*
Free space propagation	$\begin{pmatrix} 1 & d \\ 0 & 1 \end{pmatrix}$
Refraction at planar boundry	$\begin{pmatrix} 1 & 0 \\ 0 & \frac{n_1}{n_2} \end{pmatrix}$
Refraction at curved boundry	$\begin{pmatrix} 1 & 0 \\ -\frac{(n_2-n_1)}{n_2 R} & \frac{n_1}{n_2} \end{pmatrix}$
Thin lens	$\begin{pmatrix} 1 & 0 \\ -\frac{1}{f} & 1 \end{pmatrix}$
Reflection from planar mirror	$\begin{pmatrix} 1 & 0 \\ 0 & 1 \end{pmatrix}$
Thin lens	$\begin{pmatrix} 1 & 0 \\ \frac{2}{R} & 1 \end{pmatrix}$

1.2 Wave optics and the beam model of light

"I brought into the sunbeam a slip of card" (Thomas Young in [56]).

It would be nice if one could describe all phenomena of light with the simple model of ray optics described in section 1.1, but unfortunately this is not the case. An indication of this is given in figure 1.5 where we have plotted the radius of our HeNe-laser beam as a function of the distance after the collimator when it leaves the optic fiber[3]. Although no optic element has been inserted into the path, the beam radius decreases to a minimum before it increases back symmetrically around this minimum. As we will see in chapter 4, the beam will have a Gaussian intensity distribution after having propagated through the fiber. The radius in the figure is the radius where the intensity has decreased to e^{-2} of its central value.

The beam model will provide the intuitive picture that will lay the basis for most of our arguments in the experimental section of this work.

[3]For a description of the optic fiber and collimation, see chapter 4.

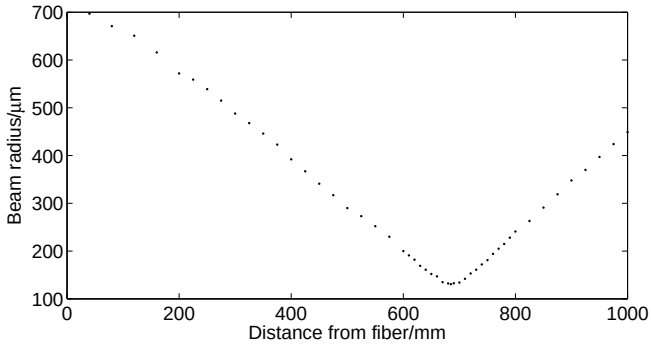

Figure 1.5: The profile of the laser beam after it leaves the collimator on the outgoing side of the optic fiber.

Young's double slit experiment

One of the first demonstrations of the wave nature of light was the famous "double slit experiment" performed by the British physicist Thomas Young at the beginning of the 19^{th} century. When bringing a thin piece of cardboard into a beam of sunlight and examining the pattern of the light falling on a screen behind the card, he found that the one piece of card produced a pattern of several dark and bright fringes. The idea of light having wave-like properties was not new. Refraction phenomena of light had been observed by physicists before Young, and some had concluded that light possessed wavelike, or oscillating, properties. It is nontheless the article in which Young presented his ideas to the Physical Society of London that has come to be considered the modern revival of the wave theory of light [22].

Young himself never uses the word "waves" in his article, but he argues that one may infer from his experiments that light

> *"...is possessed of opposite qualities, capable of neutralising or destroying each other, and of extinguishing the light, where they happen to be united; that these qualities succeed each other alternately (...) at distances which are constant for the same light passing through the same medium" [56].*

He equally urges *"those who are attached to the Newtonian theory of light"*, that is, those who believe in a corpuscular theory of light [32], to make an effort to explain his results using their own theory or

> *"...if they fail in the attempt, to refrain at least from idle declamation against a system which is founded on the accuracy of its application to all these facts, and to a thousand others of a similar nature"* [56].[4]

[4]Though of no relevance to the theme of this thesis, let us, purely for the sake of its beauty, offer one more example of the poetic langage of Young's article, in which he discusses the pos-

The beam model from Maxwell's equations

Standard electromagnetism tells us that light is a type of electromagnetic phenomena. Maxwell's equations state that if $\mathbf{E}$ denotes the electric and $\mathbf{H}$ the magnetic field, one has:

$$\nabla \times \mathbf{E} = -\mu \frac{\partial \mathbf{H}}{\partial t} \tag{1.4a}$$

$$\nabla \times \mathbf{H} = \epsilon \frac{\partial \mathbf{E}}{\partial t} \tag{1.4b}$$

$$\nabla \cdot \mathbf{E} = 0 \tag{1.4c}$$

$$\nabla \cdot \mathbf{H} = 0 \tag{1.4d}$$

given that the media is linear[5], isotropic[6], and dielectric[7] without currents or free charges. Taking the curl of equation (1.4a) gives

$$\nabla \times (\nabla \times \mathbf{E}) = -\mu \frac{\partial}{\partial t} \nabla \times \mathbf{H}$$

and using the identity

$$\nabla \times (\nabla \times \mathbf{v}) = \nabla(\nabla \cdot \mathbf{v}) - \nabla^2 \mathbf{v}$$

together with (1.4c) on the left hand side, and (1.4b) on the right hand side gives

$$\nabla^2 \mathbf{E} = \epsilon\mu \frac{\partial^2 \mathbf{E}}{\partial t^2}.$$

Equivalently, one can find that

$$\nabla^2 \mathbf{H} = \epsilon\mu \frac{\partial^2 \mathbf{H}}{\partial t^2}.$$

These equations must be satisfied for all the components of the electric and magnetic field separately. To simplify the notation we write

$$\nabla^2 u = \frac{1}{c^2} \frac{\partial^2 u}{\partial t^2}. \tag{1.5}$$

where $u = u(\mathbf{r}, t)$ is any of the six components of the electric and magnetic fields, and $\mathbf{r} = (x, y, z)$ is the position vector. Equation (1.5) is a wave-equation, and

sibility of light moving through an ether: *"I am disposed to believe, that the luminiferous ether pervades the substance of all material bodies with little or no resistance, as freely perhaps as the wind passes through a grove of trees" [56].*

[5]**Linear**: Having the property that the polarisation-vector is parallel and proportional to the electric field [51].

[6]**Isotropic**: "Denoting a medium whose physical properties are independent of direction" [12].

[7]**Dielectric**: "A nonconductor (...) in which an applied electric field causes a displacement of charge but not a flow of charge" [12].

the electromagnetic field may therefore be interpreted as a phenomenon exhibiting wave-like properties.

It will prove useful to expand the wave function u with an imaginary part. We can then write this new complex wave function as

$$U(\mathbf{r},t) = U(\mathbf{r})e^{i2\pi\nu t} = a(\mathbf{r})e^{i\phi(\mathbf{r})}e^{i2\pi\nu t} \tag{1.6}$$

and define our real wave function to be $u = Re\{U(\mathbf{r},t)\}$. In equation (1.6), ϕ is some parameter that describes the phase of the beam at a certain point $\mathbf{r}$. The *wave fronts* of the beam are surfaces of constant phase ϕ, that move with speed $c \equiv 1/\sqrt{\epsilon\mu}$. All information about the electromagnetic wave and its propagation is now contained in $U(\mathbf{r},t)$.

The time-independent part, $U(\mathbf{r}) = a(\mathbf{r})e^{i\phi(\mathbf{r})}$ is commonly referred to as the complex amplitude of the wave. In the following, when we write only U, we will take it to mean $U(\mathbf{r})$. The complex wave function has to obey the same wave-equation as its real part. When putting the expression for $U(\mathbf{r},t)$ into equation (1.5), the exponential containing all the time-dependence is kept constant and cancels out, and we are left with

$$\nabla^2 U + k^2 U = 0, \tag{1.7}$$

where we have used the definition $k = \frac{2\pi\nu}{c}$.

We will in the following see how equation (1.7) brings fourth the *Gaussian beam* as a possible allowed solution for propagating light. In chapter 4 we will show how to experimentally shape a beamfront to become Gaussian, and see why this is essential in carrying out experiments in optics.

The paraxial approximation

It is possible to show more subtly the connection between the models of waves and rays, but suffice it here to simply state that the rays of ray optics are parallel to the normals of the wave fronts of wave optics. As a consequence of this, the mathematics of wave optics may be carried out in the paraxial approximation if their normals are paraxial rays, that is, if the wavefront bends only slightly.

A wave whose wavefront does not bend at all is called a plane wave. If it propagates in the z-direction its complex amplitude can be written out

$$U(\mathbf{r}) = Ae^{-ikz},$$

where A is a constant.

To allow for the wavefront to bend, we let A become a function of $\mathbf{r}$, and write

$$U(\mathbf{r}) = A(\mathbf{r})e^{-ikz}.$$

Putting this into equation (1.7), we are left with an equation for $A(\mathbf{r})$:

$$\nabla_T^2 A + \frac{\partial^2 A}{\partial z^2} - i2k\frac{\partial A}{\partial z} = 0. \tag{1.8}$$

In the above equation, $\nabla_T^2 = \frac{\partial^2}{\partial x^2} + \frac{\partial^2}{\partial x^2}$ is the transverse Laplacian operator.

For the wavefront to *be* and *remain* in the paraxial approximation, the variance of A and its derivative must be very small within distances in the order of a wavelength [44]. We then have

$$\delta\left(\frac{\partial A}{\partial z}\right) = \frac{\partial^2 A}{\partial z^2}\delta z \;=\; \frac{\partial^2 A}{\partial z^2}\lambda \;<<\; \frac{\partial A}{\partial z}.$$

Since $\lambda = 2\pi/k$ and the factor of π is of the order of unity, the term with the double derivative in z in equation (1.8) may be neglected, and we are left with the simpler equation

$$\nabla_T^2 A - i2k\frac{\partial A}{\partial z} = 0. \tag{1.9}$$

The solutions to equation (1.9) define the set of possible waves that propagate in the z-direction and obey the paraxial aproximation.

The Gaussian beam

Although simpler solutions to equation (1.9) exist, let us jump directly to the one that will be relevant in the continouation of the thesis: The Gaussian beam.

A Gaussian beam may be described by [44]

$$A(\mathbf{r}) = \frac{z_0\sqrt{I_0}}{q(z)}\exp\left\{-ik\frac{\rho^2}{2q(z)}\right\}, \qquad \rho = x^2 + y^2. \tag{1.10}$$

In equation (1.10), q(z) is called the q−parameter of the beam, and is equal to z plus a constant imaginary term, $q(z) = z + iz_0$. The quantity $z_0\sqrt{I_0}$ is for the time being just an arbitrary constant. Its somewhat peculiar appearance will prove useful in a moment.

To show the physical meaning of the q-parameter, let us look at its inverse:

$$\frac{1}{q} = \frac{1}{z + iz_0} = \frac{z}{z^2 + z_0^2} - i\frac{z_0}{z^2 + z_0^2} \equiv \frac{1}{R} - i\frac{\lambda}{\pi W^2}, \tag{1.11}$$

where we have defined

$$\begin{aligned} R &= R(z) \equiv z\left[1 + \left(\tfrac{z_0}{z}\right)^2\right] \\ W &= W(z) \equiv W_0\sqrt{\frac{z^2 + z_0^2}{z_0^2}}, \qquad W_0 \equiv \sqrt{\frac{\lambda z_0}{\pi}}. \end{aligned} \tag{1.12}$$

Using the expressions for W and R with equation (1.10), the complex envelope may be written out

$$U(\mathbf{r}) = -i\sqrt{I_0}\frac{W_0}{W(z)}\exp\left\{-\frac{\rho^2}{W^2(z)}\right\}\exp\left\{-ikz - i\frac{k\rho^2}{2R(z)} - i\tan\left(\frac{z_0}{z}\right)\right\}. \tag{1.13}$$

The intensity of a beam is the square of its complex envelope [44]. In our case this is:

$$\begin{aligned} I(\mathbf{r}) = I(\rho, z) &= |U(\mathbf{r})|^2 = |A(\mathbf{r})|^2 \\ &= \frac{I_0 z_0^2}{|q(z)|^2}\exp\left\{\frac{-k\rho^2\lambda}{\pi W^2(z)}\right\} \\ &= I_0\left[\frac{W_0}{W(z)}\right]^2\exp\left\{\frac{2\rho^2}{W^2(z)}\right\}. \end{aligned} \tag{1.14}$$

As seen from the last part of the equation, the beam is a Gaussian function of the radial distance from the beam axis. On the beam axis, where $\rho = 0$, the intensity is equal to

$$I(0, z) = I_0\left[\frac{W_0}{W(z)}\right]^2.$$

From equation (1.12), $W(z = 0) = W_0$ so that

$$I_0 = I(\rho = 0, z = 0).$$

The parameters W and R defined in equation (1.12) are called the *waist* and *radius of curvature* of the beam. We will now show the physical meaning of the two parameters.

Beam width

The ratio of the total energy of the beam within a circle of radius $W(z)$ is

$$\frac{E}{E_{total}} = \frac{\int_0^{W(z)} I(\rho, z)2\pi\rho\, d\rho}{\int_0^{\infty} I(\rho, z)2\pi\rho\, d\rho} = 1 - e^{-2} \approx 0.86.$$

Since a high fraction of the energy is contained within a circle of radius $W(z)$, and since this fraction is independent of z, $W(z)$ is called the beam width, and is often given as one of the parameters needed to completely describe the propagation of the beam. The smallest beam width is $W_0 = W(z = 0)$, and the $z = 0$-plane is called the beam waist.

Radius of curvature

To justify giving the name *radius of curvature* to the quantity R let us first look at the radius of curvature of a spherical wavefront. Spherical waves have complex amplitude $U(\mathbf{r}) = Ae^{-ikr}$, every point on the wavefront has the same radius of

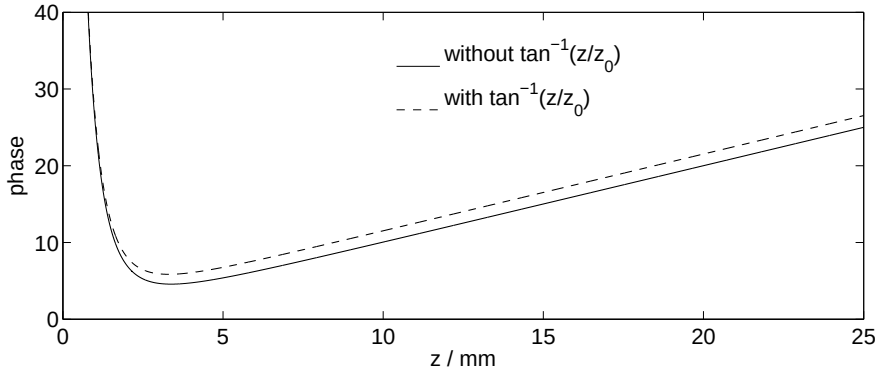

Figure 1.6: Equation 1.16 with and withouth the $\tan^{-1}(z/z_0)$-term. In the graphs, $\rho = 10$ mm, $W_0 = 1$ mm and $k = 1$ mm^{-1}. In visible light, k would be many orders of magnitude larger, and the effect of the $\tan^{-1}(z/z_0)$-term would not be visible in the graph.

curvature r. Remembering that the wavefronts were defined as surfaces of constant phase, we may write

$$\text{constant} = kr = k\sqrt{\rho^2 + z^2} = kz\sqrt{\frac{\rho^2}{z^2} + 1} \approx kz\left(1 + \frac{\rho^2}{2z^2}\right) \approx kz + \frac{k\rho^2}{2r}, \quad (1.15)$$

where the last two steps are only valid in the paraxial approximation where $\rho << |z| \approx r$.

The phase of a Gaussian wave was written out in equation (1.13). Setting this phase to be constant, we find that for Gaussian wavefronts, it holds that

$$kz + \frac{k\rho^2}{2R} + \tan\left(\frac{z_0}{z}\right) = \text{constant}, \qquad R = z\left[1 + \left(\tfrac{z_0}{z}\right)^2\right]. \quad (1.16)$$

If we make a plot as in figure 1.6 of the left hand side of equation (1.16) with and without the $\tan z_0/z$, we see that this term may be neglected. Without this term, equation (1.15) and equation (1.16) are identical with the R defined in equation (1.12) indeed playing the role of radius of curvature. As we will see in chapter 5, for measuerments of coherence length to be possible, the wavefronts of two beams must be completely overlapping, that is, both the beam waist and radius of curvature must be similar for the overlapping beams.

ABCD-matrix in beam optics

At a first glance, it may not seem obvious that the ABCD-parameters from ray optics can be used with a model of a propagating and developing beam. However, using the fact that the rays of ray optics are parallel to the wavefront normals, we will see that this is indeed the case. Though qualitatively different from the matrix representation of the ray model, the ABCD-equation of the beam optics will have

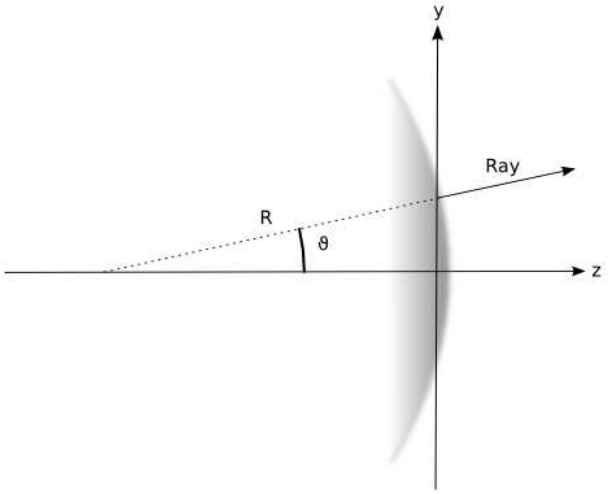

Figure 1.7: The rays are normal to the wavefront normals. Accordingly, to work in the paraxial approximation in the beam model means that the wavefront bends little enough for its normals to be paraxial rays.

an appearance very similar to what we previously saw.

Recall that in the representation of paraxial rays,

$$y/R = \sin\theta \approx \theta. \tag{1.17}$$

Now, let R be the radius of curvature of the beam itself (and *not* of a lens). From figure 1.7 we see that the relation (1.17) still holds. Since the rays we had earlier correspond to the wavefront normals, we can use the same set of equations as before, and we get

$$\begin{aligned} y_2 &= Ay_1 + B\theta_1 \\ \theta_2 &= Cy_1 + D\theta_1. \end{aligned}$$

Dividing the former by the latter and using equation (1.17), one finds directly [35]

$$R_2 = \frac{AR_1 + B}{CR_1 + D}.$$

It has been shown ([10], [54]) that this can be generalized to

$$q_2 = \frac{Aq_1 + B}{Cq_1 + D},$$

q being the q-parameter of the beam, whose relation to R is defined by equation (1.11).

Chapter 2

Coherence

The title of this work is *Spectral linewidth and coherence*. Coherence in light is closely tied with *interference*, a physical phenomenon found in many situations that involve wavelike behaviour. We will therefore begin with a short discussion of interference before moving on to defining coherence, and to define and calculate some quantities that will help us measure the coherence of a signal.

2.1 Interference

Imagine throwing a pebble into a lake and watching the waves spread in circles from where it hits the water. If you trow several pebbles into the water, they will start out in the same way: Several circular wavefronts spreading from each point where a pebble hit. After a while, when the circles have grown large enough, they begin to mix. The resultant wave depends on the amplitude and relative phase of the wavefronts of each of the partial waves, and the result is an interference pattern with very many more speckles and nuances than of the original circular pattern.

Interference patterns in water is an idea intuitively easy to accept. If two wave tops of equal amplitude meet, it is only natural that the new wave has an amplitude larger than each of the two partial waves. If a wave top meets a trough, the result would be no wave at all - at least if the partial waves were identical and conducted in a way so that a wave top *always* would hit a trough and vice-versa. Doing a similar experiment with light is perhaps more astonishing. In chapter 1 we saw that light may be described as electromagnetic waves. In daily life, the wave-nature of light for the most part remains hidden. Even our best detectors do not have the temporal resolution to be able to resolve field oscillations in the order of 10^{14} Hz; what they actually measure is the time average of the intensity, proportional to the square of the electric field, taken over a time window much larger than a period of oscillation of the light. With the help of an interferometer, light waves may be brought together and mixed in a way that lets us examine the relative phase of their electric field.

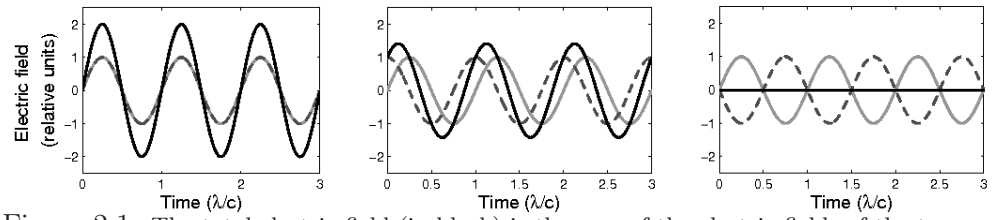

Figure 2.1: The total electric field (in black) is the sum of the electric fields of the two partial waves. If the electric field is completely in phase, constructive interference will occur (a). If there is a slight phase difference between the two waves, the difference of value between the maxima and the minima will be smaller, as in (b). If the difference in the two paths, Δl, is an odd integer of half of the wavelength, the interference will be destructive (c).

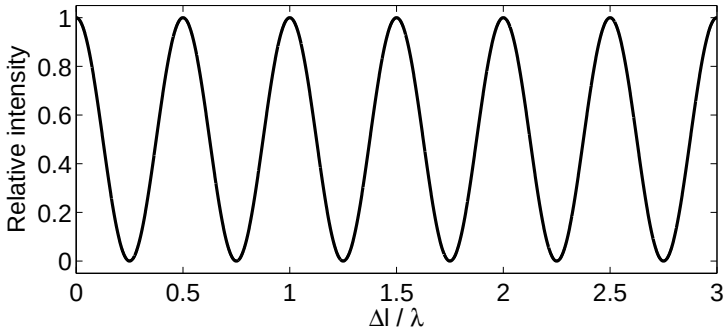

Figure 2.2: The intensity is proportional to the square of the electric field, and changing the path difference Δl therefore makes the intensity oscillate.

An interferometer is an optical device that splits a beam into two and lets the two parts follow different paths before recombining them. The recombination of the two partial beams follow the principle of superposition. If the two paths are equal, the beams will recombine to form the original beam[1] as in the first graph in figure 2.1. If, however, one of the partial beams has followed a path whose distance differs with an amount Δl with respect to the path of the other, the measured intensity may be significantly different from what it would have been if no interference had taken place. The second and third graphs in figure 2.1 show the total wave created from superposing waves that have a slight phase difference, and that are completely out of phase. The intensity as function of phase difference will oscillate as shown in figure 2.1.

To be able to measure the quality of an interference pattern, we define the quantity *visibility*:

$$V = \frac{I_{max} - I_{min}}{I_{max} + I_{min}}, \tag{2.1}$$

where I_{max} is the intensity maximum closest to $I(\Delta l)$ and I_{min} is the intensity of the following minimum. It then follows that a visibility of 1 means that the wave-

[1]Or rather, they will recombine to form two beams, each with intensity half of the original

fronts are perfectly overlapping, so that destructive interference brings I_{min} to zero.

As we will see in chapter 4, no physical light source emits purely monochromatic light. In addition, there will always be random fluctuations that over time can change a beam significantly. A beam with a visibility of nearly unity when Δl in the order of 1 mm may have been subject to many fluctuations, and therefore not show any sign of an interference pattern when Δl becomes close to, say, a meter. This brings us to the main topic of this chapter: Coherence.

2.2 Coherence

In the introduction we defined coherence as *the time τ one may predict the state of the system if one knows its current state*, though we admitted that this definition was only *passable*, and promised to make it more precise.

In the following, we will sometimes write intensities and electric fields as functions of time, sometimes as functions of frequency. This has been done to make the mathematics as intuitive as possible. It is implied that when we use quantities as functions of time, we mean the instantaneous intensity and electric field, and that when we are working with frequency-dependent quantities, the quantity in question is a time-average.

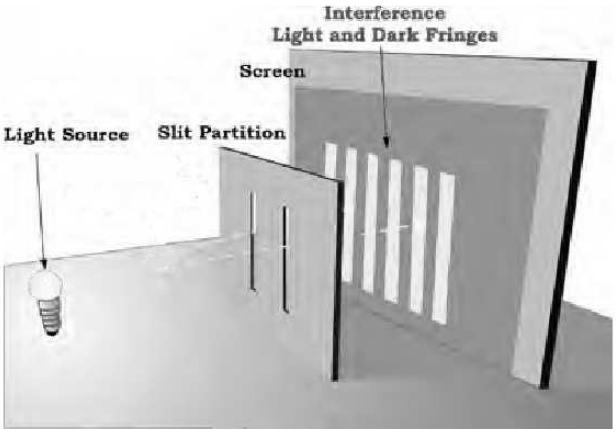

Figure 2.3: The double slit experiment (Figure from [28], slightly modified)

.

2.2.1 The n'th order correlation function

To be able to give a more precise definition and a quantitative measure of coherence, we define the n'th order correlation function of a two-beam system as:

$$g^{(n)}_{1,2}(p_1, p_2, \tau) = \frac{\langle |E_1(p_1, t)E_2(p_2, t+\tau)|^n \rangle}{\langle |E_1(p_1, t)E_2(p_2, t)|^n \rangle} \tag{2.2}$$

where p_1 and p_2 are the points in the (x, y)-plane from which the two beams originate, and τ is a time-delay, due, at least in our case, to the difference in optical path length of the two beams [5]. The angle brackets denote a time average:

$$\langle f(t) \rangle = \frac{1}{T} \int_T f(t)dt. \tag{2.3}$$

In our analysis of the experimental results, the period T will usually mean the entire data set.

If p is the point where the two beams are brought together to interfere[2], $\tau = (l_1 - l_2)/c$, where l_i is the length of the path of the beam originating from p_i. $l_i = |p - p_i|$.

If the path lengths l_1 and l_2 are equal, that is if $\tau = 0$, the coherence is said to be purely spacial. If, on the other hand, the two points p_1 and p_2 should coincide but the light from that point is divided to follow two different paths of different lengths, $g^{(n)}_{1,2}(\tau)$ is called the n^{th} order *auto*-correlation function, and the coherence is called temporal. In that case equation (2.2) reduces to:

$$g^{(n)}_{1,2}(\tau) = \frac{\langle |E_1(t)E_2(t+\tau)|^n \rangle}{\langle |E_1(t)E_2(t)|^n \rangle}. \tag{2.4}$$

The only significance of the index $i = 1, 2$ is now to show that the fraction of the electric field that follows each path may differ. We will from now on assume that we are working with two beams of equal intensity so that our final expression for the auto-correlation function is a further simplification of (2.4):

$$g^{(n)}(\tau) = \frac{\langle |E(t)E(t+\tau)|^n \rangle}{\langle |E(t)|^{2n} \rangle}. \tag{2.5}$$

The first- and second order auto-correlation functions are then given as:

$$g^{(1)}(\tau) = \frac{\langle E^*(t)E(t+\tau) \rangle}{\langle |E(t)|^2 \rangle}, \tag{2.6}$$

$$g^{(2)}(\tau) = \frac{\langle E^*(t)E(t)E^*(t+\tau)E(t+\tau) \rangle}{\langle |E(t)|^4 \rangle} = \frac{\langle I(t)I(t+\tau) \rangle}{\langle I(t)^2 \rangle}. \tag{2.7}$$

[2]In the two split experiment in figure 2.3, p is the point of detection, in a Michelson's interferometer it is where the beams meet the beam splitter for the second time.

We will define the n'th order coherence time of a signal to be the time τ_{coh} where the absolute value of the envelope of the n'th order correlation function $|g^n(\tau)|$ has decreased to e^{-1} of its value at $\tau = 0$, and we say that the signal is n'th order coherent for $\tau < \tau_{coh}$. The coherence length of a signal is defined to be $l_{coh} = c\tau_{coh}$.where c, as always, is the speed of light.

It should be mentioned that the quantity we have called the auto-correlation function often in the literature is named the *degree of coherence*, while the term *temporal correlation function* or *auto-correlation function* is reserved for the unnormalized numerator $\langle E^*(t)E(t+\tau)\rangle$. Since, as mentioned in the introduction the thesis is only concerned with relative quantities, we will use the two terms interchangeably.

In reality almost all coherence measurements will be a mix between temporal and spacial coherence, though it may be *more* spacial than temporal or vice versa. The double slit experiment depicted in figure 2.3 is one example of this. It is only purely spacial along the middle line of the interference pattern, where the lengths from the two slits to the screen are the same. For all other points, there will be a difference in the length of the two paths, and we will therefore have a mix between temporal and spacial coherence. In our work, we have assumed that the effect of temporal coherence is much greater than that of spacial coherence. When talking about *coherence* in the rest of the thesis, it will be implied that we are talking about temporal coherence. Also, when talking about the first order auto-correlation function, it will simply be referred to as the auto-correlation function. If we are talking about a higher order function, this will be specified.

The second order correlation function can be found directly from experimental data using the program in appendix C. The first order correlation function may seem more tricky, since our detectors measure *intensities*, not *electric fields*. In the next two sections we will look at two methods to determine the first order auto-correlation function of a light source. First, we will see how equation (2.6) may be re-written to show $|g^1(\tau)|$ to be equivalent to the earlier mentioned, very useful experimental quantity: *Visibility*, secondly how the auto-correlation function may be determined by looking at the frequency distribution of the original signal.

Visibility and the first order correlation function

The electric field of the total beam in the previous section is the superposition of the electric fields of the two partial beams: $E = E(t) + E(t+\tau)$. The detected

intensity is then:

$$\begin{aligned} I_{det} &= \langle I(t) \rangle \\ &= \langle |E(t) + E(t+\tau)|^2 \rangle \\ &= \langle |E(t)|^2 \rangle + \langle |E(t+\tau)|^2 \rangle + \langle E^*(t)E(t+\tau) + E(t)E^*(t+\tau) \rangle \\ &= \langle |E(t)|^2 \rangle + \langle |E(t+\tau)|^2 \rangle + 2Re\langle E^*(t)E(t+\tau) \rangle \\ &= \langle |E(t)|^2 \rangle + \langle |E(t+\tau)|^2 \rangle + 2|\langle E^*(t)E(t+\tau) \rangle| \cos\left[\phi(\tau)\right]. \end{aligned} \tag{2.8}$$

The first two terms in the last line are just the intensity of the two partial beams. Since we have assumed to be working with a 50-50 beam splitter, only half of the original incoming intensity takes the path towards the detector[3], and we will have $\langle |E(t)|^2 \rangle = \langle |E(t+\tau)|^2 \rangle = I_{partial\ beam} = I_{in}/4$. The third term in the last line in equation (2.8) can be re-written using equation (2.6) with the fact that $|E(t)|^2 = I(t)$, so that in the end we find

$$I_{det} = 2I_{partial\ beam}\{1 + |g^1(\tau)| \cos\left[\phi(\tau)\right]\} = \frac{I_{in}}{2}\{1 + |g^1(\tau)| \cos\left[\phi(\tau)\right]\}. \tag{2.9}$$

In equation (2.1) we defined visibility to be:

$$V(\Delta l) = \frac{I_{max} - I_{min}}{I_{max} + I_{min}}$$

If we have a interference maximum at $\tau - \delta\tau/2$, we will have a minimum at $\tau + \delta\tau/2$, where $\delta\tau$ is the time it takes for light to move the distance of one half wave length. In terms of equation (2.9) we may write the visibility as[4]

$$V(l) = \frac{2I\{1 + |g^1(\tau - \delta\tau/2)|\} - 2I\{1 - |g^1(\tau + \delta\tau/2)|\}}{2I\{1 + |g^1(\tau - \delta\tau/2)|\} + 2I\{1 - |g^1(\tau + \delta\tau/2)|\}} \approx |g^1(\tau)|, \tag{2.10}$$

where the last approximation holds if the first order correlation function changes very little within a time difference of $\delta\tau$, so that $|g^1(\tau + \delta\tau)| \approx |g^1(\tau)|$. Since $\Delta l = c\tau$, writing visibility and the correlation as functions of Δl or τ is equivalent. First-order coherence may in this case be directly measured through measuring the visibility of a signal.

The Wiener Khinchine-theorem

The intensity as a function of frequency of a signal of light is known as *power spectral density*:

$$I(\nu) = |E(\nu)|^2 = E^*(\nu)E(\nu).$$

[3]The other half (the light that is twice reflected and twice transmitted in the beam splitter) takes the path back towards the light source. See also the figures 2.4 and 5.9 for an illustration of this.

[4]Since $\cos(\phi)$ will be $+1$ when $I = I_{max}$ and -1 when $I = I_{min}$.

If we let $E(t)$ denote the Fourier transformed of $E(\nu)$, we have

$$\begin{aligned} I(\nu) &= \int_{-\infty}^{\infty} E(t)e^{i2\pi\nu t}\,dt \int_{-\infty}^{\infty} E(t')e^{-i2\pi\nu t'}\,dt' \\ &= \int_{-\infty}^{\infty}\int_{-\infty}^{\infty} E(t)e^{i2\pi\nu t}E(t')e^{-i2\pi\nu t'}\,dtdt' \\ &= \int_{-\infty}^{\infty}\int_{-\infty}^{\infty} E(t)E(t')e^{i2\pi\nu(t-t')}\,dtdt'. \end{aligned} \tag{2.11}$$

We now define τ to be the difference between t and t': $\tau = t - t'$. Writing equation (2.11) as a function of t and τ, it becomes

$$I(\nu) = \int_{-\infty}^{\infty}\left\{\int_{-\infty}^{\infty} E(t)E(t+\tau)dt\right\} e^{-i2\pi\nu\tau}\,d\tau. \tag{2.12}$$

Recognizing the quantity inside the curly brackets as part of the definition of the auto-correlation function, equation (2.6) we have[5]

$$I(\nu) = \langle|E(t)|^2\rangle \int_{-\infty}^{\infty} g^{(1)}(\tau)e^{-i2\pi\nu\tau}\,d\tau.$$

In other words, the intensity as a function of frequency is (apart from a constant) the Fourier transformed of the first order auto-correlation function. This is known as the *Wiener-Khinchine theorem* [24].

2.2.2 Classical theoretical value of coherence length

Following, but somewhat modifying and adapting to our use the method described by Salamon [43], we will now make a classical estimate of expected coherence length of light with a Gaussian and Lorentzian frequency distributions. Although we will not make express use of the concept of Fourier transforms, the Wiener-Khinchine theorem will be shown to hold for these cases. It should be stressed that the Gaussian shape refers to the distribution of the *frequency contents in a signal,* centered around some central frequency ν_0. This distribution is *not* related the shape of the Gaussian beam described in chapter 1.

General expression for outgoing electric field in a two-beam interferometer

As explained above, in an interferometer, the incoming beam is split, and the partial beams follow separate paths until recombined to form an interference pattern.

[5] One may wonder how we may say that an integral that spans the interval between $\pm\infty$ may be said to be the same as an integral that we specifically defined to be over a period only, as we did in equation (2.3). However, if the function is not periodic, *one period* really *is* infinitely long. If, on the other hand, the function *is* periodic,taking the integral over *many* whole periods and dividing by the total number of periods will yield the same answer as if one took the integral over a single period. If the integral is taken over time that is not an integer times the duration of a period, any error due to the "leftover" after the last whole will be minute since it will be divided by the total number of periods.

The electric field of the beam leaving the interferometer is the superposition of the electric fields of the partial beams. We will again look at only one component of the electric field.

$$E_{out} = \sum_j E_j.$$

For a two-beam interferometer, such as the Michelson's interferometer, this is:

$$E_{out} = E_1 + E_2 = k_1 E_{in}(\nu) e^{i\phi_1(t)} + k_2 E_{in}(\nu) e^{i\phi_2(t)},$$

where $E_{in}(\nu)$ is the electric field entering the interferometer, k_j is a constant modifying the amplitude of the electric field, and $\phi_j(t)$ is the phase of the partial wave.

Detected intensity in a Michelson's interferometer

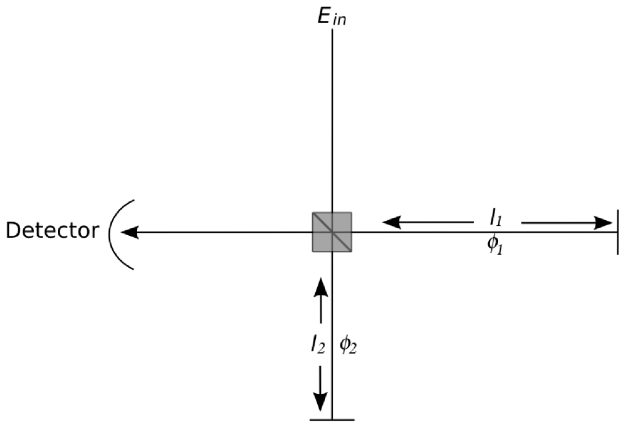

Figure 2.4: The path difference in a Michelson's interferometer will cause a phase difference $\Delta l = 2(l_2 - l_1)$ between the two paths.

In a Michelson's interferometer, each partial wave that leaves the interferometer on the side of the detector will once be reflected and once transmitted through the beam splitter. Assuming all mirrors to be identical and perfect reflectors, these will not affect the constants k_j, and any phase change due to the beam splitter or mirrors will be the same for both paths. The phase change due to the beam propagating a length l is given by $\phi = 2\pi l/\lambda = 2\pi\nu l/c$. Since only the phase *difference* between the paths is of any importance, we may write:

$$E_{out}(\nu) = RTE_{in}(\nu)e^{i\phi_1} + TRE_{in}(\nu)e^{i\phi_2} = RTE_{in}(e^{\frac{i2\pi\nu(2l_1)}{c}} + e^{\frac{i2\pi\nu(2l_2)}{c}}).$$

The quantities R and T are the fraction of the original electric field being reflected and transmitted, and c is again the speed of light. Note that the distance that enters the equation is actually $2l_i$, since the beam will have to travel the distance

of the arm twice.

The intensity of the light is -apart from a constant- the absolute square of the electric field:

$$I_{out}(\nu) = |E_{out}(\nu)|^2 = R^2T^2|E_{in}(\nu)|^2 \left| e^{\left(\frac{i4\pi\nu l_1}{c}\right)} + e^{\left(\frac{i4\pi\nu l_2}{c}\right)} \right|^2 .$$

Assuming a perfect 50-50 beam splitter[6] with $R^2 = T^2 = 1/2$ this is[7] :

$$I_{out}(\nu) = \frac{1}{2} I_{in}(\nu) \left[1 + \cos\left(\frac{2\pi\nu\Delta l}{c}\right) \right], \qquad \begin{array}{c} \Delta l = 2(l_1 - l_2) \\ I_{in}(\nu) = |E_{in}(\nu)|^2 \end{array}.$$

The total detected intensity will be the integral of this over all frequencies[8]:

$$I_{det} \;=\; \frac{1}{2} \int_{-\infty}^{\infty} I_{in}(\nu) \left[1 + \cos\left(\frac{2\pi\nu\Delta l}{c}\right) \right] d\nu. \tag{2.13}$$

Coherence length of a light source with a Gaussian intensity distribution

Let us now have a look at the expected coherence length of a light source of which the intensity is a Gaussian function of frequency, centered around a central frequency ν_0:

$$I_{in}(\nu) \;=\; I_0\, e^{-4\ln 2\left(\frac{\nu-\nu_0}{\Delta\nu}\right)^2}, \qquad I_0 = I(\nu = \nu_0).$$

The constant $\Delta\nu$ is called the full width at half maximum (FWHM). If calculating the value of the intensity at the points $\nu_0 \pm \Delta\nu/2$, one finds:

$$I(\nu_0 \pm \Delta\nu/2) = I_0/2,$$

so $\Delta\nu = (\nu_0 + \Delta\nu/2) - (\nu_0 - \Delta\nu/2)$ is indeed the width of the intensity graph at the height where it has decreased to half of its maximum value.

[6]Half of the intensity reflected, half transmitted.

[7]The energy of a beam of light is proportional to its intensity. Conservation of energy therefore requires that the sum of the intensity leaving each side of the beam splitter is equal to the incoming intensity. Since intensity is proportional to the *square* of the electric field, and R and T represent the fractions of the reflected and transmitted electric field, we require R and T *squared* to be equal to one half for a 50-50 beam splitter.

[8]Technically, one should weight the frequencies with the detection efficiency $P(\nu)$ of the detector. However, since we will be working with Gaussian and Lorentzian distributions that go very fast to zero, and light with a fairly narrow bandwidth, our assumption of a perfect and universal detector should be well grounded.

Putting this into the expression for the detected intensity in equation (2.13), we find[9]:

$$\begin{aligned} I_{det} &= \frac{I_0}{2}\int_{-\infty}^{\infty} e^{-4\ln 2\left(\frac{\nu-\nu_0}{\Delta\nu}\right)^2}\left\{1+\cos\left(\frac{2\pi\nu\Delta l}{c}\right)\right\}d\nu \\ &= \frac{I_0}{4}\Delta\nu\sqrt{\frac{\pi}{\ln 2}}\left[1+\exp\left\{\frac{-1}{\ln 2}\left(\frac{\pi\Delta l\Delta\nu}{2c}\right)^2\right\}\cos\left(\frac{2\pi\Delta l\nu_0}{c}\right)\right]. \end{aligned}$$

Integrating over all frequencies, we have for the incoming intensity

$$I_{in} \;=\; I_0\int_{-\infty}^{\infty} e^{4\ln 2\left(\frac{\nu-\nu_0}{\Delta\nu}\right)^2}d\nu \;=\; \frac{I_0}{2}\Delta\nu\sqrt{\frac{\pi}{\ln 2}},$$

so that the outgoing intensity normalized to that of the incoming is:

$$\frac{I_{det}}{I_{in}} \;=\; \frac{1}{2}\left[1+\exp\left\{\frac{-1}{\ln 2}\left(\frac{\pi\Delta l\Delta\nu}{c}\right)^2\right\}\cos\left(\frac{2\pi\Delta l\nu_0}{c}\right)\right]. \tag{2.14}$$

The intensity has been plotted in figure 2.5. Comparing equation (2.14) with equation (2.9) and (2.10), we see that we have

$$V(\Delta l) = \exp\left\{\frac{-1}{\ln 2}\left(\frac{\pi\Delta\nu\Delta l}{2c}\right)^2\right\}. \tag{2.15}$$

Above we found that visibility should be proportional to the Fourier transform of the intensity distribution $I(\nu)$. From Table A.1 we find as predicted:

$$V(\Delta l) = \exp\left\{\frac{-1}{\ln 2}\left(\frac{\pi\Delta\nu\Delta l}{2c}\right)^2\right\} \quad \rightleftharpoons \quad e^{-4\ln 2\left(\frac{\nu-\nu_0}{\Delta\nu}\right)^2} = I_{in}(\nu).$$

In this case, the expression for the coherence length is given by:

$$\begin{aligned} & V(l^g_{coh}) = \exp\left\{\frac{-1}{\ln 2}\left(\frac{\pi\Delta\nu l^g_{coh}}{2c}\right)^2\right\} = e^{-1} \\ \Rightarrow \qquad & l^g_{coh} = \frac{2\sqrt{\ln 2}c}{\pi\Delta\nu}. \end{aligned} \tag{2.16}$$

Coherence light for Lorentzian light

As we will see in chapter 4, the other far side of the possible range of intensity distributions of atomic light sources is the Lorentzian:

$$I(\nu) = I_0\frac{\Delta\nu^2}{4(\nu-\nu_0)^2+\Delta\nu^2},$$

[9] We solved the integral by making the substitution $u = (\nu-\nu_0)/\Delta\nu$, writing the cosine as a sum of exponential functions, and then looking up in [42]. An alert reader may also notice that the integral is actually the same as the integral solved to find the Fourier transform of the Gaussian function, which we solve in appendix A.

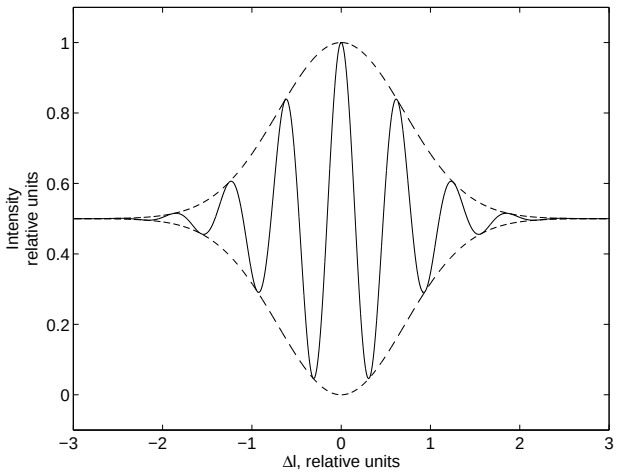

Figure 2.5: The output intensity of a Michelson's interferometer using a light source with a Gaussian $I(\nu)$-distribution.

where $\Delta\nu$ is again the FWHM-width of the distribution.

Inserting this into equation (2.13) we have

$$I_{det} = \frac{I_0}{2}\int_{-\infty}^{\infty}\frac{\Delta\nu^2}{4(\nu-\nu_0)^2+\Delta\nu^2}\left[1+\cos\left(\frac{2\pi\nu\Delta l}{c}\right)\right]d\nu.$$

Looking the integral up in [39] we find:

$$I_{det} = I_0\frac{\pi}{4}\Delta\nu\left\{1+e^{\frac{-\pi\Delta\nu}{c}|\Delta l|}\cos\left(\frac{2\pi\nu_0}{c}\Delta l\right)\right\}.$$

The total incoming intensity is given by

$$I_{in}(\nu) = I_0\int_{-\infty}^{\infty}\frac{\Delta\nu^2}{4(\nu-\nu_0)^2+\Delta\nu^2}d\nu = \frac{I_0}{2}\pi\Delta\nu.$$

This gives a relative intensity of:

$$\frac{I_{det}}{I_{in}} = \frac{1}{2}\left[1+e^{\frac{-\pi\Delta\nu}{c}|\Delta l|}\cos\left(\frac{2\pi\nu_0}{c}\Delta l\right)\right]. \tag{2.17}$$

The intensity is plotted in figure 2.6.

Again comparing with equation (2.10), we have

$$V(\Delta l) = |g^1(\Delta l)| = e^{\frac{-\pi\Delta\nu}{c}|\Delta l|}. \tag{2.18}$$

The coherence length is now:

$$\begin{aligned} & V(l^g_{coh}) = \exp\left\{\frac{-\pi\Delta\nu}{c}l^l_{coh}\right\} = e^{-1} \\ \Rightarrow \qquad & l^l_{coh} = \frac{c}{\pi\Delta\nu}. \end{aligned} \tag{2.19}$$

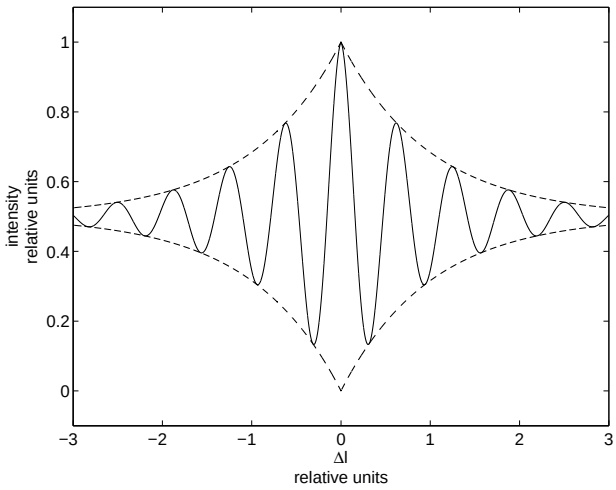

Figure 2.6: The output intensity of a Michelson's interferometer using a light source with a Lorentzian $I(\nu)$-distribution.

Again comparing with table A.1 we find

$$\frac{1}{\omega^2 + a^2} \rightleftharpoons \frac{\pi}{a} e^{-a|t|}.$$

In finding the auto-correlation function of Gaussian and Lorentzian intensity distribution, we have also shown that the Wiener-Khinchine theorem holds.

In chapter 4, we will have a closer look at the physical meaning of the two shapes of the frequency distribution. We will see that a light source consisting of an ideal, dilute gas will have a Gaussian frequency distribution, while a dense gas of high temperature will be closer to Lorentzian.

It should perhaps be mentioned that the figures 2.5 and 2.6 have been made for illustrative purposes only, to show the shapes of the expected curves after the light has been sent through an interferometer. The curves depicted can hardly be said to satisfy the requirement that the auto-correlation function (and therefore also the visibility) changes *very little* within a wavelength. With a signal similar to those depicted, it would be impossible to measure a visibility close to unity even for very small Δl. From equation (2.14) and (2.17), we see that the number of oscillations within the enveloping curve depends on the ratio $R = \Delta\nu/\nu_0$. If R is small, the intensity will oscillate fast compared to the damping time of the Gaussian or Lorentzian envelope, and the requirement will be satisfied. If R is large, we will have a situation as in figure 2.5 and figure 2.6.

Comparing the coherence length of Lorentzian light sources, equation (2.19), with that of light of Gaussian intensity distributions, equation (2.16), we see that the Gaussian coherence length is a factor $2\sqrt{\ln 2}$ larger that the coherence length for

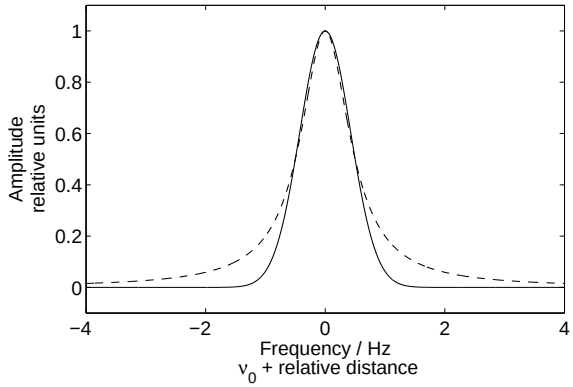

Figure 2.7: A Gaussian distribution (whole drawn line) has more of its intensity concentrated within a narrower FWHM-width, and therefore has a longer coherence length than Lorentzian distributed light (dotted line).

light of a Lorentzian distribution with the same $\Delta\nu$. This can be explained by examining figure 2.7. In Gaussian light, a higher fraction of the total intensity is concentrated in frequencies between $\nu_0 \pm \Delta\nu/2$ than for Lorentzian light.

One could argue that it would make more sense to define a width of the graph that took this intensity distribution into account, but as we will see, light from physical light sources tend to be a mix between the two extremes: A pure Gaussian and a pure Lorentzian. It is then useful to have a common convention of spectral width.

2.3 Coherence as predictability

Let us again return to the way we described coherence in the introduction, and that was repeated at the beginning of this chapter. We claimed that *[Coherence time is] the time τ one may predict the state of a system if one knows its current state.* From the above discussion, it should be clear that the predictability in question is *not* a matter of whether we are able to mathematically calculate the behavior of a signal. In that case, the coherence length of a light source would depend on our subjective knowledge of its evolution in time. The *predictability* is rather a question of how sensitive the average intensity of a superposition of a signal with a shifted[10] version of itself is. If the intensity is highly dependent on the value of τ, it is an indication that the signal is highly periodic, and that a change at one point of the signal to a great extent is matched by a similar change in the rest of the signal. In that sense, the signal may be said to be predictable. If, on the other hand, the average intensity does not change significantly with different values of τ, it is an indication that the parts of the signal are not strongly correlated, and the signal may thus be said to not be predictable.

[10] In time or space.

Chapter 3

Simulations

In the previous chapter, we saw several examples of relations between quantities that may be calculated from a signal of light. We will now analyze some of these relations through numerical simulation. We will also try to give an estimate of the coherence length of the signal, and in the end we will discuss coherence length in relation to the concept of the *photon* or *quantum of light*. The original signals have been generated using Matlab-code produced by Borys Jagielski [23]. The analysis has been done using code made by the author, which may be found in appendix C.

Graphs representing quantities that do not in general have magnitudes relative to one have been normalized for easily comparison.

It is worthwhile saying a few words to clarify the terms that will be used. When we talk about a *pulse*, we will mean the quantity that is emitted from a light source, as in figure 3.1. The term *wave-packet* will be used for a wave enveloped by a function, periodic or not, that groups some of the periods of the wave into separate entities, as in figure 3.7(a2)[1]. In this definition, a pulse will always be a wave packet, while a wave packet is not necessarily a pulse.

In the discussion of figures 3.9 and 3.10, we will talk about the *background*, the *pulse-like structure*, the *central peak* and the *classical coherence length*. The first term will refer to the flat background that is especially visible in the last graph in figure 3.9. The second term refers to the larger structure in the background, enveloped by a Gaussian function. The third and fourth terms will both refer to the peak of the envelope, a few wave lengths thick, that becomes increasingly dominating and visible for an increasing number of emitters.

[1] See figure text for letter-labeling of figures.

3.1 Generation of signals

Generation of all signals builds on a model where light is emitted in the form of electromagnetic pulses, or wave-packets as in figure 3.1. Each pulse is a pure sine with a Gaussian envelope. The author finds this the most intuitive way to picture light emittance from atoms, as it allows for keeping some ideas from both the wave and particle interpretation of light. It is nevertheless understood that this picture imposes some strong constraints on the simulations and the interpretation of their results.

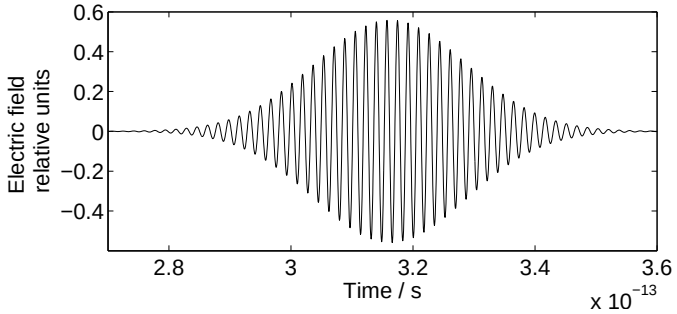

Figure 3.1: An electromagnetic pulse or wave-packet.

To generate a signal in the simulations, the user must choose *how many* emitters there will be in the sample, and the *probability per data-point* for an emitter to emit a pulse. Each pulse is characterized by three parameters: Wavelength, amplitude and damping factor. While the wavelength and amplitude refer to the wavelength and amplitude of the sine-function mentioned above, the damping factor determines the width of the Gaussian envelope. Each pulse has a sharp value for all three parameters, but the values vary randomly from pulse to pulse, following a normal distributed probability function [23]. The generation program allows for the user to determine the central value and width of the distribution function of all three parameters. In our simulations, we have set the amplitude to be equal to unity for all pulses, that is, with a normal distribution of width equal to zero, The central wavelengths were chosen to be 633±10 nm or 633±100 nm, corresponding to a small or large spectral width, respectively (cf. figure 3.8). For the most part, a wide spectral width has been used, as the correspondingly short coherence length is clearly discernible from the pulse width. The damping factor was set for each separate simulation to give the best possible visualisation of the point being discussed. It was, of course, kept constant where required for a fair comparison of different figures. This applies especially to the figures 3.6 and 3.7, figure 3.11, and figures 3.9 and 3.10.

3.2 Matlab code for analysis

We will now give a description of the Matlab code used in the analysis of the generated signals. The code may be found in appendix C, and the line numbering of the text refers to the lines in the code.

In the main program, the user is asked to enter the set of data to be plotted, and to choose a τ_{cut} (lines 55 and 72 of the code respectively). A τ_{cut} is chosen partly to speed up calculation time, since the loops that generate $g^{(n)}(\tau)$ run from $\pm\tau_{cut}$. The chosen value of τ_{cut} should be much smaller than the total length of the data set to avoid unphysical effects due to low statistics in the end of the function. If the original data does not include a time-column, the user is also asked to state the sampling time (lines 78-85). The user is then given the following choice:

1. To plot the original *signal* and its Fourier transform

2. To plot the *auto-correlation function* of arbitrary order, and its Fourier transform

3. To simulate the intensity as a function of the length difference $\Delta l = c\tau$ in a *Michelson's interferometer*, and to plot its *visibility*

4. To plot *power spectral density*.

In the following, we will briefly describe the algorithms of the points (2)-(4), the code of which may be found in section C.3, C.4 and C.5 in the appendix. As in the code, we will take a to be the amplitude of the original signal, t to be the time in data-points, and τ to be the retardation in time, related to the path difference Δl in an interferometer through $\Delta l = c\tau$.

3.2.1 The auto-correlation function

The user is asked to choose the order n of the auto-correlation function (cf. the definition of $g^{(n)}(\tau)$ on page 22), and the n^{th} order auto-correlation function is generated (lines 193-212). In generating $g^{(n)}(\tau)$, a loop runs between the values $\tau = \pm\tau_{cut}$. The auto-correlation function is then calculated as $a(t) \times a(t+\tau)$ for all t in the interval defined by τ_{cut} from each end of the total data set. The program will also calculate the Fourier transform of $g^{(n)}(\tau)$ (lines 238-242), which the user is offered to save (lines 248-257) for later comparison with the visibility function (cf. equation (2.10)).

If the user has chosen to plot the *first* order auto-correlation function, the program automatically also finds and plots its absolute value, and offers to save the information for later comparison with the power spectral density (lines 250-286).

3.2.2 Simulation of a Michelson's interferometer

The algorithm is similar to that of the auto-correlation function, but this time calculating the sum (instead of the product): $a(t) + a(t + \tau)$ (lines 303-309). The output intensity is the square of this, normalized by the intensity at $\tau = 0$.

To find the visibility, we defined two vectors, *pks_n* and *pks_p* where we entered the minimum and maximum values of the intensity function (lines 321-323). A visibility-vector was defined as *visibility(i) = (pks_p(i) - pks_n(i))/(pks_p(i) + pks_n(i))*, with i being the element number of the vectors (line 337). The position of *visibility(i)* was defined as the mean value of the positions of *pks_n(i)* and *pks_p(i)* (lines 335-337). The program offers to save the visibility graph for later comparison with the absolute value of the Fourier transform of the first order auto-correlation function (lines 347-355).

3.2.3 Power spectral density

The user may choose to divide the original signal into a number of sub-segments (line 359). The program then calculates the Fourier transform of *the square* of each sub-segment separately, and superposes them (lines 379-389). If the number of sub-segments is chosen to be high, the average obtained from sub-segmenting will be better, but at the cost of adding to the edge-effects and effects stemming from decreased statistics, of each Fourier transform due to shorter segments. Sub-segmenting should not be used if the original data is not stationary.

3.3 The Wiener-Khinchine theorem

On page 24, we showed that power spectral density is equal to the Fourier transform of the first order auto-correlation function. In figure 3.2, we have plotted the power spectral density described in section 3.2.3 in red together with the Fourier transform of $g^1(\tau)$ from section 3.2.1 in blue.

In the figure, a sub-segmenting of 14 was used to obtain the graph of the spectral density. The upper frame shows the calculated Fourier transform. In the lower frame the graphs have been smoothed using the built-in Matlab-function *smooth(data,n)*, where *data* is the set of data that is to be smoothed, and n is an integer. The function *smooth* makes a moving average of n points around each data point in *data*.

As seen in the figure, our signal is in very good agreement with the theoretical prediction that says that $g^{(1)}(\tau) \rightleftharpoons I(\nu)$ (equation (2.12)). The curve describing spectral density has slightly lower values than the curve generated from the auto-correlation function. Examining the upper figure, the red line has one peak significantly higher than the rest, and in using the very simple normalization of

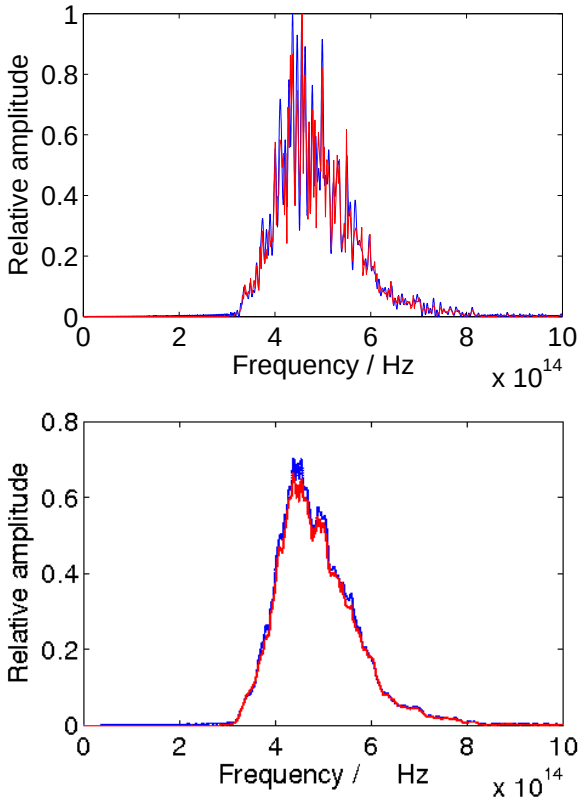

Figure 3.2: Numerical test of the Wiener-Khinchine theorem

defining the highest peak to be equal to one, this will cause the bulk of the curve to be shifted towards lower values.

3.4 Visibility and the auto-correlation function

The first frame in figure 3.3 shows the first order correlation function of the signal (cf. section 3.2.1), the second the intensity as as function of $\tau = c\Delta l$ that one would obtain if sending the light through a Michelson's interferometer, as described in section 3.2.2. If one neglects the fact that the second graph is shifted to have only positive values (since the intensity cannot be negative), the two graphs are identical[2]. Comparing the third line of equation (2.8), which shows the intensity from an interferometer, with equation (2.6) defining the first order correlation function, this is not surprising[3].

[2]As in chapter 2 we have normalized the intensity to that of the incoming intensity

[3]In a Michelson's interferometer, it does not matter which arm is defined to give the electric field $E(t)$ and which arm gives the field $E(t+\tau)$. This is equivalent to saying that the the intensity of the light from an interferometer should be the same for positive and negative τ. We may then write $\langle E^*(t)E(t+\tau)+E(t)E^*(t+\tau)\rangle = \langle E^*(t)E(t+\tau)+E(t)E^*(t-\tau)\rangle = \langle E^*(t)E(t+\tau)+E^*(t-$

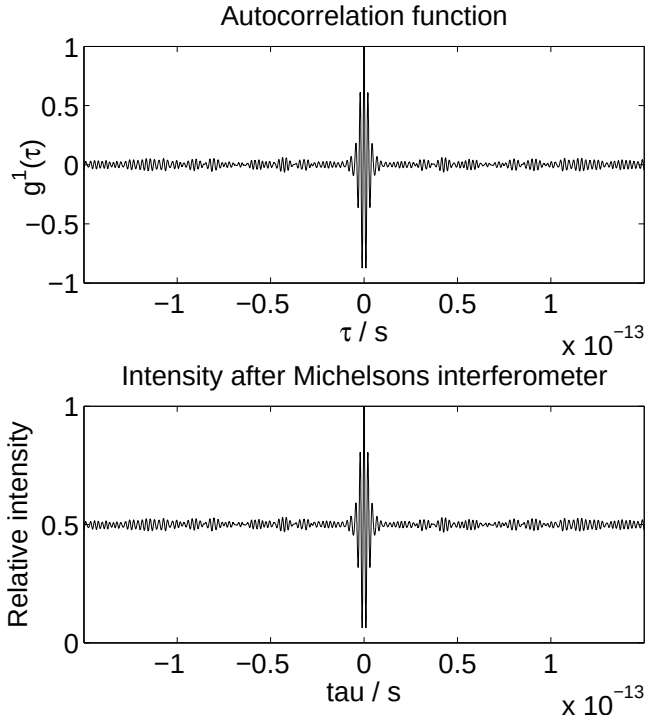

Figure 3.3: The shape of the intensity as a function of $\tau = c\Delta l$ from a Michelson's interferometer is identical to the shape of first order correlation function, but their absolute values are different.

On page 23 we showed that the absolute value of the first order correlation function is equal to the visibility. In figure 3.4 we have plotted the absolute value of the autocorrelation function together with the visibility of the same signal as in figure 3.3. Again, our simulations are in good agreement with the theory.

$\tau)E(t)\rangle$. Making the shift $t' = t - \tau$ this is: $\langle E^*(t)E(t+\tau) + E(t')E^*(t'+\tau)\rangle = 2\langle E^*(t)E(t+\tau)\rangle$, where the last equation is valid because we are taking the integral over all t. The two equations mentioned in the paragraph are now directly comparable.

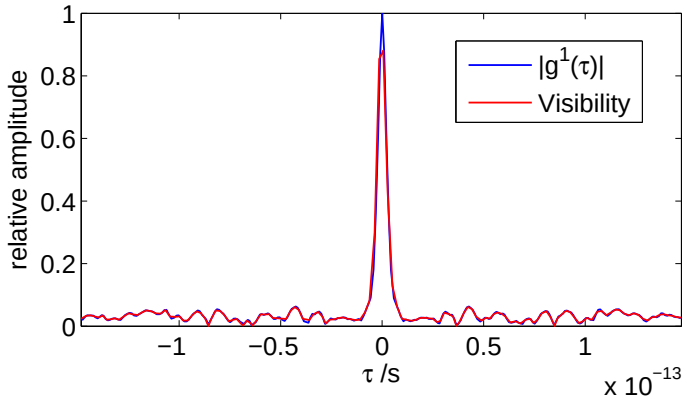

Figure 3.4: The visibility is equal to the absolute value of the first order auto-correlation function $|g^1(\tau)|$.

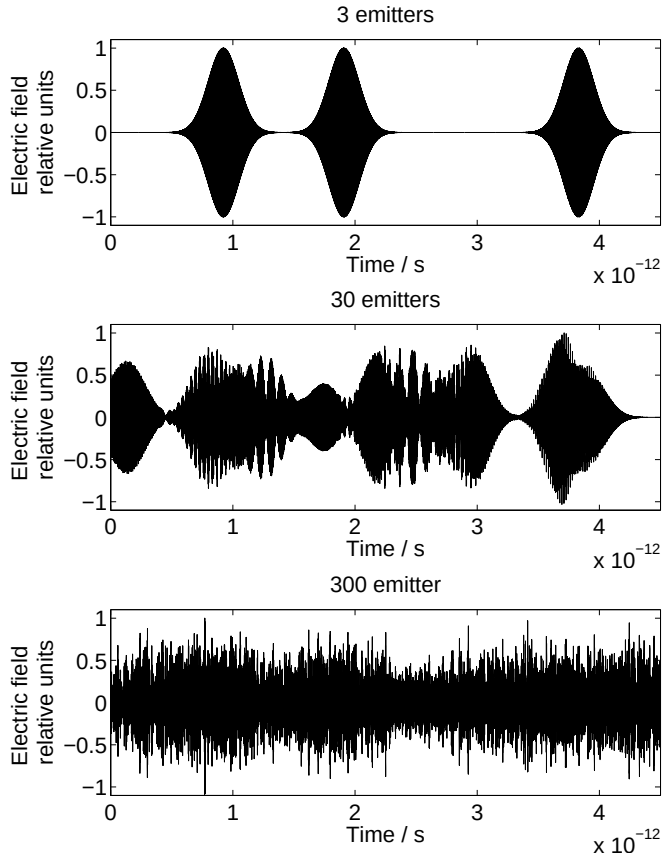

Figure 3.5: When the number of emitted pulses become large, the pulse pattern gradually becomes hidden in the interference pattern of superposed pulses.

3.5 Wave packets, photons and coherence length

As it was briefly mentioned in the introduction, some authors seem to suggest that the coherence length of a signal may be identified as the size of a photon or quantum of light [2], [25]. In our model, this size would intuitively correspond to the dimensions of the curve enveloping the pulse in figure 3.1. We will in the following examine some methods of determining coherence, and see how the coherence length depends on the number of emitters.

3.5.1 Does the coherence length correspond to the photon size?

In chapter 2, the coherence length and time of a signal was defined to be the $\Delta l = c\tau$ where the value of the auto-correlation function had decreased by a factor e^{-1}. This definition was shown, theoretically and numerically to be equivalent with the half-width of the visibility function. Other ways of finding the coherence time of a signal have been suggested, some have also been proved. In this section, we will numerically examine the following methods of calculating coherence time:

1. The size of a photon, which in our pulse-model would correspond to the temporal length of a pulse
2. The width of the visibility function
3. Calculation from the width of the power spectral density, according to the classical value for a Gaussian intensity distribution.

We have chosen to use the visibility function rather than the auto-correlation since we have shown that the two are equivalent, and it is easier to make a rough estimate of the former through examination of figures 3.6 and 3.7.

Examine for a moment figure 3.6(a) and figure 3.7(a1 and a2). The only difference between the two figures is the number of light emitters; figure 3.6 depicts a single light pulse from a single emitting atom, while figure 3.7, shows a signal that is a superposition of pulses from one hundred emitters[4]. The pulse in 3.6 has a e^{-1}-width of about 0.35×10^{-12} sec, the value of the visibility graph, figure 3.6(d), when its amplitude is e^{-1} is about 0.25×10^{-12}, that is in the same order of the pulse. The signal in figure 3.7(a2) also shows a wave-packet pattern, but this time one wave-packet lasts for a much shorter time; a rough estimate gives 0.01×10^{-12} sec per wave-packet. Again, the number is approximately equal to that found through an examination of graphs showing the visibility function, figure 3.7(d).

According to the results found in chapter 2, the coherence length of a source of a Gaussian frequency distribution is

$$l^g_{coh} = \frac{2\sqrt{\ln 2}c}{\pi\Delta\nu} \quad \Rightarrow \quad \tau^g_{coh} = \frac{2\sqrt{\ln 2}}{\pi\Delta\nu}, \tag{3.1}$$

[4]As described in section 3.1, each emitter has a given probability per data point of emitting a pulse. If a signal contains n pulses, the pulse density is such that there are n pulses within a distance $l_{max} = c\tau_{max}$, where l_{max} is the maximum length difference of the interferometer.

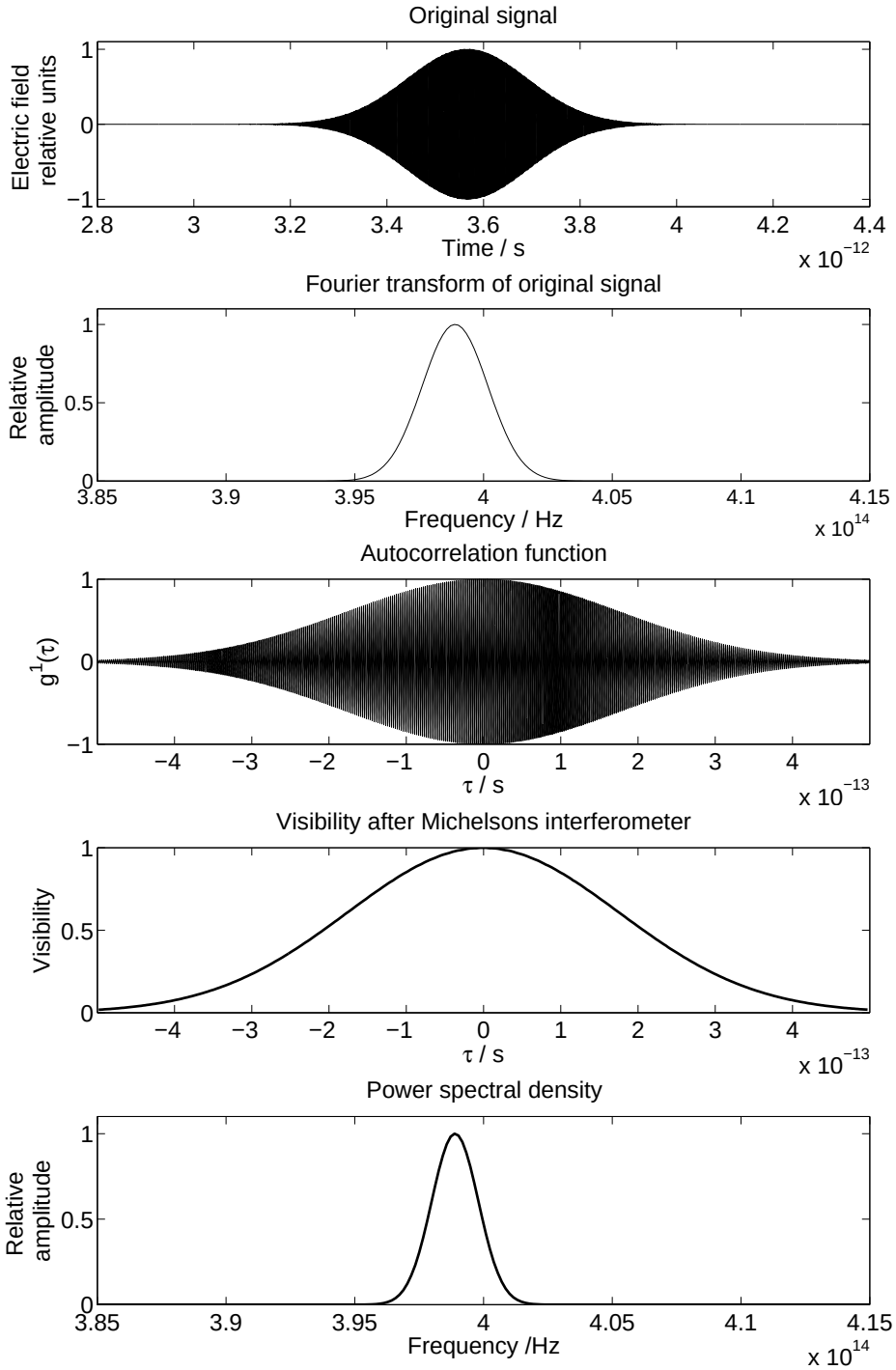

Figure 3.6: A single pulse. From the top down: (a) Electric field, (b) Fourier transform of the electric field, (c) auto-correlation function, (d) visibility and (e) power spectral density.

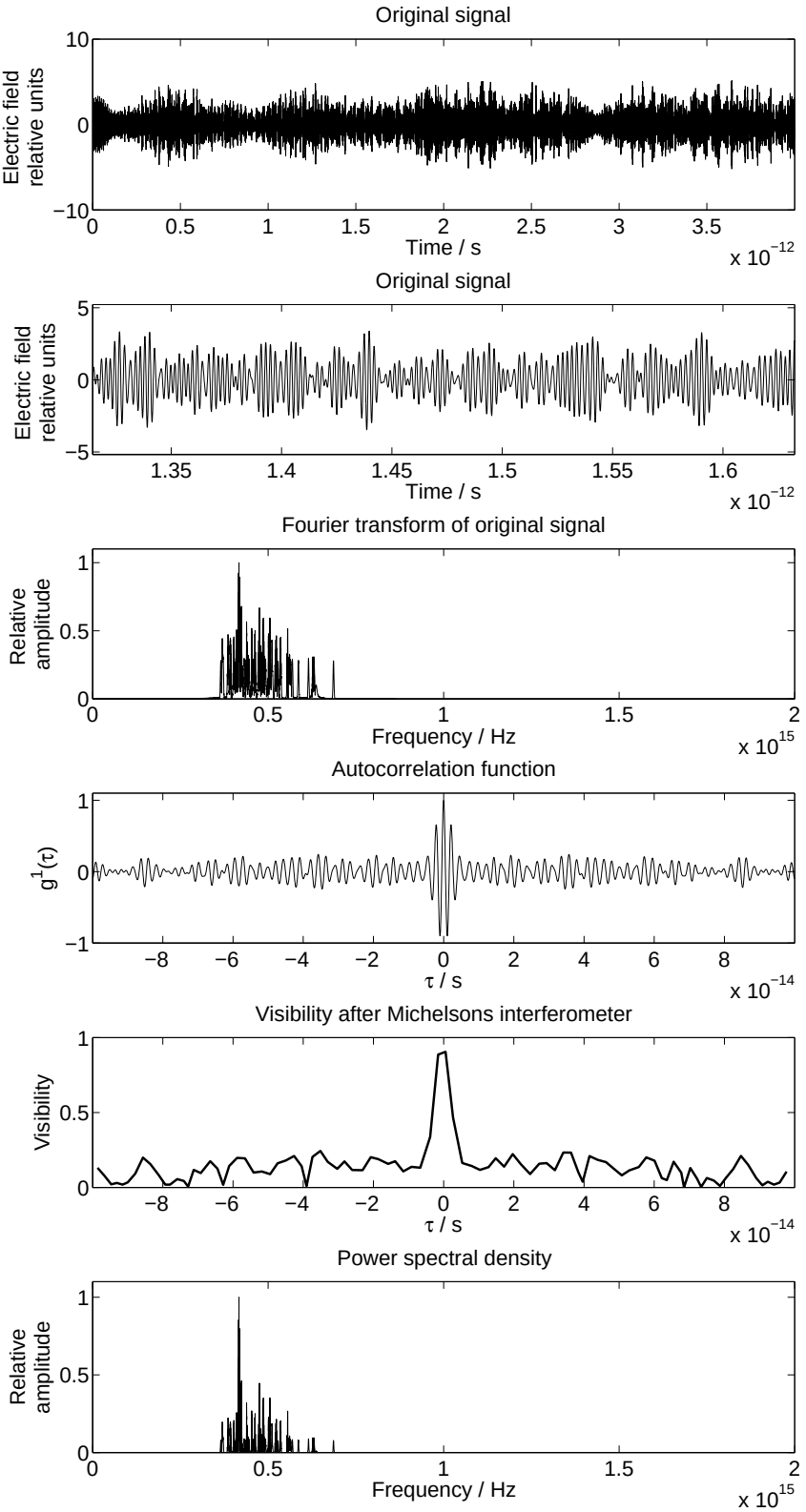

Figure 3.7: A superposition of one hundred pulses. From the top down: (a1) Electric field, (a2) enlarged section of the electric field, (b) Fourier transform of the electric field, (c) auto-correlation function, (d) visibility and (e) power spectral density.

The FWHM-width of the power spectral density of the single pulse is approximately $\Delta\nu = 0.021 \times 10^{14}$ Hz. Plotting this value into equation (3.1) gives a theoretical value of the width of the visibility graph:

$$\tau^g_{coh} = \frac{2\sqrt{\ln 2}}{\pi\Delta\nu} = \frac{2\sqrt{\ln 2}}{0.021 \times 10^{14}\pi \text{ Hz}} = 0.25 \times 10^{-12} \text{ sec}, \tag{3.2}$$

in exact agreement with the above estimate.

The width of the power spectrum of the light from the hundred emitters is harder to define, but a value of 0.2×10^{15} Hz seems to be of the right order. The shape of the spectrum may hardly be said to be a well defined Gaussian, but in lacking a proper expression, we will use equation (3.1). We then find:

$$\tau^g_{coh} = \frac{2\sqrt{\ln 2}}{\pi\Delta\nu} = \frac{2\sqrt{\ln 2}}{0.2 \times 10^{15}\pi \text{ Hz}} = 0.27 \times 10^{-14} \text{ sec}, \tag{3.3}$$

As expected, the match is not as good as for the single graph. The coherence length found from the width of the pulse is a little less than a factor 4 longer than that found from the power spectral density. The disagreement may be due to the fact that the power spectral density is composed of several distinct peaks, which together would not decrease the coherence length as much as our roughly determined FWHM suggests.

As mentioned at the beginning of this section, the only difference between the two sets of graphs in figure 3.6 and figure 3.7 is the *number* of light emitters. Seeing the difference between the coherence lengths in the two cases, it is very difficult to explain how coherence length may correspond to the size of a photon *unless* one is willing to sacrifice the idea of a photon as an indivisible and unique link between two events (cf. the introduction chapter) [19]. If one, on the other hand is willing to see the photon as a statistical feature arising from the superposition of several pulses of electromagnetic radiation, the picture of light in the form of particles or wave-packets may be kept, and the photon may then be identified as the wave packets defined in the introduction of this chapter. In the case of *a single pulse*, the photon will be identical to a pulse, while in the case of many such pulses as in figure 3.7(a2), we will be forced to identify the photon as the wave packets of much shorter coherence length than each original pulse.

It may be clarifying to briefly return to the analogy that opened our description of interference in chapter 2. In the case of a single pebble being thrown into the quiet lake, the waves that emerged could truly be said to stem from that pebble hitting the water. In the case of many such pebbles, there is no longer a one-to-one link between a specific pebble to a resultant wave-top far from where the pebbles hit. Each wave-top[5] is a superposition of a collection of original waves, and each original wave may be part in the formation of several such new wave-tops.

[5]It may be confusing that a photon now corresponds to a wave in water, but hopefully the reader is able to understand the analogy.

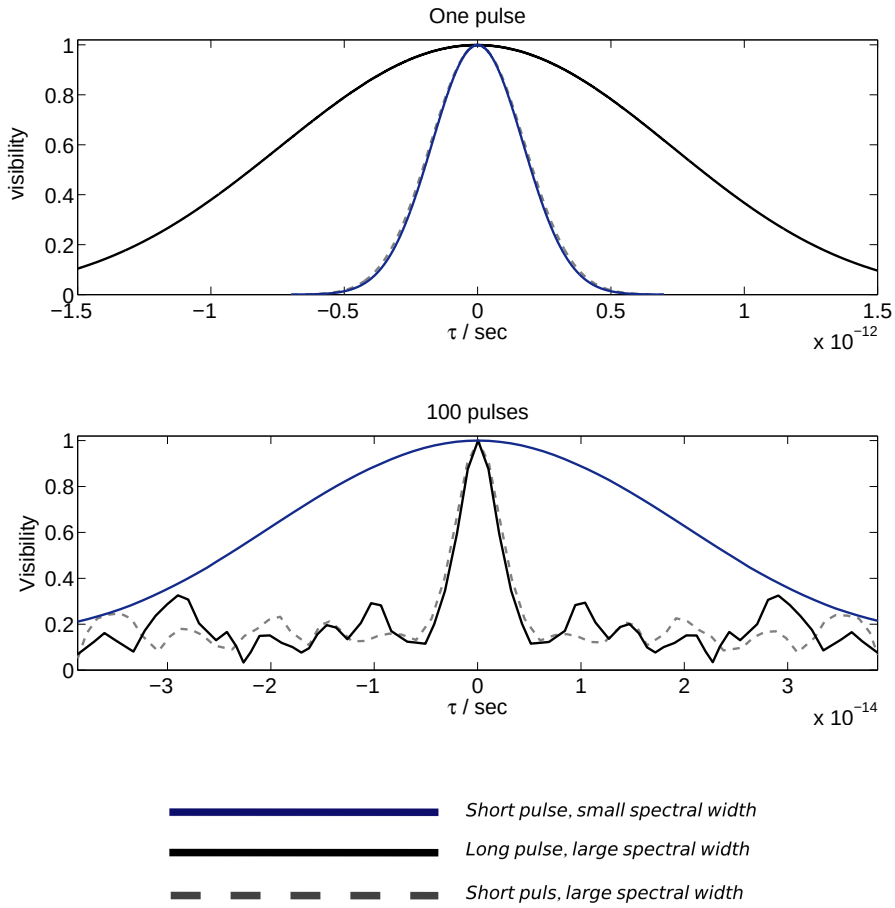

Figure 3.8: The visibility, and therefore the coherence length of single pulses is highly dependent on the length of the pulse. When the number of pulses increases, the coherence length no longer depend on this length. Note the color/pattern coding of the graphs and the difference scaling of the τ-axis.

In figure 3.8, the dependence of coherence length on pulse size and line width is further investigated. The upper frame depicts the visibility of single pulses. As we saw and discussed in the previous paragraphs, the coherence length of a single pulse is comparable to the length of the pulse. The second graph in figure 3.8 depicts the coherence length of light from one hundred emitters with the same statistical settings as for the pulses in the upper graph.

In both sub-figures in 3.8, the damping factor (corresponding to the temporal size of a pulse) of the blue and dashed gray pulse is the same, while the damping factor of the black pulse is significantly longer. On the other hand, when it comes to the *statistical properties* of *a collection of pulses*, the picture is another: The black and the dotted gray lines both have a standard deviation of wave length of 100 nm, while the blue has a standard deviation of 10 nm. In all three cases, each single

pulse contains only one wavelength[6], but the *probability* for a pulse to be emitted with a given wavelength follows a Gaussian probability distribution with the standard deviations just mentioned. In each case, this distribution is centered at 633 nm, the nominal wave length of our laser.

As implied from the previous paragraph, the statistical properties of the pulses do not matter in figure 3.8(a). When comparing with figure 3.8(b), however, it becomes clear that the standard deviations are important, as it is the two graphs with *the same* standard deviation that have similar widths. In our case, the collective properties are very dominant for the signal from 100 pulses. It should not be forgotten that the Fourier transform of the signal and the power spectral density will depend on both the damping factor and standard deviations of the wavelengths It would be interesting to see how varying the values of these would change the graphs in 3.8. Standard deviations of 10 and 100 nm are rather large, and will therefore tend to make the coherence length of the light very short. The physical meaning of a given standard deviation will be further investigated in chapter 4.

The auto-correlations function of an increasing number of emitters

Let us again look at the auto-correlation function of the pulse-signal, this time over a larger range of τ. Figure 3.9 shows the absolute value of $|g^1(\tau)|$ for light emitted from 10, 100, 1000, and 10000 atoms. Figure 3.10 shows the same graphs zoomed in on the central maximum. The auto-correlation function seems to have a less defined value. Even with as many as 1000 emitters, there is a structure higher than than the flat background but not belonging to the central peak. The width of the structure is of the same order as in the figures for 10 and 100 emitters, so it seems natural to assume that the structure stems from the shape of the original pulse. The value of the highest point of this structure is decreasing with an increasing number of emitters, until it is barely discernible when the number of emitters becomes very large. At the same time, the fluctuations of the background seem to increase, and comparing the two lowest frames in figure 3.9, it does not seem impossible that it reaches a constant level, and that this level is reached when the number of emitters become large enough for the pulse-structure to be indiscernible.

Examining the figures 3.8 and 3.10, it looks like the width of each of the small tops of the fluctuations in the background are of approximately the same width as the central maximum.

Figure 3.9 and 3.10 seem to contain more information than what we have seen contained in the auto-correlation function discussed in the literature. An experimental verification of the pattern shown in the figures would significantly strengthen the

[6]Strictly speaking, a *pulse* is *never* entirely monochromatic, since, according to the discussion of Fourier transforms in appendix A that would imply that the length of it is infinite, and it would no longer be a pulse. What we mean is that the wavelength "inside" the pulse is well-defined.

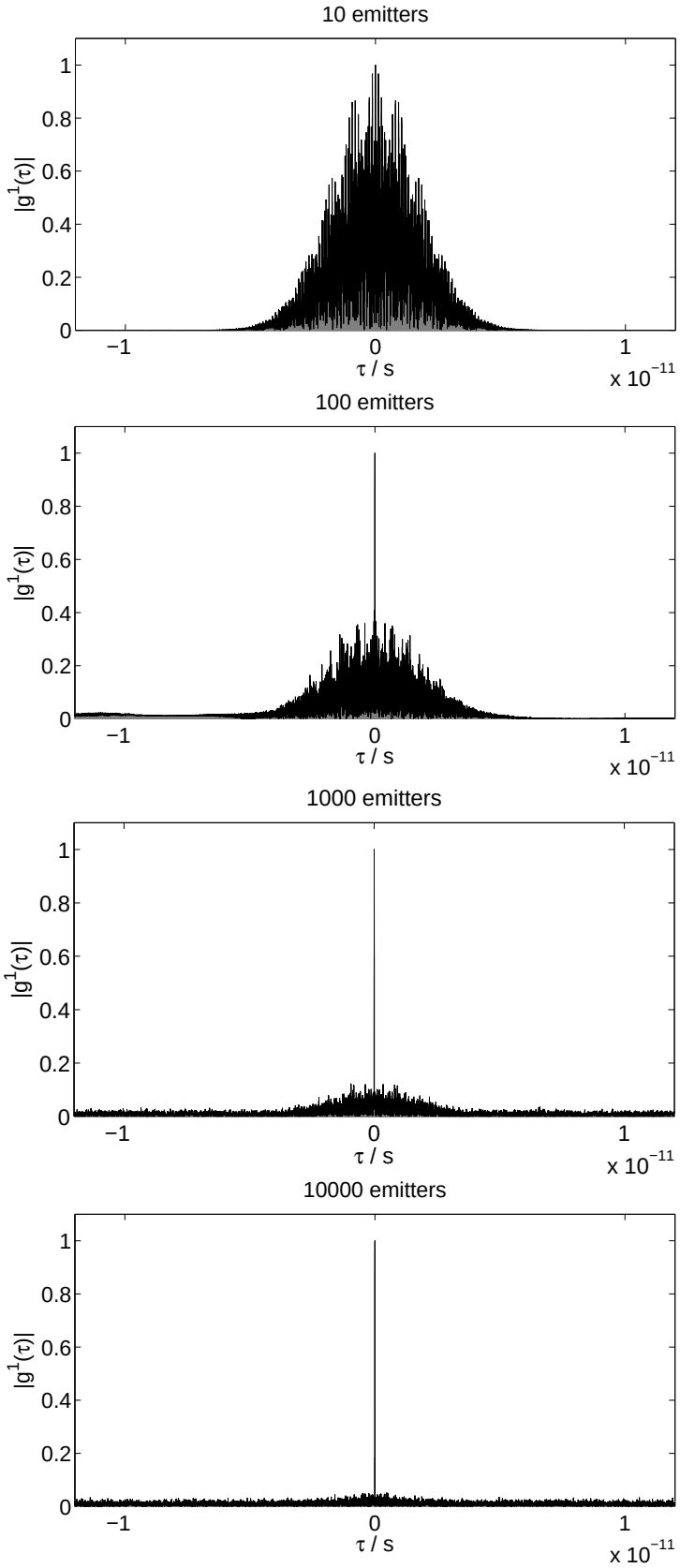

Figure 3.9: The absolute value of the first order auto-correlation function for 10, 100, 1000 and 10000 emitters.

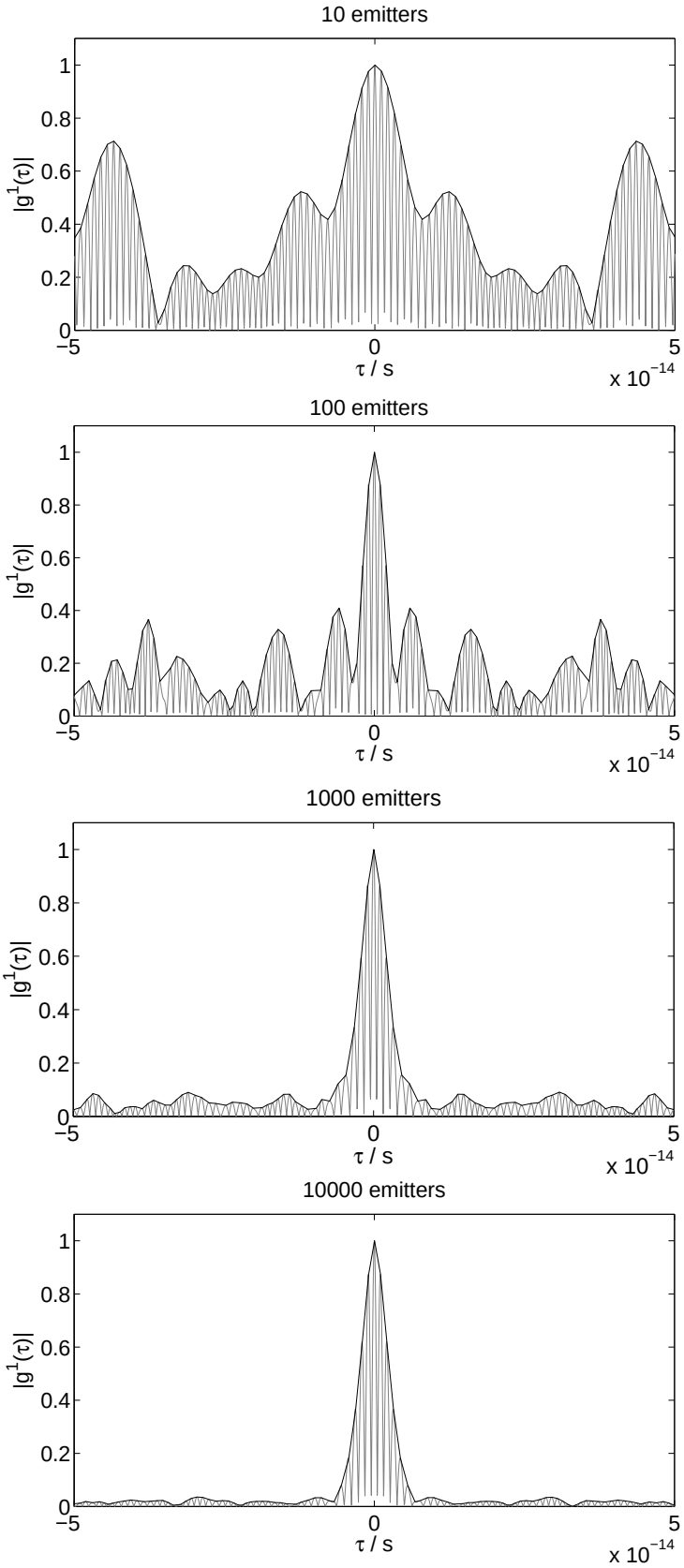

Figure 3.10: The absolute value of the first order auto-correlation function for 10, 100, 1000 and 10000 emitters, zoomed in on the central maximum.

pulse model of light emission[7] As shown on page 37, the first order auto-correlation function of a signal is equal in shape to the signal from a Michelson's interferometer, and measurements should in principle be possible.

A few words should be said on the attenuation of a beam of light down to very low intensities. One may perceive the attenuation of a beam in at least two ways.

1. The shape of the signal remains the same as when the intensity was higher, but the amplitude is scaled down gradually as the attenuation factor increases

2. Decreasing the intensity would cause the signal to become a superposition of fewer pulses, and it would therefore regain the pulse-like appearance we saw in figure 3.5.

The first option is closely related to a classical wave-description of light, the second favours a quantum description where the pulses emitted from atoms are indivisible photons. It is possible to argue that the method chosen to attenuate the beam would play a significant part. If the intensity of the light source itself is lowered, it seems natural that one would return to a pulse-like signal[8]. If, on the other hand, the light source is kept at a constant intensity and the beam is attenuated using a filter, both of the possibilities i and ii seems perceivable. Experimentally, a direct measurement of a beam at very low intensities is difficult, since it would require using a detector similar to our SPCM-detector which *by its nature* has single pulses as output (see chapter 5 for a discussion of the SPCM). Using the auto-correlation function instead of the raw signal, it may be possible to distinguish between the two.

In figure 3.9, the value of the maximum point of the pulse shaped background is decreasing with an increasing number of emitters. When the number of emitters becomes very large, this background is no longer visible. In figure 3.11 we have plotted the maximum value of the background as a function of the number of emitters[9]. The graphs seems to be decreasing towards a constant value. It seems natural that a function describing the graph in the figure would be a function of the number density, damping factor and wavelength of the pulses. In the figure, we have included a curve fit on the form $A = a/(n+b)$ where A is the amplitude of the graph at point n, and a and b are constants. A function on the form of a simple fraction was chosen from purely visual arguments, as it seemed to give a better fit than an exponentially or logarithmically decreasing function, or more complicated fractions of polynomials. Intuitively, in light of the arguments above, it seems as if

[7] Given, of course, that one is not able to find another model that predicts the same behaviour.

[8] It is implied that the energy of each pulse remains the same, so that the decrease of intensity is due to a lowering of the number of pulses emitted.

[9] The reader should be warned that the original code was meant simply to *visualize* the auto-correlation function, and consequently did not include a way of calculating any numerical values. The values in the graph are the maximum value of a Gaussian function that was visually fitted to the pules-structure. Accordingly, the values given are due to the (possibly large) correction factor of a human being that would like to be right.

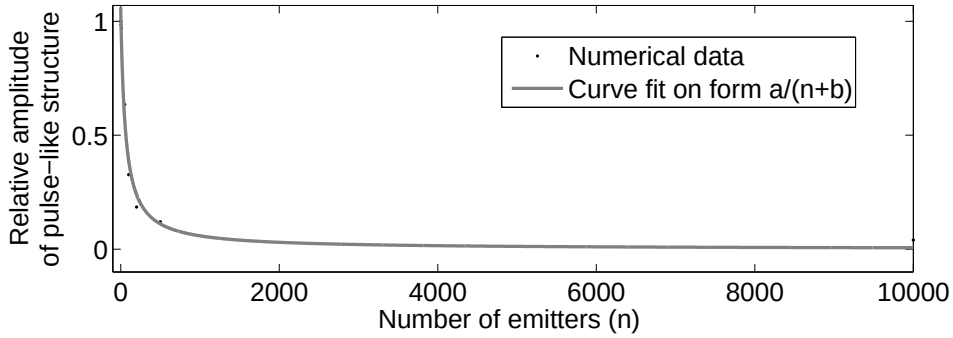

Figure 3.11: The maximum value of the background as a function of the total numbers of emitters.

a function on the form of a simple fraction would not be complete, since it does not take the flat background into account, but becomes equal to zero as the number of emitters, n, approaches infinity. A separate constant or slowly increasing term describing the background could be added to make up for this. Unfortunately, time did not allow us to make the necessary theoretical speculations or simulations to give other hints of the dependence on the factors suggested above.

Increasing the number of emitters, and therefore the intensity of the light corresponds to moving from the quantum mechanical to the classical domain. If the behaviour suggested in figure 3.11 is confirmed by experiment, the coherence length could be a measure of the extent to which a system belongs to the quantum of classical domain.

Pulse-shape

As described at the beginning of the chapter, the models we use are based on pulses with a *Gaussian* envelope. It would be interesting to repeat the analysis of the previous sides with different-shaped pulses. Two possibilities would be to choose a square envelope as in figure 3.12(a), or an exponentially decaying envelope as in figure 3.12(b). The second of these would perhaps be the more interesting for two reasons: 1) It is probably more physical than a box-shape, as it could be directly related to the quantum mechanical state function that we will find in chapter 4, and 2) we predicted in chapter 2 that the auto-correlation function is symmetric around $\tau = 0$. Using an un-symmetric pulse-shape would possibly show some interesting features. On the other hand, doing the simulations with simple pulse-shapes, such as a box, would allow us to investigate closer the shape of the pulse-structure of the auto-correlation. In that respect, the Gaussian envelope we chose is maybe a little too well-behaved for all details to emerge in the plot.

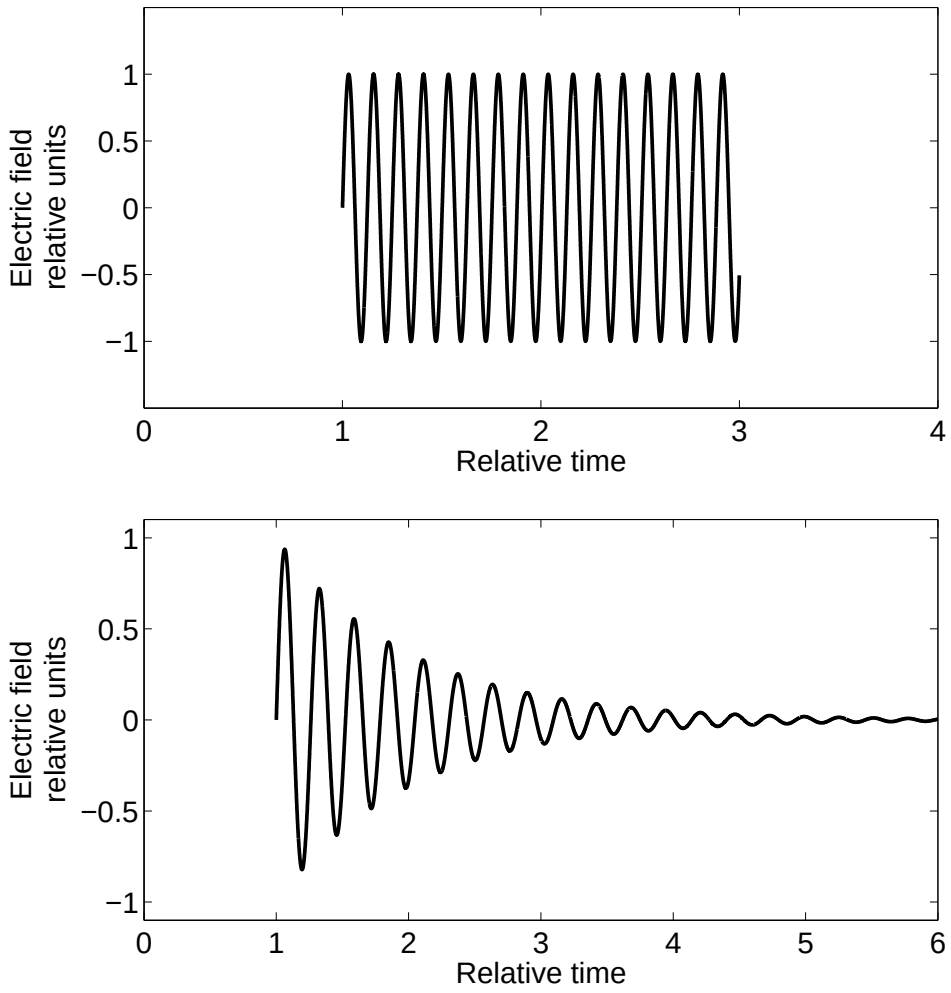

Figure 3.12: Possible interesting pulse-shapes for future simulations: (a) A square box, and (b) and exponentially decreasing function.

Problems with a common definition of coherence time

Some authors define coherence time to be [44]

$$\tau_c = \int_{-\infty}^{\infty} |g^{(1)}(\tau)|^2 d\tau. \tag{3.4}$$

This is a definition that works for functions that decrease to zero fast enough for equation (3.4) to be well defined. If, on the other hand the fluctuations appearing in our simulations should prove to be aspects of a physical reality, not only due to the limitations of numerical simulation, the integral in (3.4) will diverge. To resolve this problem, we see two possible solutions:

1. To redefine coherence time and length to include the width of the central

peak only, make a fit of the peak with a function $f(\tau)$ of which the integral $\tau_c = \int_{-\infty}^{\infty} |g^{(1)}(\tau)|^2 d\tau$ is well defined, and define this to be the true expression for the coherence time.

2. To introduce a cut-value τ_{cut} and redefine the coherence time to be

$$\tau_c = \int_{-\tau_{cut}}^{\tau_{cut}} |g^{(1)}(\tau)|^2 \, d\tau. \tag{3.5}$$

The first approach seems unsatisfactory in that it neglects some possibly important features of the auto-correlation function. Having to fit a graph with an almost freely chosen function also introduces an element of subjectivity into the definition, as the choice of function may not be obvious. By examining the uppermost graphs in the figures 3.9 and 3.10 it is also not obvious how to make such a fit for signals from very few emitters.

The second approach allows for the inclusion of features apart from the central maximum to be included in the definition of coherence length, given that one is able to make a sensible choice τ_{cut}. Using the wave-packet structure in figure 3.9 as a basis may open for a definition of τ_{cut} less arbitrary than what has hitherto been possible. One possibility is to define that:

> *The cut value τ_{cut} should be equal to the value of τ where the the envelope of pulse-structure is a factor κ_1 larger than the average value of the background when the number of emitters approaches infinity. If the top of the pulse structure is smaller than a factor κ_1 times the average of the background, τ_{cut} should be at the position of this first minimum after the central peak.*

A definition of τ_{cut} similar to the definition above would allow for inclusion of features of the auto-correlation function aside from the central maximum, and being well defined even for a signal with many fluctuations in the auto-correlation function.

Another possible way to define τ_{cut} would be to find the enveloping curve for some very few emitters, choose a cut value where the curve is equal to some κ_2, and keep that value of τ_{cut} constant regardless of the number of emitters. This definition would in practice probably be more time consuming, since it would require a knowledge of the auto-correlation function of a single or very few pulses.

On the other hand, it could well be argued that if we have already found a characteristic time τ_{cut} of a graph, then τ_{cut} *itself* could well be used as a definition of coherence time, and the integral in (3.5) would be superfluous.

Chapter 4

Components of the experimental setup

> *"There is another much stronger motive which fascinates the good scientist in connection with practical application, namely: to see that is works; to see that one has correctly understood nature"* (Werner Heisenberg in [21]).

As the choice of opening quote suggests, one of the author's fascinations with the natural sciences is nature's ability to be described in the language of mathematics, and the possibility to make predictions for practical application based on the rules of that language[1]. It was to a large part this fascination that motivated the present chapter.

4.1 Spectral lamps

The structure of the atom, and why an atomic element emits light of certain wavelengths

Examining the colors of light emitted from matter under certain conditions is an old and effective technique of identifying chemical elements. The wavelengths of the visible spectral lines of the hydrogen atom was mathematically described by Johann Balmer in 1885, and in the years that followed, descriptions of other lines in the non-visible part of the spectrum were added.

At the beginning of the 20^{th} century, Max Planck presented his idea of quantization of energy to explain the black-body spectrum, and shortly thereafter Albert Einstein suggested that the electromagnetic field itself is quantized into what is now known as *photons*. Experiments showing the photoelectric effect[2] were seen

[1] Whether she may be counted among the *good scientists* is a question subjective in nature that the author herself will not attempt to answer. The fascination, however, remains.

[2] The **photoelectric effect** is the phenomenon that electromagnetic radiation hitting a metal plate will cause electrons to loosen, and therefore create an electric current if and only if the

as hard proof of these particles of light[3].

In 1913 Bohr introduced his model of the atom in which he used Planck's idea of quantization of energy to explain the mechanism behind the observed wavelengths in the hydrogen spectrum. The idea was that the electron moves around the nucleus in circular orbits, the radius of which corresponds to a given energy. In the transition from a larger to a smaller radius, the atom loses energy which is emitted in the form of quanta of electromagnetic radiation.

Although a tremendous achievement and a great leap forward for theoretical physics, several steps in the derivation of Bohr's formula were highly questionable[4], the most fundamental of which was the way he used classical mechanics to find the stable energy levels. Nevertheless, the idea that the spectrum has something to do with the energy of the electrons in the atom was born [52].

Inspired by classical wave mechanics and Louis de Broglies idea that matter may be assigned a wavelength, Erwin Schrödinger invented a wave equation for quantum mechanics, the validity of which was proven through experiments [17].

Light can be emitted from or absorbed in an atom if the energy of the light corresponds to the energy difference between two of the atomic energy levels allowed by the Schrödinger equation.

$$i\hbar\frac{\partial\psi}{\partial t} = \left(-\frac{\hbar^2}{2m}\nabla^2 + V\right)\psi = E\psi, \tag{4.1}$$

where ψ is the state, V is the potential, m the mass, and E the energy of the system we are working with. For electrons belonging to an atom in a gas where the interactions between the separate atoms may be neglected, the potential can be assumed to be the total coulomb potential of the protons in the nucleus plus that of the other electrons. It is typically only the valence electrons of an atom that undergo optical transitions [44].

For atoms of chemical elements, the solutions to (4.1) are discrete. The light that is emitted from an atom can therefore have only certain wavelengths determined by the difference between the energy levels of the atom, as given by Planck's law:

$$\nu = \frac{\Delta E}{2\pi\hbar} = \frac{E_2 - E_1}{2\pi\hbar}, \tag{4.2}$$

quantity $2\pi\hbar\nu$ where ν is the frequency of the radiation is larger than the binding energy of the electron. A voltage V_0 may be set up in the other direction to prevent the current. This voltage is only dependent on the frequency, and not on the intensity of the light [52] (see also the discussion of equation (4.2)).

[3]Whether the photoelectric effect is *really* a proof of the particle nature of light has later been questioned. See for example the discussion of the effect in [22].

[4]That is, highly questionable to the *modern* physicist familiar to the rules of quantum mechanics.

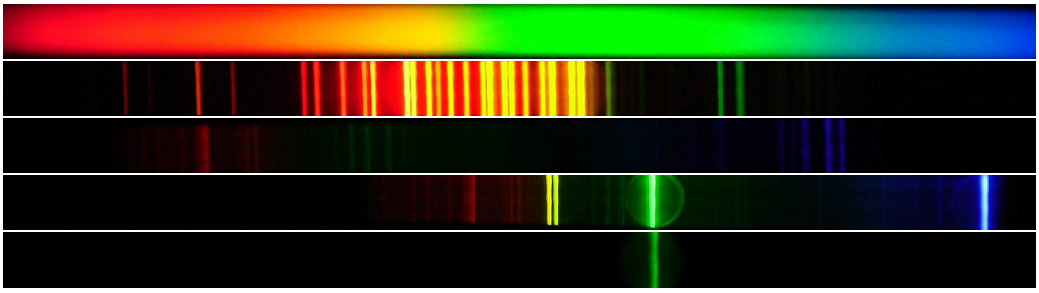

Figure 4.1: The spectra of our gas discharge lamps. From the top down: White light, neon, argon, mercury, and mercury lamp with interference filter (for a brief discussion on interference filters, see section 4.2). The camera settings were adjusted to give each separate picture the best possible quality. The relative intensities may therefore not be compared between two different photographs. The circle around the bright green line in the mercury spectra is a reflection of the lamp holder (photographs by author).

E_1 and E_2 being the energies of the higher and lower electron level. As a result of this, each element has a spectrum of possible wavelengths, something that is reflected in figure 4.1 for Neon, Argon and Mercury. The uppermost photograph in figure 4.1 shows the spectrum of white light.

4.1.1 Broadening mechanisms

From our discussion of the energy levels of the atom, one could think that the frequency of each spectral line of the emitted radiation would have a sharp value. This is not the case even in principle. The mechanisms that govern the spectral width of the intensity function of each line are called broadening mechanisms. It is common to distinguish between two main families of broadening mechanisms: Homogeneous broadening, that affect all the separate microscopic light sources (that is, all atoms) in the same way, and *in*homogeneous broadening due to actual differences between the light sources, and to the statistical properties of the collection of sources.

As we will see, homogeneous mechanisms give rise to a Lorentzian shaped intensity function, whereas inhomogeneously broadened lines of ideal gases are Gaussian [44].

Lifetime broadening

In the formalism of quantum mechanics, a physical state may be written as[5] $\psi(t) = \sum_n \psi_n(t)$, where the ψ_n's constitute a complete set of basis-vectors. A measurement of a property, or physical observable A of $\psi(t)$ may be described

[5]In anticipation of the calculation of natural linewidth, we have chosen *not* to normalize the ψ_n's to have length equal to unity.

through an operator $\hat{A}$ acting on the state. The Dynamics of $\psi(t)$ may be said to follow two main principles [8]:

1. The wavefunction $\psi(t)$ evolves *continuously* and *deterministically* according to the Schrödinger equation (equation (4.1)). The Schrödinger equation is linear so that if $\psi(t)$ and $\phi(t)$ are solutions, then $\alpha\psi(t)+\beta\phi(t)$, where α and β are constants, will also be a solution.

2. Upon a measurement, the state $\psi(t)$ is *discontinuously* reduced to some ψ'_n which is an eigenvector of the operator describing the measurement, and the measurement will return the corresponding eigenvalue a_n. The reduction is *stochastic*, not deterministic. The probability of obtaining a_n is equal to the absolute square of ψ_n; $P(a_n) = |\psi'_n|^2$.

According to the second dynamic principle of quantum mechanics, a measurement of a single quantum system will necessarily return one of the eigenvalues of the system, and the state will collapse to the corresponding eigenvector $\psi_n(t)$. It is therefore impossible to find the total original state $\psi(t)$ doing measurements on only one quantum system. Since after a measurement the state of the system will be changed, repeated measurements on the same system will be void[6].

Heisenberg's uncertainty principle of position and momentum states that

$$\Delta x \Delta p \geq \frac{\hbar}{2},$$

where $\Delta x = \sigma_x$ and $\Delta p = \sigma_p$ are the standard deviations of the data-set of multiple measurements or position and momentum on identical sets of quantum systems[7]. A similar uncertainty principle holds for time and energy:

$$\Delta t \Delta E \geq \frac{\hbar}{2}. \tag{4.3}$$

In this case, the interpretation that "Δ" really means the standard deviation of repeated measurements is problematic. *Time* is a running parameter, not a dynamical variable[8]. *There is no time-operator*, you simply cannot measure *the time* of a system! How then should we understand Δt?

[6] It is far beyond our aim to discuss the problem of the reality of the wavefunction. Whether this *collapse* of the wavefunction is something that happens within the state itself or only in our knowledge of the state, has been, and is still, a matter of dispute.

[7] Actually, in the standard interpretation of quantum mechanics, σ_A is the standard deviation of the quantum system *itself*. Quantum mechanics states that one cannot measure every property with arbitrarily good precision at the same time. This is closely related to the theory of Fourier transforms. The sets of position- and momentum eigenstates are Fourier pairs. If the position of a state is measured, the wavefunction will become a delta function in the position-state. According to table A.1, the wavefunction will then become a constant in momentum space, its standard deviation will become infinite, and we will not know anything about the momentum of the state. At this point, however, we have gotten dangerously close to breaking our promise of not discussing the reality of the physical meaning of $\psi(t)$.

[8] Assuming that we stay clear of relativistic quantum mechanics.

To answer that question, we will need to look at the other input in equation (4.3): ΔE. This is again a variable to which repeated measurements may be assigned a standard deviation. Now, some time t after a given atom of our spectral lamp has been exited, there is a given possibility that the atom will have already emitted a quantum of light. In the words of David J. Griffiths we may then say that: Δt *represents the amount of time it takes the expectation value of E to change by one standard deviation* [18]. From now on, in anticipation of what is about to be said, we will write τ instead of Δt. It should be mentioned that alternative approaches and formulations of the uncertainty relation of time and energy exist [18], [9].

Let A_{jk} denote the rate of transition due to spontaneous emission between two energy levels j and k. For historical reasons, A_{jk} is called the *Einstein coefficient* of the given transition [44]. The total transition rate from an energy level k is then the sum over the Einstein coefficients of transitions from k to all lower energy levels:

$$R_k = \sum_j A_{jk}.$$

Tables of the Einstein coefficients for various elements, along with other properties of various atoms, may be found in for example the web-pages of the National Institute of Standards and Technologies [34].

The τ that we have just defined and defended is often referred to as the *lifetime* of a given energy level and it is therefore the inverse of the rate:

$$\tau = R_k^{-1} = \left(\sum_j A_{jk} \right)^{-1}.$$

The uncertainty of energy level k may then be rewritten

$$\Delta E_k = \frac{\hbar}{2\tau} = \frac{\hbar}{2} R_k = \frac{\hbar}{2} \left(\sum_j A_{jk} \right).$$

The uncertainty of the difference in energy between the two levels that take part in the transition of the electron is equal to the sum of the uncertainties of each energy level

$$\Delta E_{jk} = \Delta E_k + \Delta E_j.$$

Using Planck's law (equation (4.2)) and Heisenberg uncertainty relation this gives the uncertainty of the frequency of the radiation emitted[9]:

$$\Delta \nu_H \geq \frac{1}{4\pi}(R_j + R_k) \equiv \frac{1}{4\pi} R.$$

[9]We have added a subscript H on the frequency to remind the reader that we are talking about the natural linewidth that stems from Heisenberg's uncertainty principle.

Imagine looking at a sample of atoms, with $N_k(t)$ of them being in the excited state k at time t. The speed with which the number of excited electrons decreases is proportional to the number of atoms still in the excited state, and with the rate of photon emission from an atom:

$$\frac{dN_k}{dt'} = -RN_k.$$

Integrating from time $t' = 0$ to $t' = t$, we find

$$\int_{N_0}^{N_k(t)} \frac{dN_k}{N_k} = -R \int_0^t dt'.$$

where $N_0 = N_k(t' = 0)$. After integrating we find

$$N_k(t) = N_0 e^{-Rt}.$$

So that at a time t, $N_0 e^{-Rt}$ atoms will be found in the excited state. The probability to find a given atom in the excited state at time t after we *know* that it was in the excited state will then be

$$P_k(t) = e^{-Rt}.$$

The probability that a quantum mechanical system is in a certain state, is equal to the absolute square of that state:

$$P_k(t) = |\psi_k(t)|^2 \quad \Rightarrow \quad \psi_k(t) = e^{-\frac{R}{2}t}.$$

From the discussion above, and from appendix A, we know that the state as a function of frequency is the Fourier transform of this. Looking up in table A.1, we find that:

$$\psi_k(t) \; = \; e^{-\frac{Rt}{2}} \quad \rightleftharpoons \quad \frac{i}{2\pi(\nu - \nu_0) + i\frac{R}{2}} \; = \; \psi_k(\nu), \tag{4.4}$$

where $\psi(\nu)$ is the state written out in the frequency domain.

The probability that the atom will send out light of frequency ν is then

$$P_k(\nu) = |\psi_k(\nu)|^2 = \left| \frac{i}{2\pi(\nu - \nu_0) + i\frac{R}{2}} \right|^2 = \frac{1}{4\pi^2(\nu - \nu_0)^2 + \left(\frac{R}{2}\right)^2}. \tag{4.5}$$

Making the variable shift $\nu \rightarrow \nu' = \nu + \nu_0$ will not make any difference since $d/d\nu = d/d\nu'$, and since the Fourier integral is taken over the interval from $-\infty$ to $+\infty$.

In a collection of many atoms, the intensity of the emitted light is proportional to the probability that a single atom will emit light. The intensity as a function of frequency for a collection of atoms will then be:

$$I(\nu) = I_0 \frac{1}{4(\nu - \nu_0)^2 + \left(\frac{R}{2\pi}\right)^2},$$

where we have pulled a factor of $1/\pi$ from equation (4.5) into I_0. The expression on the right hand side of equation (4.4) is the Lorentzian curve that we saw in chapter 2, with $\Delta\nu_{FWHM} = R/2\pi$, and it is the shape we expect from a single, stationary light source [7].

The above use of quantum mechanics may be said to be questionable, since we are doing calculations on the de-excitation of single atoms while at the same time, we expressly say that there are several atoms in the gas, and use this to find the probability function. One may think of the above calculation as valid in the limit of an infinitely diluted ideal gas, so that the radiation from one atom may not excite another. In the next two sections, we will look at the more probable and not-so-ideal case, with a gas of interacting atoms, and where the statistical properties of the gas come into play.

Collision broadening

When there is more than one particle in a volume, there is a finite possibility that the particles will collide. This possibility increases with the number and speed of the particles. Using statistical quantities for a gas of many particles, this corresponds to the collision rate increasing with increasing temperature and pressure.

Each time an excited atom undergoes collision, it may gain or lose energy. The total transition rate will therefore be higher than the rate one gets from Heisenberg's uncertainty relation only:

$$R = R_{total} = R_{collision} + R_{Heisenberg}.$$

The mathematics of finding the lineshape has not changed, so the spectral line will still have a Lorentzian shape. It will, however, be broadened since the numeric value of the rate will be higher.

Since the rate now is a function of the pressure of the gas, $R = R(p)$, the broadening due to collisions between the atoms is often referred to as *pressure broadening* [6]. Lifetime- and collision broadening are the two most important contributions to the homogeneous broadening of a spectral line. In a gas and under normal conditions, collision broadening will often give the greater contribution of the two [35].

Doppler broadening

In addition to the spread in frequency due to the physics of the individual atoms, the statistics of a collection of these will also give a contribution to the total linewidth. As mentioned above, the broadening coming from statistical differences between light sources is called *in*homogeneous. The most significant inhomogeneous effect comes from the Doppler shift due to the motion of the atoms in the gas [35].

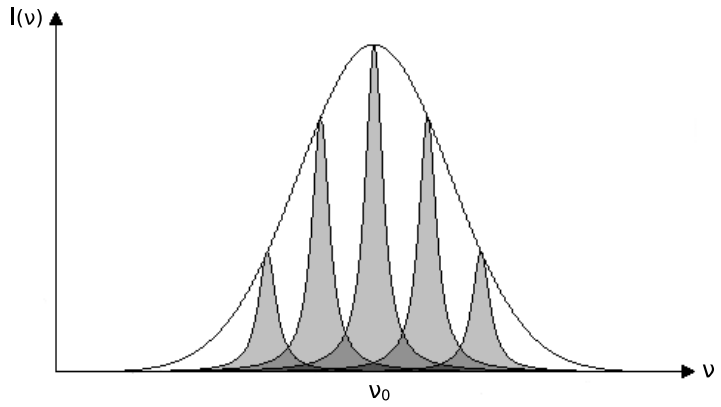

Figure 4.2: If the homogeneous broadening is much less than the inhomogeneous, and the number of light sources approaches infinity, the total broadening of the spectral line will be approximately Gaussian. Note that in the figure, only the peaks of five different ν have been drawn. (figure is self-made, but strongly inspired by [44]).

A light source at rest will emit light of frequency ν_0. If the source is moving with respect to the observer, the observed frequency will be shifted with an amount $\pm(v_z/c)\nu_0$, where v_z is the speed of light parallel to the direction of observation. Assuming our gas to be ideal, that is with no forces at work between the individual particles, the probability distribution of the velocity of one particle is proportional to the Boltzmann factor

$$P(\mathbf{v}) \propto e^{-m\mathbf{v}^2/2kT}, \tag{4.6}$$

where $\mathbf{v}$ is the velocity vector, m the mass of the particles, k the Boltzmann constant and T the temperature of the gas. The distribution of each directional component of the velocity vector follow the same distribution[10] as in (4.6) ([40], [45]). Since the frequency shift is a linear function of v_z, the probability distribution of frequencies will also be Gaussian, centered about ν_0.

If the spectral line from each photon were infinitesimally thin[11], the lineshape function would become Gaussian as the number of light-emitting atoms approached infinity. If the spread in frequency due to the homogeneous broadening is much smaller than that due to *in*homogeneous broadening $\Delta\nu_{hom} << \Delta\nu_{inhom}$, this is still to a good approximation true, as in figure 4.2. In real life, however, the total line shape will be somewhere between a pure Lorenzian and a pure Gaussian [44].

Recall our discussion of figure 3.8, where the standard deviation of the wavelength of electromagnetic pulses were discussed. We may now recognize one physical realization of that standard deviation as due to Doppler shift and the velocity distribution of our microscopic light sources.

[10] This is seen by writing $\mathbf{v}^2 = v_x^2 + v_y^2 + v_z^2$ and integrating over all v_x and v_y.
[11] That is, if there were no natural or homogeneous broadening

Choosing which lines to use

The spectral lines used in the experiments were chosen based on a set of criteria:

1. The line had to be part of an atomic spectra of an element in easily available commercial lamps. Effectively, this narrowed the choice down to five elements: Mercury (Hg), neon (Ne), argon (Ar), krypton (Kr), and Xenon (Xe).

2. The spectral lines should be within the range of good detection efficiency for our detector. The detection efficiency of our detection device as a function of the wavelength is shown in figure 5.21 under the discussion of the detectors in chapter 5. We thus only considered wavelengths between approximately 500-900 nm.

3. To facilitate filtering and avoid signals coming from other lines, the lines being used should be intensive, and there should not be other intensive lines too close.

4. Choosing lines with very different FWHM-width would be desirable to test the theory for a wide range of parameters. However, this had to yield to the more important requirements of points 1 through 3. In addition, the technical information from the manufacturer was very limited, and values for the spectral widths could not be obtained prior to the purchase. Although not ideal, testing sources of similar widths would still be a strong test of the theory, which predicts a coherence length nearly independent of the value of the central frequency.

The *Oriel Pencil Style Calibration Lamps* from Newport [29] seemed to be a convenient choice of light sources. Comparing data from [29] and [34] three spectral lines were decided upon:

$$\begin{aligned} &\text{Hg} : 546.1 \text{ nm}, \\ &\text{Ne} : 692.9 \text{ nm}, \\ &\text{Ar} : 696.5 \text{ nm}. \end{aligned}$$

The spectral lines will in the future be referred to as Hg546, Ar696, and Ne692.

4.2 Fabry-Perot interferometer and interference filter

An interference filter is a bandpass filter based on the principles of the Fabry-Perot interferometer. This type of interferometer consists of two almost perfect reflectors separated by a layer of transparent material of distance d, see figure 4.3. The transparent middle layer is called a *spacer*. Most of the light that enters the interferometer will be reflected back and forth between the two reflectors, and

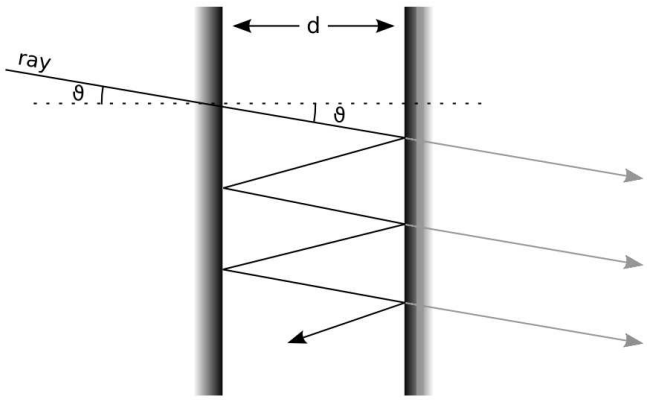

Figure 4.3: Fabry-Perot interferometer.

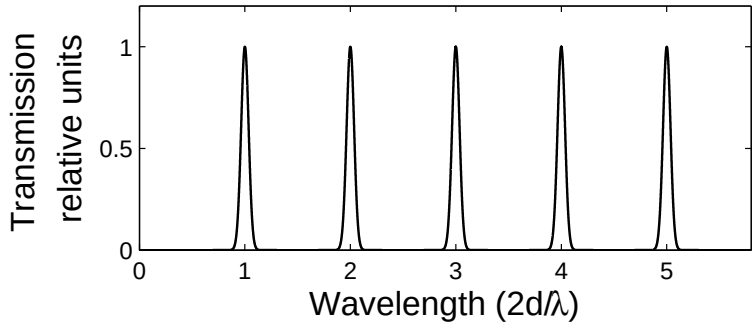

Figure 4.4: If the light rays hit the interferometer normal to the reflective surfaces, only bands of wavelengths sharply peaked around a Central wavelength whose value is an integer of twice the distance between the reflectors will be able to escape from the interferometer.

interference between the waves will be overall destructive for all wavelengths significantly different from twice the distance that the ray travels between the two reflectors divided by an integer n, that is, for wavelengths far from $2d/n \cos\theta$, see figure 4.3. In the following, we will assume that the beam of light is normal to the plane of the interference filter, so that $\cos\theta = 1$. Alternatively, one may look at the total electric field as analogous to a standing electromagnetic wave between two perfect conductors. On a perfect conductor, the electric field has to be zero. Therefore, between such two, only standing waves with nodes on the conductors will survive, and as a consequence, there will only be waves with wavelengths of $2d/n$, in the cavity, with n being an integer. Only a small fraction of the light will be able to escape through the reflectors.

Each of the reflective mirrors in an interference filter are stacks of several layers of materials of alternating high and low refractive indices. The spacer is also a thin film of thickness of one half of the wavelength one wants to transmit [11]. A system of two reflective stacks and a spacer film is commonly referred to as a cavity.

A filter typically consists of up to eight such cavities, and in addition has layers of film to block unwanted frequencies further from the desired frequency band [3]. That is, to ensure that only frequencies within one of the peaks of figure 4.4 are transmitted through the filter. The higher the number of cavities within a filter, the sharper is the cutoff of the bandwidth transmitted.

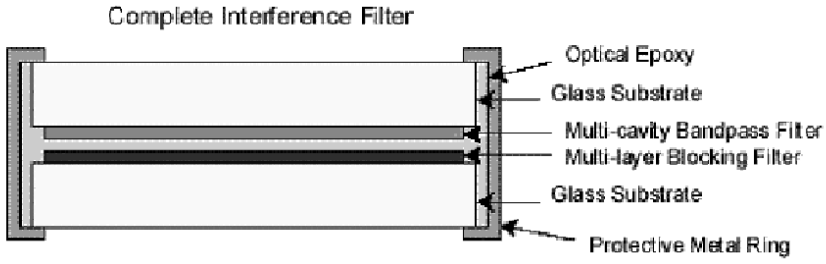

Figure 4.5: Structure of an optical interference filter. Figure from C& L Instruments [11].

4.3 Optic fibers

The physics behind optic fibers

The propagation of light in an optic fiber is based on the principle of total reflection, which can be deduced from Snell's Law of refraction:

$$n_1 \sin\theta_1 = n_2 \sin\theta_2, \tag{4.7}$$

where, as in equation (1.1), n_1 and n_2 are the refractive indices of the incoming and outgoing medium respectively, and $\sin\theta_1$ and $\sin\theta_2$ are the incoming and outgoing

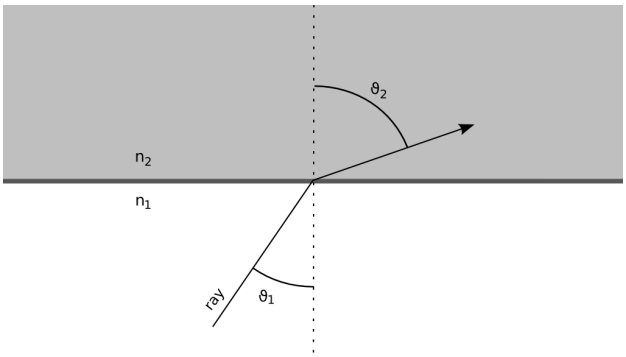

Figure 4.6: Diffraction of light ray between to transparent media of different refractive indices

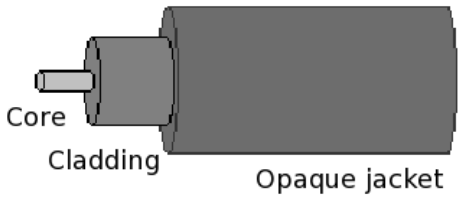

Figure 4.7: A typical optic fiber consists of a thin core with a thicker cladding, and a non-transparent jacket

angles with respect to the normal of the surface between the two media [15].

The angle θ_2 has its maximum value at $\pi/2$, which gives $\sin\theta_2 = \sin\pi/2 = 1$. For a given set of n_1 and n_2, this also gives the maximum value θ_1 can have before all the light is reflected back into the incoming media. We define the critical angle to be the incoming angle for which $\sin\theta_2 = 1$. From equation (4.7) it then follows that

$$\theta_c = \sin^{-1}\left(\frac{n_2}{n_1}\right). \tag{4.8}$$

An optic fiber consists of a thin transparent core with refractive index n_1, and a cladding of a slightly smaller refractive index n_2. Often a fiber or a bundle of fibers will also be covered by a layer of rubber called a jacket for further protection and easier handling of the fiber [15].

Since we also have diffraction in the surface at each end of the fiber, θ_c will in general differ from the angle at which the light enters the fiber, as indicated in figure 4.8. The sine of the critical angle of the fiber is

$$\sin\theta_c = \frac{n_2}{n_1}, \tag{4.9}$$

and from using Snell's Law (equation (4.7)) on the surface where the light enters

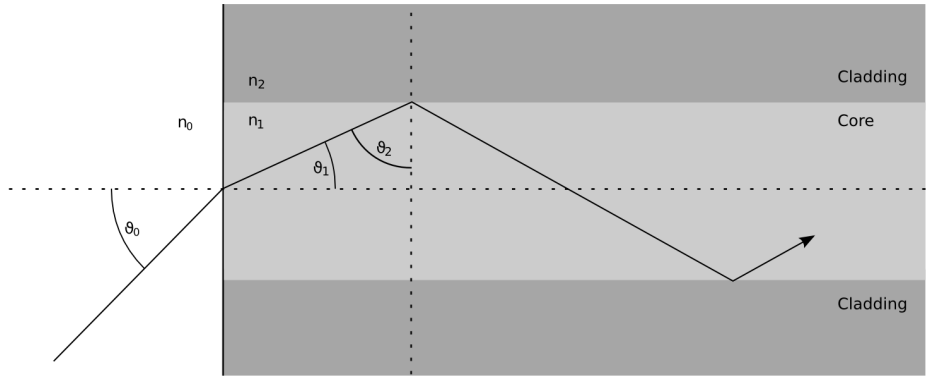

Figure 4.8: The concept of numerical aperture comes from the fact that the light ray is bent according to Snell's law when entering the fiber.

the fiber we find

$$n_{air} \sin\alpha = n_1 \sin\left(\frac{\pi}{2} - \theta_c\right) = n_1 \cos\theta_c = n_1\sqrt{1 - \sin^2\theta_c}.$$

Together with using $n_{air} = 1$, this gives[12]

$$\sin\alpha = \sqrt{n_1^2 - n_2^2}.$$

The expression $\sin\alpha$ is commonly referred to as "numerical aperture" and is, as follows from the discussion above, a limit on the maximum angle a ray entering the fiber can have with respect to the fiber axis and still undergo total reflection. In other words, it describes the light-gathering capacity of the fiber [44].

Single-mode vs. mulitmode fibers

As we saw in chapter 1, much information is lost in picturing light as propagating as single rays through a fiber. Our light sources do not emit light of infinitely thin rays. Instead, one has to consider a beam that varies in width as the light propagates. The cross section of the beam will have a certain intensity profile, which depends upon the source and the optical path of the light.

A beam of light can be described as a sum of different modes of electromagnetic radiation. A multimode fiber is one that lets several modes pass, while a single mode fiber only lets one or very few modes pass through. The physical difference between a multimode and a single mode fiber is the radius of the core. To explain why this is, and to make more clear the concept of a mode of light, we will in the following deduce the intensity of a cross-section of the beam as a function of distance from the center of the fiber. The following discussion follows the line of thought of [15] and [44].

[12] The refractive index of air is actually about $n_{air} = 1.00029$ [26].

Earlier we found that all allowed electromagnetic waves have to satisfy the wave equation[13]

$$\nabla^2 u = \frac{1}{c^2}\frac{\partial^2 u}{\partial t^2}. \tag{4.10}$$

where u is any of the six components of the electric or magnetic field, and $c = \sqrt{1/\epsilon\nu}$ is the speed of light in the fiber. Since the fiber is essentially a very long and very thin cylinder of a circular cross section, we will do the mathematics in cylindrical coordinates (the conversion from Cartesian coordinates is straight forward, but tedious, so we looked it up in [42]). Equation (4.10) then becomes

$$\frac{\partial^2 u}{\partial r^2} + \frac{1}{r}\frac{\partial u}{\partial r} + \frac{1}{r^2}\frac{\partial^2 u}{\partial \phi^2} + \frac{\partial^2 u}{\partial z^2} = \frac{1}{c^2}\frac{\partial^2 u}{\partial t^2}. \tag{4.11}$$

The z-axis is the axis of propagation, r and θ define the distance to the center of the fiber and the position angle in the cross-section of the fiber. We use the fact that u must be periodic with respect to ϕ so that $u(\phi) = u(\phi + 2\pi)$. Let us assume that $u(r, \phi, z, t)$ is separable and can be written in the form

$$u = u(r, \phi, z, t) = u(r)u(\phi)u(z, t) = u(r)e^{-ip\phi}e^{-i(k_z z - 2\pi\nu t)},$$

where p is an integer and $k_z = k \cdot \hat{z}$ is the z-component of the wave vector. Putting this into equation (4.11) leaves

$$\frac{\partial^2 u(r)}{\partial r^2} + \frac{1}{r}\frac{\partial u(r)}{\partial r} + \left(q_n^2 - \frac{p^2}{r^2}\right)u(r) = 0, \tag{4.12}$$

where

$$q_n^2 \equiv (2\pi\nu)^2/c^2 - k_z^2 = k_{vac}^2 n^2 - k_z^2. \tag{4.13}$$

The quantity $k_{vac} = 2\pi/\lambda$ is the wavenumber in vacuum, and k_z the z-component of the wavevector in the fiber.

The solution to equations on the form of (4.12) are in the family of Bessel functions in the variable qr [4].

For the solutions to make physical sense, we require all field values to go to zero as r approaches infinity, and that they be finite at $r = 0$, that is

$$\lim_{r\to\infty} u(r) = 0 \qquad \text{and} \qquad u(0) < \infty.$$

These requirements are fulfilled if

$$u(r) = A_p \mathcal{J}_p(q_n r) \qquad \text{for } r < a, \text{and}$$
$$u(r) = B_p \mathcal{K}_p(q_n r) \qquad \text{for } r > a$$

[13]The assumptions of a linear, dielectric and isotropic media of no currents and free charges are all satisfied for an optic fiber.

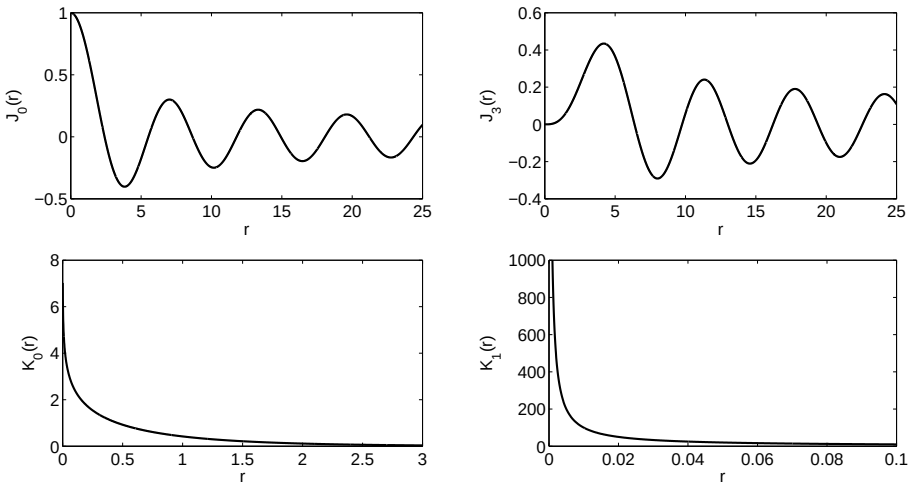

Figure 4.9: The Bessel-functions as function of radius. The upper two figures are the Bessel-functions of the first kind, $J(r)$, of the zeroth and third order. The lower two are the modified Bessel-functions of the second kind, $K(r)$ of the zeroth and first order. Since the upper two oscillate they cannot be the solutions to the field propagating along the fiber as $r \to \infty$. Similarly, the lower two become infinite at $r = 0$, and therefore cannot be solutions in the core of the fiber.

where a is the radius of the core of the fiber, A_p and B_p are constants, $\mathcal{J}_p$ is the Bessel function of the first kind, and $\mathcal{K}_p$ is the modified Bessel function of the second kind. Further descriptions of the Bessel solutions can be found in for example [4], [41]. In figure 4.9 we have plotted examples of the Bessel functions of the first and second kind for illustrating the argument above.

Let us have a closer look at the quantity q. Recall from a few pages back that for light to undergo total reflection, the minimum angle θ the wavefront normal may have with respect to the normal of the boundary between the core and the cladder is the critical angle, θ_c. The z-component of the wave vector will be proportional to the sine of θ:

$$k_z = |\mathbf{k}| \sin\theta = n_1 k_{vac} \sin\theta. \tag{4.14}$$

Since $\theta_c < \theta$, we must also have $\sin\theta_c < \sin\theta$, which, using equation (4.9) means that $n_2/n_1 < \sin\theta < 1$. Equation (4.14) then gives

$$n_2 k_{vac} < k_z < n_1 k_{vac}. \tag{4.15}$$

Plotting the limits of k_z into equation (4.13) we find that q_n^2 will be negative for $r < a$. To avoid imaginary quantities, we define

$$\begin{aligned} q^2 &= q_n^2 \qquad && \text{for } r < a, \text{ and} \\ q'^2 &= -q_n^2 \qquad && \text{for } r > a. \end{aligned}$$

Note that with this definition, the quantity $q^2 + q'^2 = (k_{vac}^2 n_1^2 - k_z^2) + (k_z^2 - k_{vac}^2 n_2^2) = k_{vac}^2(n_1^2 + n_2^2)$ is a constant independent of the incoming angle, and proportional

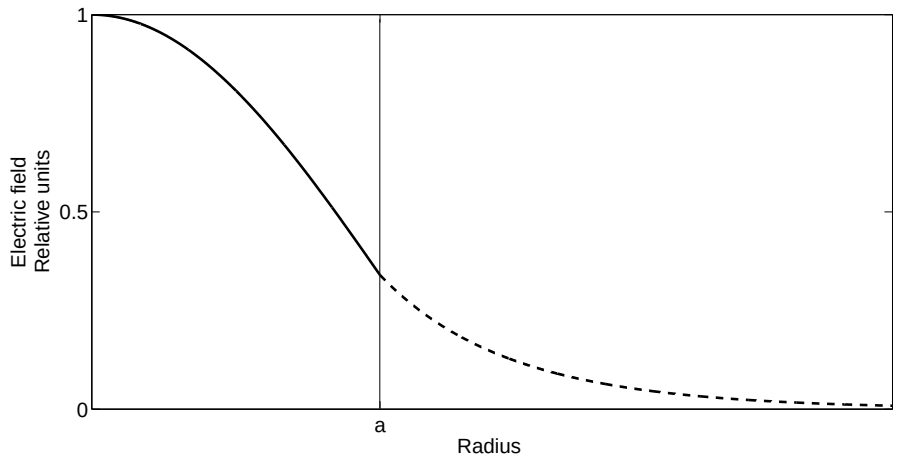

Figure 4.10: The electric field in a fiber is proportional to $J(qr)$ for $r < a$ and to $K(qr)$ for $r > a$.

to the numerical aperture found earlier.

Continuity demands that

$$A_p \mathcal{J}_p(qa) = B_p \mathcal{K}_p(q'a). \tag{4.16}$$

Generally, in an optic fiber, the refractive index of the cladding is only slightly smaller than that of the core. In this limit, the bending of the light ray will be so small that we can also require continuity of the derivative of $u(r)$ at $r = a$:

$$\left[A_p \frac{\partial J_p(qr)}{\partial r} \right]_a = \left[B_p \frac{\partial K_p(q'r)}{\partial r} \right]_a .$$

The derivative of $J_p(qr)$ is

$$\frac{d}{dr} \left[J_p(qr) \right] = \frac{p}{qr} J_p(r) - q J_{p+1}(qr), \tag{4.17}$$

and the same expression is valid also for $K_p(qr)$ [4]. We then find

$$qa \frac{\mathcal{J}_{p+1}(qa)}{\mathcal{J}_p(qa)} = q'a \frac{\mathcal{K}_{p+1}(q'a)}{\mathcal{K}_p(q'a)}. \tag{4.18}$$

Perhaps the easiest way to solve equation (4.18) is to plot the right- and left hand side together, remembering that $(qa)^2 + (q'a)^2 = k_{vac}^2 a^2 (n_1^2 + n_2^2)$. First, let us look at a plot choosing the value $k_{vac} a \sqrt{n_1^2 + n_2^2} = 10$. In figure 4.11, the discontinuous solid line is the left hand side of equation (4.18). The dotted line for the right hand side crosses it at several points, goes to zero at $qa = 10$ and then disappears. This makes sense if one compares to equation (4.18). At $qa = k_{vac} a \sqrt{(n_1^2 + n_2^2)}$,

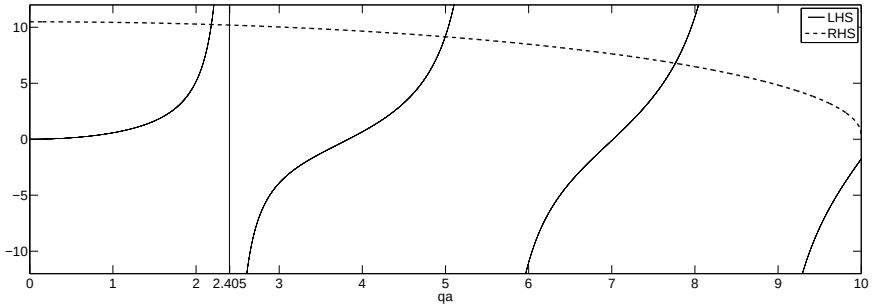

Figure 4.11: Plot of the characteristic equation for an optic fiber with $k_{vac}a\sqrt{(n_1^2+n_2^2)} = 10$. $LHS = qa\frac{\mathcal{J}_{p+1}(qa)}{\mathcal{J}_p(qa)}$ and $RHS = q'a\frac{\mathcal{K}_{p+1}(q'a)}{\mathcal{K}_p(q'a)}$, where $(qa)^2 + (q'a)^2 = k_{vac}^2a^2(n_2^2 - n_1^2)$.

the right hand side of (4.18) becomes imaginary. Physically, this corresponds to equation (4.15) no longer being valid, so that the propagating field no longer is bound to the core of the fiber, and light will be lost through the cladder and jacket of the fiber.

Each time there is an intersection between the two graphs in figure 4.11, one more mode may propagate through the fiber. To allow for only *one* mode, $k_{vac}a\sqrt{(n_1^2+n_2^2)}$ has to be small enough for the graphs to intersect only once. In other words, it must cut before the first discontinuity of the solid graph, which can be found to be at $qa = k_{vac}a\sqrt{(n_1^2+n_2^2)} = 2.405$ [44], [15]. Solving this for a, we find that a fiber is a single mode fiber if its radius a obeys:

$$a < 2.405\frac{\lambda}{2\pi\sqrt{n_2^2 - n_1^2}}.$$

Using the values given for our fiber by the manufacturer, $a = 1.65$ μm, $\lambda_{nominal} =$ 515 nm and $NA = \sqrt{n_2^2 - n_1^2} = 0.12$ [48], we find

$$k_{vac}aNA = \frac{2\pi}{515\ nm} \times 1650\ nm \times 0.12 = 2.416, \tag{4.19}$$

in good agreement with the theoretical value of 2.405. The small disagreement may be due to the fact that the value given for a is actually a calculated radius of the mode field where it has decreased to $1/e^2$ of the central value [48]. We are assuming that it is close to the actual radius of the core. The disagreement may also come from the fact that we have used a very simple model to describe the principle of a single mode fiber, where the refractive indices of both the core and the cladding, n_1 and n_2 take on constant values. In reality, graded index fibers are often used, where the refractive index has a higher value for small r than for large. The refractive index becomes constant at some $r = a$, defining the border between the core and the cladding of the fiber. One then has to solve equation (4.12) with $n = n(r)$, a task much more complicated than our calculations above [15], [44]. Our

simple model serves its purpose of explaining the physics behind single mode fibers.

After having gone through the theoretical work of explaining single mode fibers, not to mention the *experimental* work of effectively sending light through a fiber, let us at last say a few words on *why* this component is so essential.

In chapter 1 we derived a simple system of using ABCD-parameters to describe the propagation of a Gaussian beam. In addition, in appendix A, we explain the idea behind Fourier transform, and we argued that any function may be written as a sum of harmonic functions since these constitute a complete set. That argument may be generalized to higher dimensions. In our case: Any wavefront may be described as a sum of planar waves. The effect of an optical component on a planar wave is often easier to describe than its effect on a beam of random shape. Especially, a focusing lens will focus each planar wave to a point[14]. The lens therefor changes the beam to its Fourier partner[15] [44], [20]. We also show in appendix A that the Fourier transform of a Gaussian beam is also Gaussian. Effectively, this means that a Gaussian beam will remain Gaussian through an optical system as long as one does not directly divide the beam. In figure 4.12 we have plotted the zeroth order Bessel-function of the first kind together with a Gaussian. For small r, that is, in the core of the fiber, the first mode of the light able to propagate is *very nearly Gaussian*. The purpose of the fiber is in other words to shape the beam into something over which we have nearly complete control, the geometry of the beam on the outgoing side of the fiber will be the same regardless of the geometry on the incoming side. A very convenient side-effect is also that the fiber allows for a greater freedom in the arrangement of the experimental setup as the outgoing side may be moved around freely without having to adjusting the component of the experimental setup on the outgoing side of the fiber.

[14] As we saw in chapter 1 the planar wave is not actually focused to a point as that would imply $W_0 = 0$, which is impossible according to equation (1.12), but to an area much smaller than the area of the original planar wave.

[15] This implies that beams of light may actually be used to find the Fourier partner of ugly functions [44].

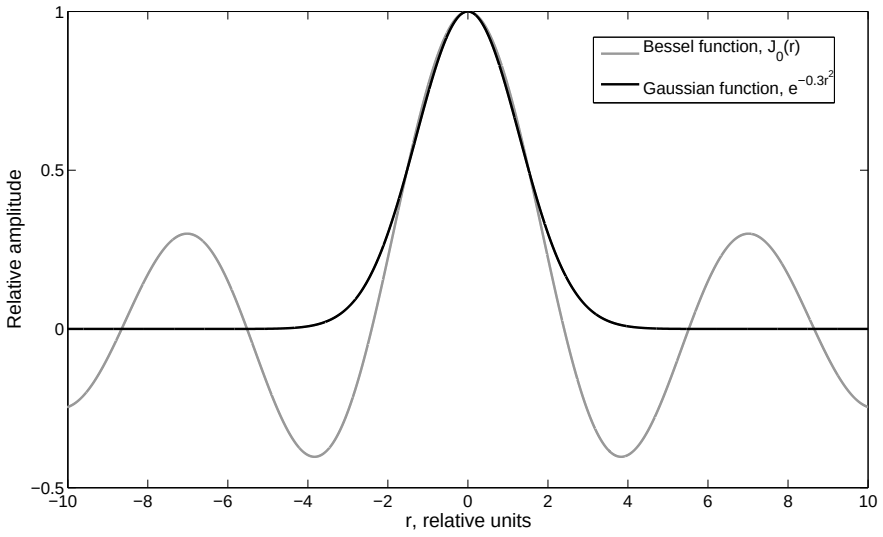

Figure 4.12: For small r, the first mode of the Bessel function of the first kind is very nearly Gaussian.

Chapter 5

Experimental setup and methods

In the present chapter we will give brief outlines of the two most important experiments that were attempted: Measurements of the spectral line width and of the coherence length of the light sources. Several smaller experiments were needed to determine the behaviour of the specific pieces of equipment used, and these have been included together with technical data and tips and procedures in laboratory work.

5.1 Measuring the spectral line widths of light sources

As may be inferred from chapter 2 and 4, any light source will have a finite, non-zero spectral linewidth. As there was no data available on the linewidth of our light sources, we wanted to determine these experimentally. To find out if these measurements were possible to carry out, we used the experimental setup shown in figure 5.1. The light was collimated into a single mode optic fiber. On the outgoing side we increased the distance between the fiber and the collimator lens[1] so that the beam width increased to fit to the area of the concave mirror. Recall from the description of the ABCD-parameters in chapter 1 that two optical system with identical final ABCD-parameter will have identical impacts on a beam. Recall also from table 1.1 that a focusing lens of focal length f has the same ABCD-parameters as a concave mirror of radius of curvature $R = -2f$. The setup depicted in figure 5.2 is therefore equivalent to the actual setup in figure 5.1.

A diffraction grating will diffract light of wavelength λ in a direction α according to the equation

$$d \sin \alpha = m\lambda, \tag{5.1}$$

where d is the center-to-center distance between adjacent slits in the grating, and m is an integer. As implied by equation (5.1) one will find several images of the same spectral line after the grating, one in each direction α corresponding to a different value of m. The image found in the direction $\alpha(m = 1)$ is called the *first*

[1] See description of collimators in section 5.2.2.

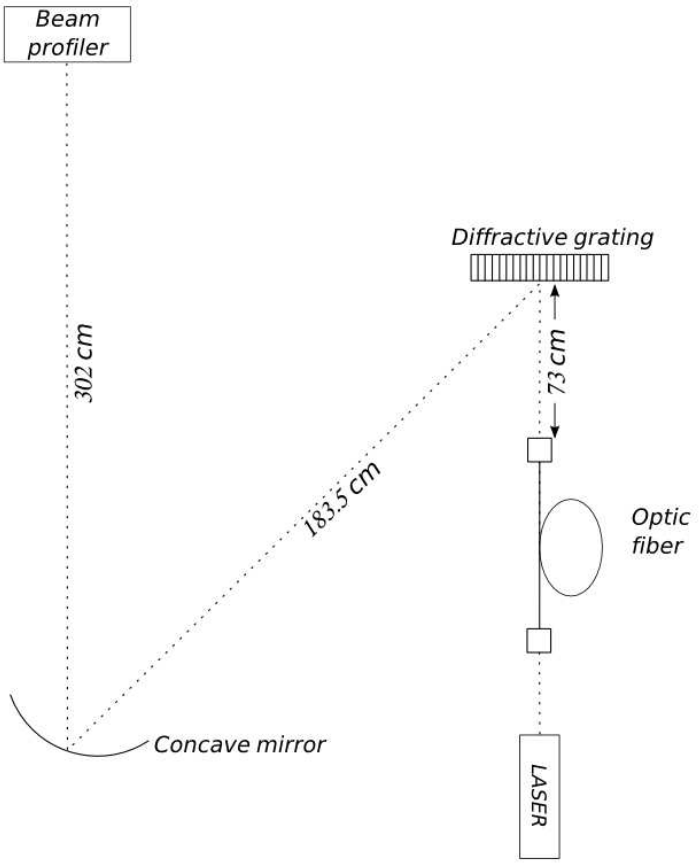

Figure 5.1: Finding the resolution of the proposed setup to measure spectral linewidth.

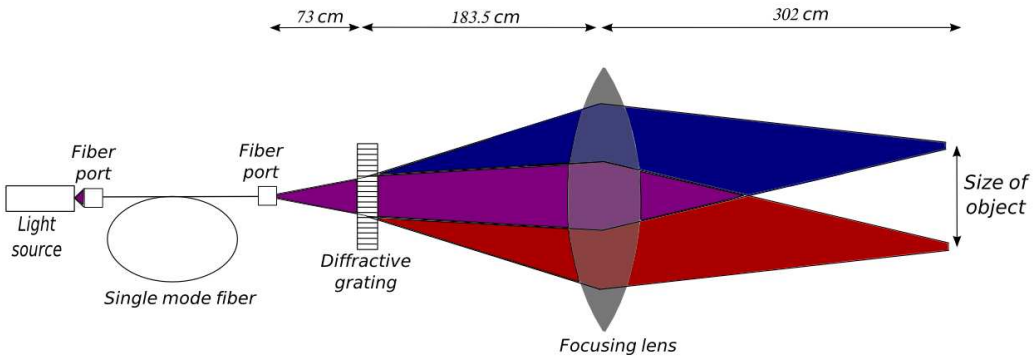

Figure 5.2: Experimental setup optically equivalent to the setup in figure 5.1. The diffraction grating will separate the original beam into monochromatic component beams. To be able to carry out the measurements, the linear size of the spectral line (the distance between the blue and red beam at the right side of the figure) must be much larger than the linear width of each of the monochromatic beams.

order image, the image at $\alpha(m = 2)$ the *second order image*, and so on [55].

Let us assume that the spectral line has a central wavelength λ_0, with a linewidth of 2δ. Light with wavelengths $\lambda_0 \pm \delta$ will be diffracted into directions

$$\alpha_\pm = \sin^{-1}\left\{\frac{m(\lambda_0 \pm \delta)}{d}\right\}. \tag{5.2}$$

The light is focused by a lens. Each spectral component may then be viewed as a separate beam, following approximately the same direction as before, but with a waist decreasing as described with the ABCD-method in chapter 1. As we saw, the waist never becomes infinitely thin, but will start to increase after it has reached a value $W(z) = W_0$. The beam waist W_0 is then a measure of the maximum spacial resolution of the experimental setup.

For linewidth measurements to be possible, W_0 must be much smaller than the linear size at the focus of what we want to measure.

Finding the resolution of an experimental setup

To determine if the spacial resolution of our setup allowed for a measurement of the spectral linewidths to be carried out, we did preliminary measurements using a laser, assuming a spectral linewidth much smaller than the linewidth of our spectral lamps so that we could set $\delta \approx 0$. The CCD-chip[2] from a Nikon D200 camera was used as detection device. Figure 5.3 shows the laser beam focused on the CCD. The image has been enlarged, for each pixel to be visible. The bright spot in the figure seems elongated. This is due to a phenomena calles astigmatism, where two directions in the plane perpendicular to the beam-axis have slightly different focal lengths [53]. In figure 5.3, the CCD-chip has been placed in the focus of the x-axis.

According to the product specifications of the camera, the CCD has a total area of 23.6 mm×15.8 mm, or 3872×2592 pixels [33]. This corresponds to a pixel size of about 6×6 μm. Counting the number of light pixels in the horizontal direction in figure 5.3, we find that the width of the focused laser beam in in the order of 20 pixels, or about $20{\times}6$ $\mu\text{m} = 120\mu\text{m}$.

Determination of d

At radial distance 170 cm from the grating, the linear distance between the first and second order image of the laser was found to be 150 cm, as in figure 5.4. The angle $\Delta\alpha \equiv \alpha_2 - \alpha_1$ between the first order and second order image then satisfies

$$\sin\left(\frac{\Delta\alpha}{2}\right) = \frac{150}{2 \times 170} \qquad \Rightarrow \qquad \Delta\alpha = 52.4^\circ.$$

[2] **CCD**-*Charge Coupled Device* is a device where electric charge is generated when light hits the surface of cells made of metaloxide semiconductors. The charges are conducted via the adjacent cell to a limited number of output nodes to be converted to voltage [13], [47].

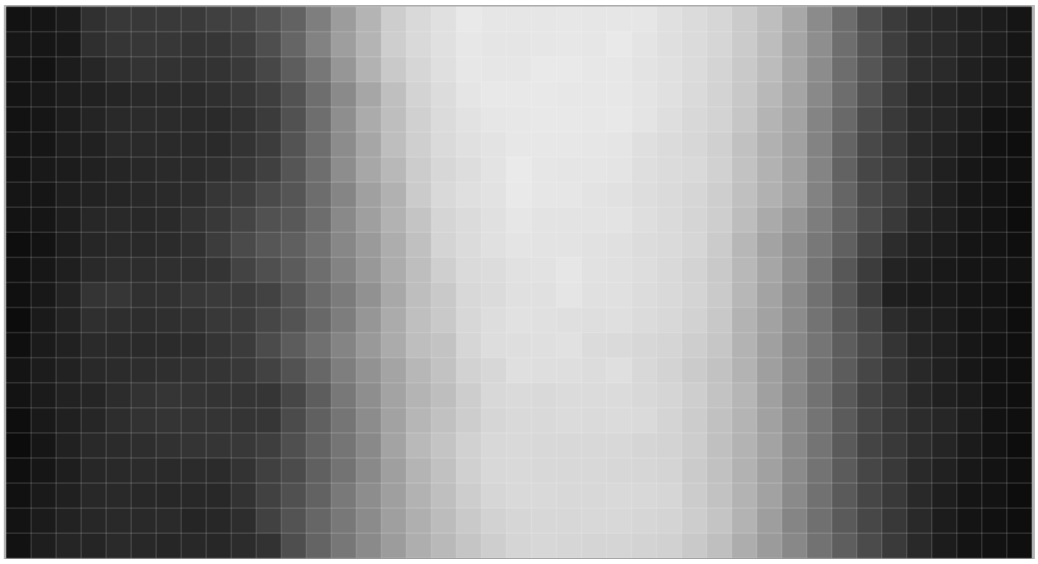

Figure 5.3: Beam waist of laser light having propagated through the setup in figure 5.2.

According to equation (5.1)

$$d \sin \alpha_1 = \frac{d \sin (\alpha_1 + \Delta\alpha)}{2}.$$

Using the property of the sine of the sum of two angles[3] and rearranging the equation, we obtain

$$\tan \alpha_1 = \frac{2 - \cos \Delta\alpha}{\sin \Delta\alpha}.$$

Inserting the value $\Delta\alpha = 52.4°$ gives $\alpha_1 = 60.3°$. Again using equation (5.1) and the nominal value of our laser $\lambda = 633$ nm, we find

$$d = \frac{\lambda}{\sin \alpha_1} = 729 \text{ nm}. \tag{5.3}$$

A more common convention for specification of diffraction gratings is to give the number of lines per unit length, N. Equation (5.3) is then equivalent to

$$N = \frac{1}{729 \times 10^{-6} \text{ mm}} = 1370/\text{mm}. \tag{5.4}$$

[3] $\sin (\alpha + \beta) = \sin \alpha \cos \beta + \cos \alpha \sin \beta$ [42].

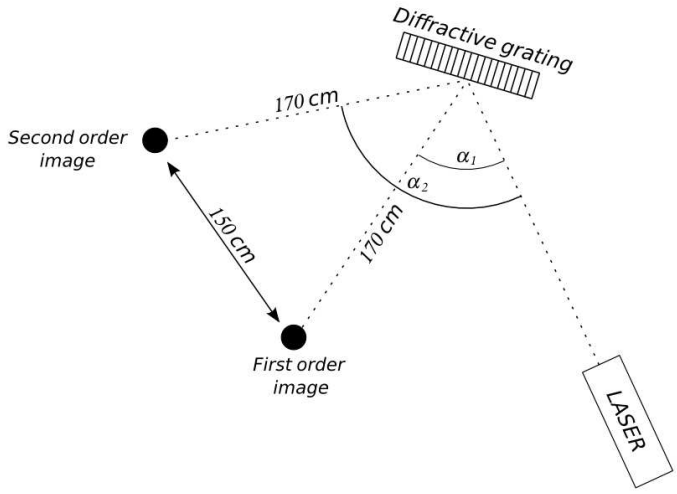

Figure 5.4: Experimental setup for finding the distance between the middle point of two adjacent slits in the diffraction grating.

Estimate of expected size of image from spectral lamps

Let us make an estimate of the size of the spectral line at the point of the beam waist. We will choose the Ne692-line as our numerical example. In chapter 6, we will see that the coherence length of Ne692 is about 30 mm. In chapter 2, we found that a source with a given coherence-length would have a frequency distribution with FWHM-width in the order of

$$\Delta\nu = \frac{c}{\pi l_{coh}} \quad \text{(cf. equations 2.19 and 2.16).} \tag{5.5}$$

Using the numbers above, this $\Delta\nu$ is about 3.18×10^9 Hz. This corresponds to a spread in wavelength of about $\delta = 0.01$ nm. According to equation (5.2) the total line will then cover an angle $\Delta\alpha_{692} = \alpha_+ - \alpha_-$, where α_+ and α_- are given by:

$$\alpha_+ = \sin^{-1}\left(\frac{692 + 0.01\text{nm}}{729\text{nm}}\right) = 71.67^\circ$$
$$\alpha_- = \sin^{-1}\left(\frac{692 - 0.01\text{nm}}{729\text{nm}}\right) = 71.66^\circ.$$

The angular spread of the spectral line is therefore $\Delta\alpha_{692} = 71.67^\circ - 71.66^\circ = 0.01^\circ$.

In figure 5.5, we have drawn the same setup as in figure 5.2, only including the quantities needed to find the size x of the spectral line. The distance L is the distance from the grating to the point where the image is focused. From the figure we see that the tangens of half the angle $\Delta\alpha_{692}$ is equal to half the size x of the spectral line divided by the total length L:

$$\tan\left(\frac{\Delta\alpha_{692}}{2}\right) = \frac{x}{2L}. \tag{5.6}$$

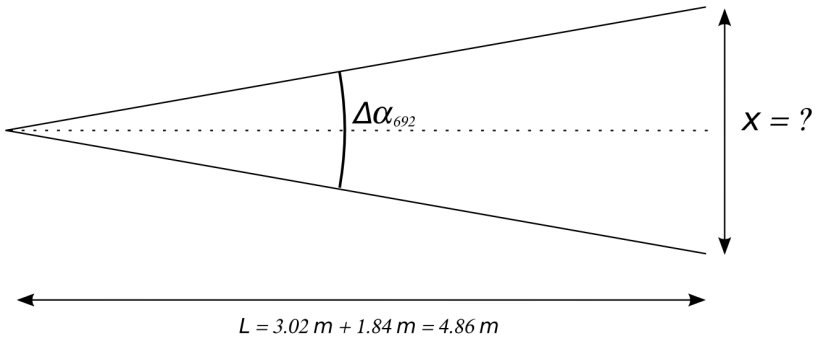

Figure 5.5: Finding the size of an spectral line.

Solving for x and inserting $L = 3.02$ m $+ 1.84$ m $= 4.86$ m (the distance from the grating to the beam waist), we find that the linear size of the spectral line is:

$$x = 2L \tan\left(\frac{\Delta\alpha_{692}}{2}\right) = 2 \times 4.86 \text{ m} \tan\left(\frac{0.01}{2}\right) = 8.48 \times 10^{-4} \text{ m} = 848 \ \mu\text{m}.$$

With the resolution of 120 μm found for the laser experiment, measuring the linewidth of Ne692 should be possible.

Although the geometry of the experiment seems to allow for the measurement of the spectral lines width of our light sources to be carried out, the low intensity of the filtered spectral lamps prevented us from continuing the spectral line measurements.

The intensity of the light sources was very low. After the light had propagated throught the fiber, it was not possible to see the beam with the naked eye. This fact would have made the alignment of the setup very difficult. In principle, one may calculate the exact position of the spectral line using the methods and equation described above, but this would require much higher accuracy in all measurements made above, and there would be a corresponding increase in the the time required for the experiments to be carried out.

In addition, the low intensity prevented us from using the CCD-chip as detection device. Accurate measurements of the intensity involved would have required the use of the single photon counting module (SPCM) described later in this chapter. The use of a SPCM is highly time-consuming even when the detector is in rest. In performing linewidth measurements with a SPCM, we would have had to move it a small distance between each measuerment, and the challenges of allinging the detector and of isolating from background light would have been considerable, possibly impossible with the equipment and within the time available.

5.2 Measuring coherence length of light sources

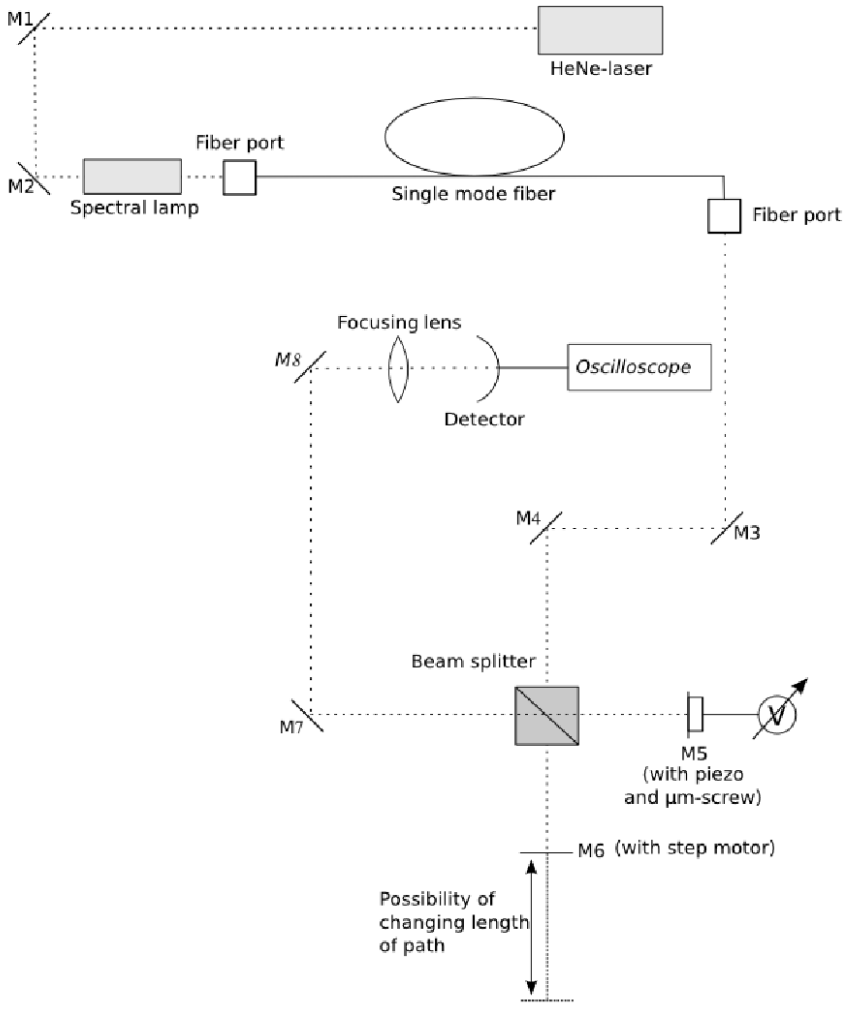

Figure 5.6: The complete experimental setup

5.2.1 General outline of the experiment

To measure the coherence length of a light source, we will need to split the light into two partial beams, let them interfere, and measure the visibility of the interference pattern as one of the arms are moved. The experimental setup requires essentially two things: 1) A light source and some way to shape it into a well-behaved beam, and 2) an interferometer that allows for changing the arm length a distance in the order of the coherence length of the source. The first of these points was treated in chapter 4, the second will be described in the current chapter. One exception to that division of the experimental setup into two chapters is the description of collimator and the process of collimation, which we chose to postpone till now since it is of a more technical than physical nature.

As seen in figure 5.6, the light is collimated into an optic fiber. On leaving the fiber, it is conducted via two mirrors (M3 and M4) into a beam-splitter. The two partial beams each are reflected in a movable mirror (M5 and M6) back towards the beam-splitter, where they are mixed to two new partial beams. One of the new partial beams follow the original path back towards the light source, the other is conducted via two mirrors (M7 and M8) to a lens that focuses the beam into the detector. The two mirrors between each part of the setup allow for adjusting both the position and the angle of the beam freely.

We will first show how to collimate light into an optic fiber. Then we will present the method used for aligning the components of the interferometer to achieve high visibility. The techniques for changing the length of the arm, and different detectors and methods of detection will then be described. In table 5.3 at the very end of the chapter, we have included the complete reference data for all parts of the experimental setup.

5.2.2 Collimating light into an optic fiber

We saw in chapter 1 that the propagation of a Gaussian beam may be described with a simple formula, and in chapter 4 we argued that it is nearly immune to unwanted side-effects of diffraction. In chapter 4 we also saw that using a single-mode optic fiber is one way to shape light into a Gaussian beam. If we try sending light directly into an optic fiber by holding the fiber into the beam, much of the intensity will never even enter the fiber, due to the very small radius of its core. In addition, in propagating through the single mode fiber, much of the intensity will as we saw, be peeled off to reshape the beam. Also, the light that leaves the fiber will have a beam waist in the order of a few micrometers and will be highly divergent.

The process of collimating the beam therefore has, in our case, two purposes:

1. To concentrate the incoming light so that as much of the intensity as possible hits the fiber core.

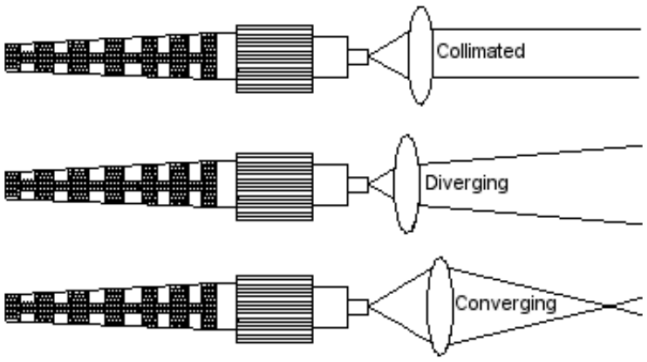

Figure 5.7: A collimator is effectively made up of a lens that may be moved with respect to the fiber opening to adjust the spread of the beam (figure from [50].

2. To avoid excessive spread of the outgoing beam, or, in the language of ray optics: To form the outgoing light into a bundle of parallel rays.

Although it may be composed of several optival components, a collimator is effectively a simple lense that can be moved with respect to the opening of the fiber to adjust the spread of the beam.

5.2.3 Achieving high visibility

The visibility defined on page 20 is a measure of the contrast of an interference pattern. In some experiments (for example related to tests of violation of Bell's inequality [1]) a high visibility is crucial for the results to be valid. In other experiments, such as ours, a high visibility is not crucial, but desirable since it increases the signal-to-noise ratio.

Since the visibility of the signal is strongly sensitive to the position of each component of an experimental setup, the measurement of coherence length requires a setup that allows changing the distance of at least one arm in the interferometer without changing the position of more components than strictly necessary. The easiest way to arrive at this is with a Michelson's interferometer, where only one mirror has to be moved. In a perfectly aligned interferometer, the interference pattern will take the form of a single spot whose intensity increases and decreases as shown in figure 5.8(a) and 5.8(b) according to the path difference of the two arms. If the interferometer is not perfectly aligned, the wavefronts will not be completely overlapping, and there will be bright and dull areas, or *fringes* within a single spot, as in figure 5.8(c). In this case, changing the arm length only causes the fringes to be shifted, while the total intensity remains nearly constant.

In light of the discussion above, and of the calculations showing the relation between coherence length and visibility in chapter 2, we may conclude that there are at least two ways that the visibility of an interference pattern may be degraded:

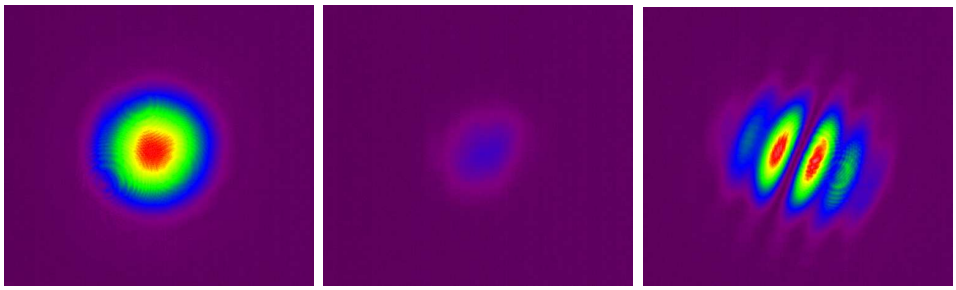

(a) Constructive **(b) Destructive** **(c) Bad overlap**

Figure 5.8: If the two beams are overlapping, the interference pattern will take form as a spot whose intensity increases and decreases periodically with path difference. If the path difference is equal to an integer times the wavelength of the light, the interference will be constructive, and we will see a bright spot (a). If, on the other hand, the path difference is equal to an integer plus one half wavelength, the interference will be destructive (b). If the beams are not completely overlapping, the interference pattern is striped (c).

- A 'true' degrading originating from the limited coherence length of the source
- Mechanical degrading caused by misaligned elements in the experimental setup.

The second of this must be avoided (or at the very least its magnitude must be known) for visibility measurements to be valid in determination of coherence length.

Recalling the derivation of the parmeters of the Gaussian beam in chapter 1, we may conclude that there is a third possible way the visibility may be degraded. The beam width and radius of curvature changes with propagation distance according to equation (1.12) on page 15. Even if the light source *in principle* has a long coherence length, and even if the interferometer is perfectly aligned, in changing the path length, the change of the beam width and radius of curvature may be so large that a complete overlap of the two partial beams is not possible. If the beam is well collimated, however, this factor of degrading of visibility should be negligible.

In chapter 1, we explained the concept and developed a mathematical expression for the wavefront of a beam. It was defined to be a surface of constant phase of the electric field. For two beams to exactly cancel each other out, it is not enough that their intensity profiles are overlapping. The electric fields must also be completely out of phase at all times: Both the beam *width* and *curvature of radius* must match. To achieve the best possible visibility, the two partial beams must therefore follow the same path from where they leave the beam splitter, it is not merely enough that they meet at the point of detection. Only then can there be a complete overlap of the wavefronts.

All mirrors used in the experimental setup were fastened to mounts that offered (at least) two degrees of freedom: Tilting in the horizontal and vertical directions.

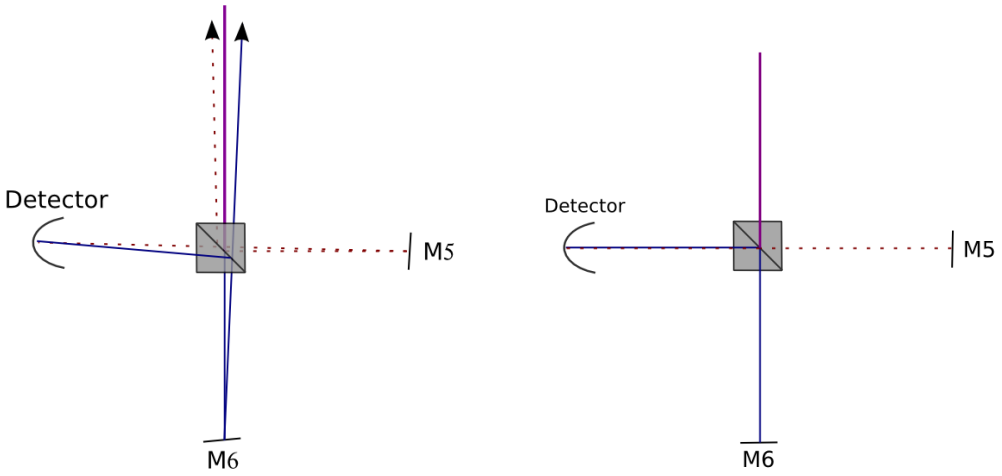

(a) Low visibility **(b) High visibility**

Figure 5.9: To achieve high visibility, it is important that the two partial beams follow the same path upon leaving the beam splitter (The rays have been colored and one has been dotted for illustrative reasons. The thick purple line on the right is the original beam. In (b), this is the same path as followed by half of the reflected re-mixed beam). The numbering M5 and M6 of the mirrors correspond with the numbering in figure 5.6

As far as possible, the first adjustment of any component should be done in the order it appears in the experimental setup. In figure 5.6, starting from the outgoing side of the optic fiber[4], this would mean collimating the fiberport before adjusting $M3$, then $M4$, then the beam-splitter, and so on. This is, however, not always possible, and in addition a fine-adjustment must be done after all components have been positioned. In the following, we will explain how one may use reflections from the components to obtain good positioning of the beam-splitter and the mirrors at the end of the arms of the interferometer.

Positioning of beam splitter

- Block the mirrors $M5$ and $M6$ so that no reflections of the light that hits these will be reflected back through the beam-splitter. There will still be a dim reflection from the front face of the beam-splitter[5].

- Adjust the beam splitter so that this reflection follows the same path as the original beam, that is, so it is positioned in the middle of the original beam at a point on the axis of propagation far from the beam splitter itself.

[4]In addition to shaping the beam, an optic fiber is an asset to the setup in that it may be moved around, and therefore allows for great freedom in the layout of the setup. The two sides of the fiber may therefore be seen as separate parts of the setup, and the adjustments of one part do not affect the other.

[5]This reflection is in every other aspect of the experiment an unwanted effect.

In principle, the same method can be used to make a good adjustment of $M5$ and $M6$. One then blocks one of the arms of the interferometer and places the reflection of the other in the middle of the original beam. The procedure is then repeated with the other arm blocked. After both reflections are placed, one uses a beam profiler to examine the output on the detector side of the beam-splitter. If everything is done right, the two partial beams should now be very close to each other. Choosing one of the two as the position standard, the other is moved to overlap with this.

For us, since the original beam was much more intense than the reflections, this proved to be a difficult procedure for two reasons: The light of the original beam made it very difficult to see the reflections as they came close (in the x-y-plane) to the original beam, and the original beam appeared to have a much larger diameter than the reflections, so that the uncertainty of the position became very large. To avoid these obstacles, we used a slightly different method:

Positioning of mirrors in interferometer

- Block the path of $M6$ so that only the light from $M5$ is reflected back through the beam-splitter.
- At a point on the axis of propagation far from the beam-splitter (close to the outgoing side of the optic fiber), position the reflection slightly on the side of the original beam, but with a very accurately determined vertical position (figure 5.10a).
- Now, block the path of $M5$, and, with the reflection from $M6$, do the same as in the previous point, this time placing the reflection just below the original beam.
- Open both paths. The partial beams should now each have one very accurately determined coordinate. Using a beam profiler on the detector side of the beam splitter, one may use only the horizontal screw on $M5$ and the vertical screw on $M6$ to move the two beams to the middle of the original beam without being disturbed by the original incoming beam (figure 5.10b).
- The most important contribution to error in the alignment should now be due to the beam splitter, and its position may be slightly altered to obtain the highest possible visibility.

Drift in system

Temperature fluctuations, equipment limitations and a non-stable environment are factors that may cause an experimental setup to expand or contract and thus change the path length between the arms or the tilt angle of the components in the interferometer. Figure 5.11 shows the measured drift in our Michelson interferometer. The drift was measured using the photo-diode detector from Newport,

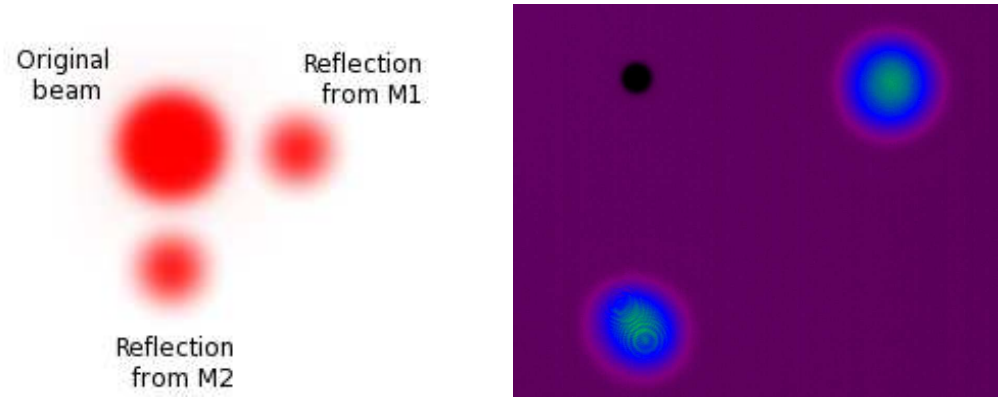

(a) Original beam and reflections of the two partial beams.

(b) The two partial beams using the beam profiler as detection devise.

Figure 5.10: Our method of adjusting the mirrors consists of placing the reflection slightly outside of the original beam, and thus obtaining very accurate coordinates for the optimal placement of the two mirrors using a graphic detection devise. The actual middle point should be very close to the black spot in the upper left corner in figure (b). This black spot was not in the original screen-shot, but has been added for clarity

described in section 5.4.2. The path length of the interferometer was not (manually) changed during the time. At the end of the measurement, the voltage over the piezo-element[6] was changed to show the value of the drift relative to the maximum and minimum intensity of a cycle of interference. Although there is certainly some drift that causes the fluctuations in intensity in figure 5.11, the intensity is always far from the maximum value seen on the far right side of the graph. On time scales of about ten minutes, the magnitude of the drift is therefore much smaller than one wavelength (633 nm).

5.2.4 Positioning of mirrors using white light interference

After having obtained good (angular) positioning of the elements of the experimental setup, it is important that the difference in distance between the two arms, $\Delta l = l_2 - l_1$ is determined as accurately as possible. As we begun trial measurements of the spectral lamps, it became obvious that their coherence lengths were much longer than first expected, in the order of centimeters rather than the first expected fraction of a millimeter. It became apparent that the span of the step motor would not allow us to cover a distance of both positive and negative τ (recall that $\Delta l = c\tau$), and determining the exact position of $\Delta l = 0$ became increasingly important.

[6] See description of piezo-elements and the piezoelectric effect below.

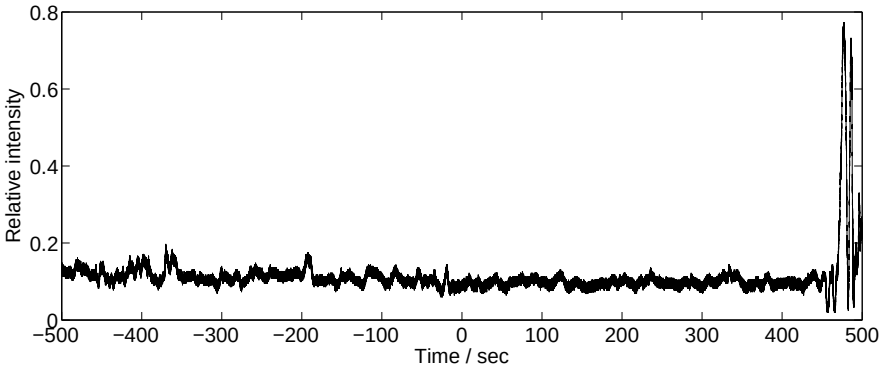

Figure 5.11: Mechanical drift in the experimental setup.

As found in chapter 2 and 4, any light with a finite linewidth should show interference for very small τ. To find the point where $\Delta l = 0$ to an accuracy of a few micrometers, we inserted a light source of white light into the experimental setup, and manually moved the mirror $M5$ with the μm-screw described below, until finding the interference pattern. Since white light has a very wide frequency range (cf. figure 4.1), the coherence length will be very short, in figure 5.12, it is found to be in the order of a few tenths of wavelengths. When positioning the mirrors, we defined $\Delta l = 0$ to be the middle point between the two extreme point where the interference pattern was observed. In figure 5.12, this point is between the second and third oscillating pulse pattern (immediately to the right of the highest peak in the figure). The graph was recorded with the detector from Newport, which is described below. The pulsating pattern in the figure may be due to the limited temporal resolution of the detector (cf figure 5.19).

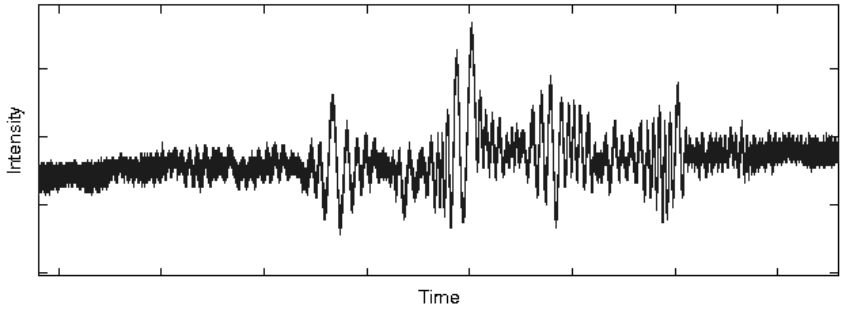

Figure 5.12: Interference pattern of a white light source.

5.3 Changing path length

Three different techniques and pieces of experimental equipment were in use to change the path lengths of the mirrors in the interferometer. Table 5.1 gives an overview of the methods, and in the following section we will further explain their use.

Table 5.1: Methods of changing path length in interferometer.

Application	*Range/step (μm)*	*Field of application*
μm-screw	25 000/5	Positioning of mirrors
Piezo-element	1.5/0.040	Visibility measurement, moving mirror short distances
Step-motor	8 000/0.060	Moving mirror large distances

5.3.1 Platform with μm-screw

One of the mirrors of the interferometer was positioned on a platform moved by a screw covering a range of 25 mm in steps of about 5 μm. The purpose of the platform was to position the mirror, since the step-motor is fastened to a block of metal difficult to move, the and piezo-element only covered a distance of about 1.5 μm. The platform was not moved during data-taking as it was difficult to achieve good angular positioning, and the mechanical degrading when moving the platform was therefore high.

5.3.2 Piezo-element

The piezoelectric effect is defined in [12] as: *"The generation of a potential difference across opposite faces of certain nonconducting crystals as a result of the application of mechanical stress between these faces"*. The opposite effect is also a property of piezo-electric materials: A potential difference across the crystal may cause it to undergo mechanical stress, and consequently change the shape of the material [57].

To be piezoelectric, the geometry of the solid must be such that mechanical stress causes an overall displacement of the charges in the solid so that the center of gravity of the negative charges does not coincide with that of the positive charges. This displacement sets up dipoles that cause a measurable potential difference between the sides of the solid. In our experimental setup, we used the opposite effect to be able to change the path difference with distances less than, and in the order

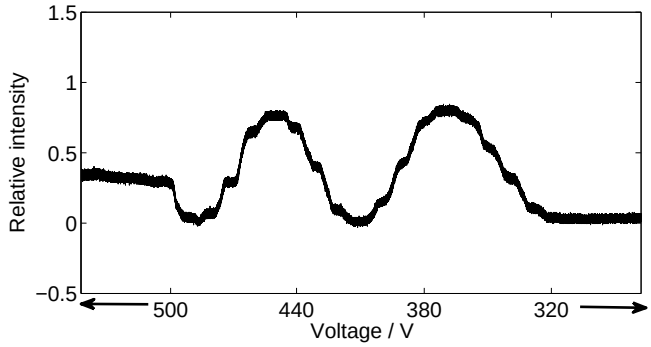

Figure 5.13: The piezo element glued to one of the mirrors enables us to change the path length with distances in the order of one wavelength. The arrow to the far left and right on the x-axis shows that the voltage is kept constant at 500 V and 320 V respectively. The wavy or step-like feature of the curve is due to an uneven rate of voltage change as described in the main text.

of one wave length: A varying potential difference between two of the sides of a piezoelectric crystal pulls the charges apart and gradually changes the size of the crystal [51], [57].

Figure 5.13 shows the intensity from the interferometer using a laser and changing the voltage by turning a knob by hand. The step-like feature of the graph is due to that hand work, as the author only managed to turn the knob about one half turn before having to take a new grip. Jagielski found in the work with his master's thesis that the expansion of our piezo-crystal is linearly dependent on the voltage applied [22].

5.3.3 Step-motor

To change the path length over a distance longer than approximately 1 μm during measurements, we used a combination of a *Travel stepper actuator* with an *ATP stepper motor controller*, both from Thorlabs. The step-motor allows for predetermining a sequence of moves to be carried out. In defining a move, the *total distance, maximum speed, and acceleration* must be defined.

As we will see below and in the next chapter, the step-motor was less stable and had larger uncertainties than expected.

Uncertainty in linear distance

According to the description from the manufacturer, the actuator may cover a distance up to 8 mm, with a minimum step size of 60 nm [49], and it should therefore be possible to use the step motor for small changes in the path length. However, in examining figure 5.14 and comparing the graphs obtained with the step-motor and the piezo-element, it seems clear that the accuracy of the piezo-element is much

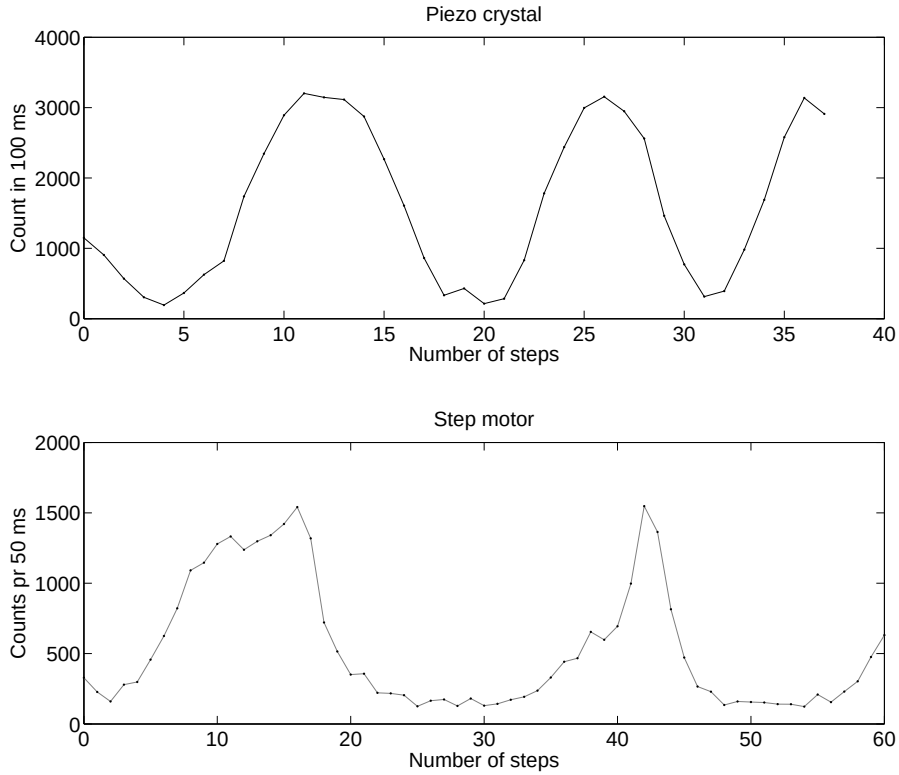

Figure 5.14: Data taken with the SPCM using (a) a piezo element and (b) a step motor. The datapoint in (b) are closer than the nominal 60 nm because the motor pushed on a device increasing the step-length, and not directly on the mirror mount.

larger than that of the step-motor, and correspondingly, the former was used during measurements.

Mechanical instability

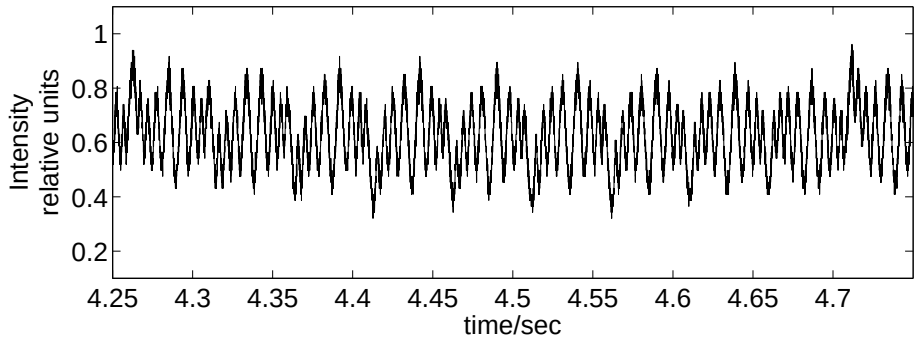

Figure 5.15: Tests with HeNe-laser and step-motor moving with a speed of 1 mm/10 sec.

During preliminary tests of the setup, we used a laser as light source, the Newport detector described below as detection devise, and the step-motor, programmed to move 1 mm in 10 sec to change the path length. The graph obtained is depicted in figure 5.15, and clearly shows an oscillating enveloping curve *in addition* to the expected interference pattern. A priori, the oscillations could have four sources:

1. Instabilities in the laser
2. The limited temporal resolution of the detector
3. Mechanical instability of the step-motor
4. External noise.

To find the source of the oscillations, we measured the intensity as the step-motor was moved with a speed of 1 mm/5 sec, 1 mm/10 sec, and 1 mm/20 sec. The data is plotted in figure 5.16.

Each of the three curves in figure 5.16 shows a segment of about 0.1 sec of the total data. In figure (a) one may see four periods of the oscillations, in figure (b) two, and in figure (c) only one oscillation. Temporally this corresponds to a period of 0.025 sec, 0.05 sec and 0.1 sec, respectively.

Taking the *speed of the motor,* v_{motor}, into the calculation, the *spatial* period P_s of the oscillation is:

$$P_s = v_{motor} \times P_t, \tag{5.7}$$

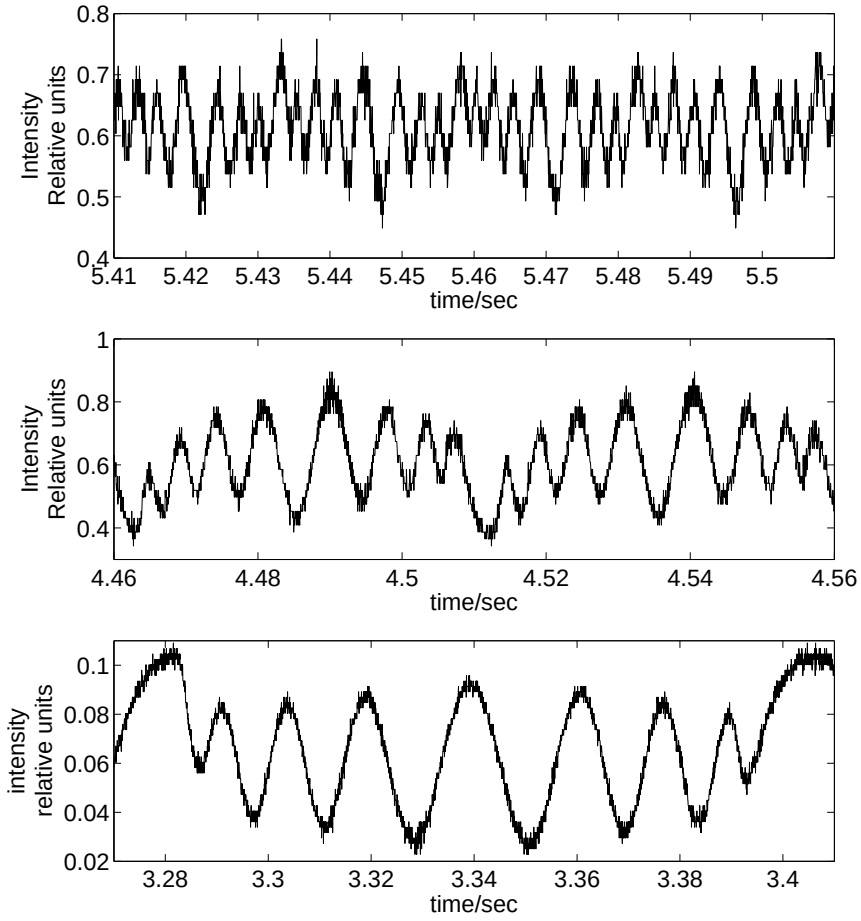

Figure 5.16: Interference pattern of laser, with the step-motor used to change path length (a) 1 mm in 5 seconds, (b) 1 mm in 10 seconds, and (c) 1 mm in 20 seconds.

where P_t is the temporal period of the oscillations.

Inserting the numbers for v_{motor} and P_t give above, we find that the spacial period in all three cases is equal to 5μm. Since the oscillations seem to have a fixed spacial, and not temporal period, we concluded that they are due to mechanical instabilities of the step-motor.

Let us examine the graph in figure 5.16 once more. The maximum and minimum values of the oscillations change, but the *shape* of each top does not seem to be significantly disorted. If the latter had been the case, it would have been an indication that the *speed* of the stepmotor is not constant. Instead, we have a periodic change of the value of the maxima and minima of the curve, and consequently of the visibility. We already showed that the periodicity of the envelope is caused by instabilities in the mechanics of the step-motor. It therefore seems natural to

conclude that in the forward motion of the mirror, there is a slight angular rocking of the mount of its mount.

5.4 Detectors

Several means of light detection were used during the experimental work: A *single photon counting module (SPCM)* from PerkinElmer, a silicon photodetector (SPD) from Newport, and a USBeamPro beam profiler from Photon Inc. Following the procedure of the section on methods of changing arm length, brief information on the use of each detector is given in table 5.2, followed by a section of a description of each. The SPD and the USBeamPro will be treated very briefly, the SPCM that were used during the actual measurements in some more detail. The data obtained from the SPD and the SPCM were analysed using a LeCroy digital oscilloscope. A brief description of this is given after the descriptions of the detectors. Since descriptions of all three detectors are readily available online, our focus will be on giving subjective discussion of our experience of the strengths and weaknesses of each module.

Table 5.2: Detectors and their use.

Detector	*Field of application*
SPCM	Numerical intensity measurement of intensities on the single-photon level
SPD	Numerical intensity measurement for low to moderate intensities
USBeamPro	Visualizing the beam, determining beam shape and size

5.4.1 USBeamPro

The colorful images in 5.8 were made using the *USBeamPro* beam profiler from *Photon Inc.* The detection device consists of a camera-based CMOS-chip[7] with 1280×1024 pixels, each of size 6.7 × 6.7 μm, giving a total active area of 8.6 × 6.9 mm. The spectral range of the device is 360 nm - 1100 nm [37]. The camera is directly connected via an USB-cabel to a computer, where the data is analysed with software following the camera. An example of the graphical interface and the possibilities of the program of analysis is shown in figure 5.17.

[7]**CMOS**: Complementary metal oxide semiconductor, similar to the CCD decribed on page 75. In a CMOS, each pixel has its own output-node, allowing for large variety in the functioning of the chip, but with lower uniformity than for the CCD [13].

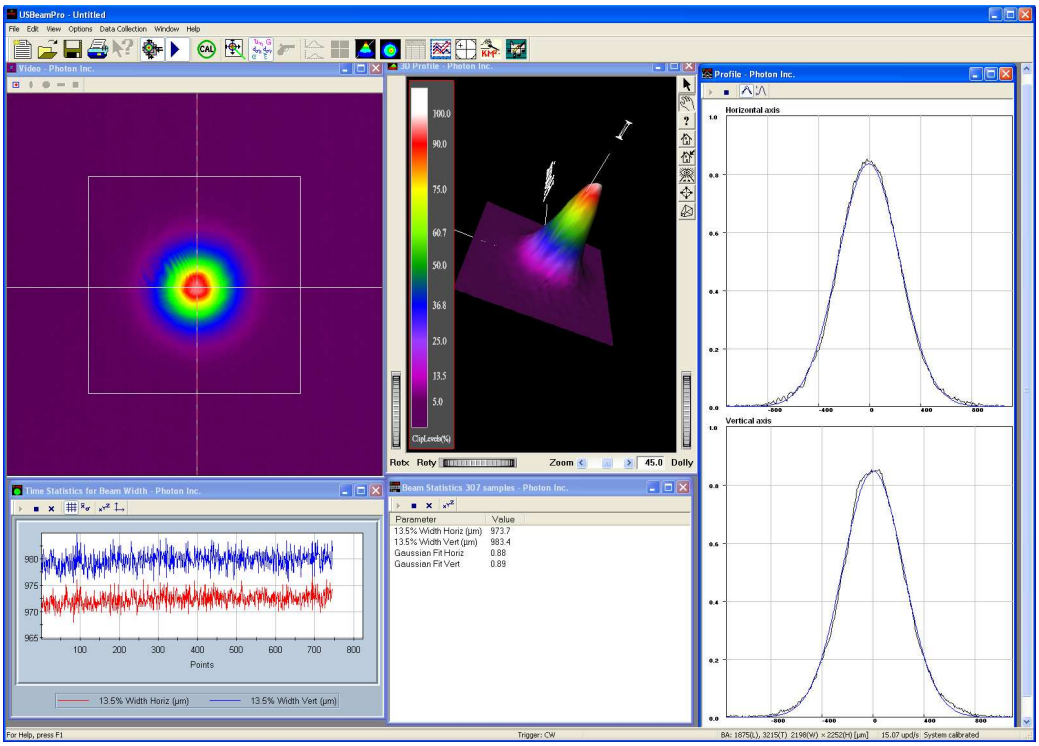

Figure 5.17: Anomg the possibility of the analysis of data obtainded with the USBeamPro are: Color coded intensity distribution in 2D and 3D, time evolution of the beam width, numerical data and gaussian fit of the intensity distribution.

5.4.2 Silicon photodetector (SPD) and power meter

While testing the experimental setup with the HeNe-laser, we combined a silicon photodetector(SPD) and a power-meter from Newport. The spectral range of the detector was 400-1100 nm [30]. The combination was not possible to use during measurements on the spectral lamps for reasons described below.

Sensitivity

According to the description from the manufacturer, the detector is sensitive to intensities down to the pW-level. On that level, however, the signal-to-noise ratio was far below a level where we could do measurements on the spectral lamps. Figure 5.18 shows the interference pattern close to $\Delta l = 0$ for the unfiltered neon lamp. The gray signal show the original signal, while the black line is the smoothed data. Experiments showed that filtering out the Ne692-line would decrease the intensity with a factor 40, and with an intensity that low, it would not be possible to distinguish the signal from the noise, at least not to the level we would need to make a good determination of the visibility of the signal.

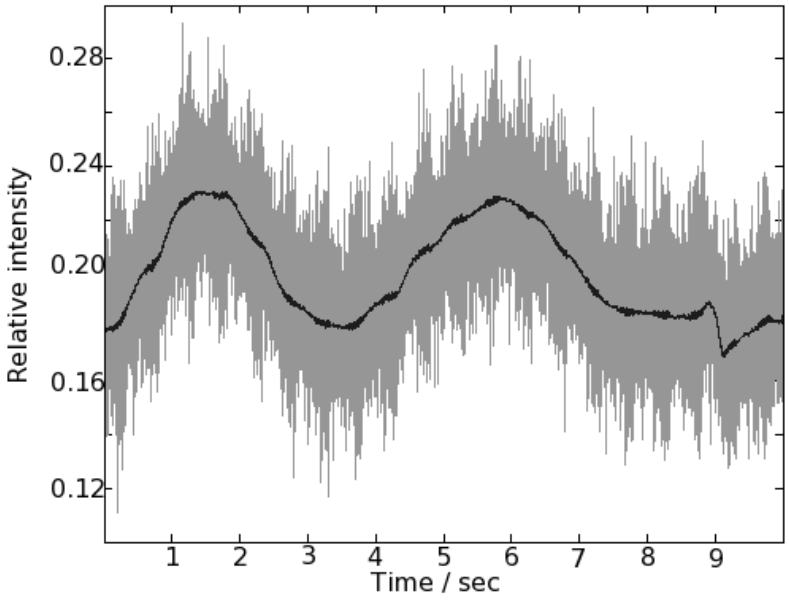

Figure 5.18: Interference of a neon lamp at $\Delta l = 0$. The gray area show the original data, to obtain the black line we have used the *smooth*-function described in chapter 3.

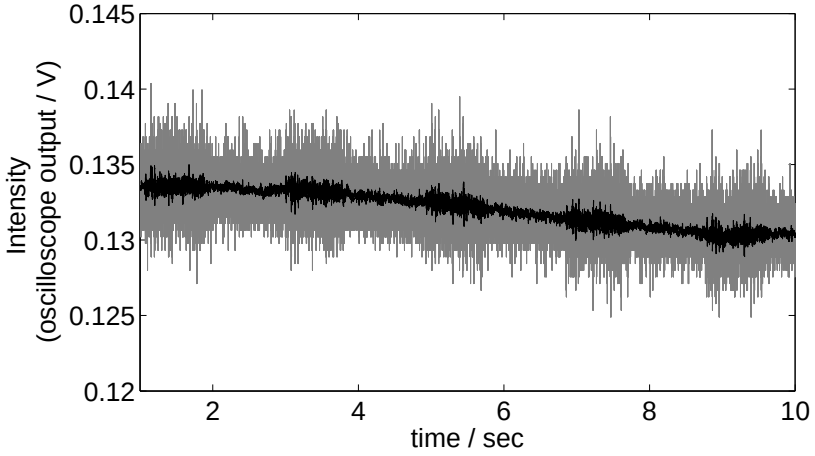

Figure 5.19: Pulsating signal due to limited temporal resolution of the SPD. The gray area is the original signal, the black line a smoothing over 50 datapoints, using the *smooth*-function.

Temporal resolution

The sensitivity of the detector was highly dependent on its temporal resolution, and using the power meter setting to obtain the highest possible sensitivity meant having the sampling rate in the order of 1 Hz. As a result, the signal showed the pulsating behaviour depicted in figure 5.19. A signal that is already weak could be significantly disorted by the pulsations. Also, to calculate the visibility of a signal, accurate values for the maximum and minimum points of a graphs is required.

5.4.3 Single photon counting module (SPCM)

General description

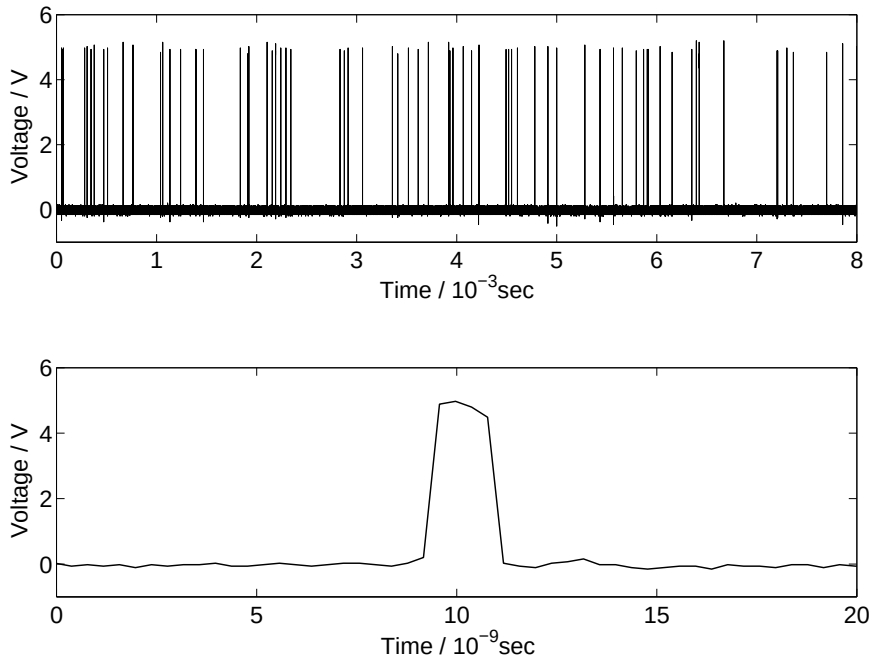

Figure 5.20: Output signal from the SPCM. Upper frame: The total signal. Lower frame: The temporal width of a single pulse.

To detect light with very low intensities, we used a *Single photon counting module* from PerkinElmer. An example of its output data is shown in figure 5.20.

The name of the module and the appearance of its output favor a picture of each pulse detected corresponding to a quantum of light as it was briefly described in the introduction to chapter 1. In any detector, the detection process involves an interaction between electromagnetic radiation and a charged particle [27]. In our opinion, the implied assumption that a pulse in figure 5.20 must correspond to the indivisible particle we normally have in mind when the word photon is used,

therefore seems somewhat hasty.

The active part of the spcm is a circular *silicon avalanche photodiode* with an active area of diameter of 180 μm [36]. The detection efficiency for light of a given frequency is given in figure 5.21. The output rate was found using a simple Matlab routine, that counted the number of pulses while taking into account the temporal width of a single pulse as shown in the upper frame in figure 5.20. The code could be run directly on the oscilloscope to avoid having to store large quantities of data.

According to the data sheet from the manufacturer [36], the actual photon rate compared to the output rate is

$$\text{ACTUAL} = \frac{(\text{OUTPUT} \times \text{CORRECTION FACTOR}) - \text{DARK COUNT}}{\text{PHOTON DETECTION EFFICIENCY}}.$$

The correction factor is a factor dependent on the count rate, that takes the detector dead time[8] into account. Its value as a function of rate is shown in figure 5.21. For count rates smaller than about one million, it is very nearly equal to unity. As explained below, we never exceeded 40 000 counts/sec in our experiments, and the correction factor was therefore neglected in our calculations. The inverse factor of the photon detection efficiency has been neglected since it cancels out in the calculation of visibility. The detection efficiency did however, as we argued in chapter 4, play a part in our choice of light sources.

Degrading, and dark count rate

According to the detector manual, the SPCM should manage a count rate exceeding 20 million counts per second [36], but according to the experience of the experimental quantum optics group of the Bohr Institute at the University of Copenhagen, the module is permanently degraded if the count rate over time exceeds 40 000 counts/sec [53].

The nominal maximum dark count rate of our module is 25 counts/sec, but approximately one year after the purchase, it was measured to be 800 ± 100 counts/sec and 150 ± 50 counts/sec respectively for two of our detectors [22]. Some months later, we measured the dark count to be 800 ± 100 counts/sec and 900 ± 100 counts/sec. During the measurements, the photodiode was covered with a black rubber cap of thickness about 2 mm, and the whole detector was covered by a black box of thickness about 5 mm. To our knowledge, the detectors have not been subject to intensities above approximately 40 000 counts/second.

5.4.4 LeCroy digital oscilloscope

As mentioned above, the data from the SPD and SPCM were displayed using a computer based oscilloscope from LeCroy. The oscilloscope has a maximum

[8] **Dead time**: The time from a pulse is registered till the detector is ready to detect the next pulse.

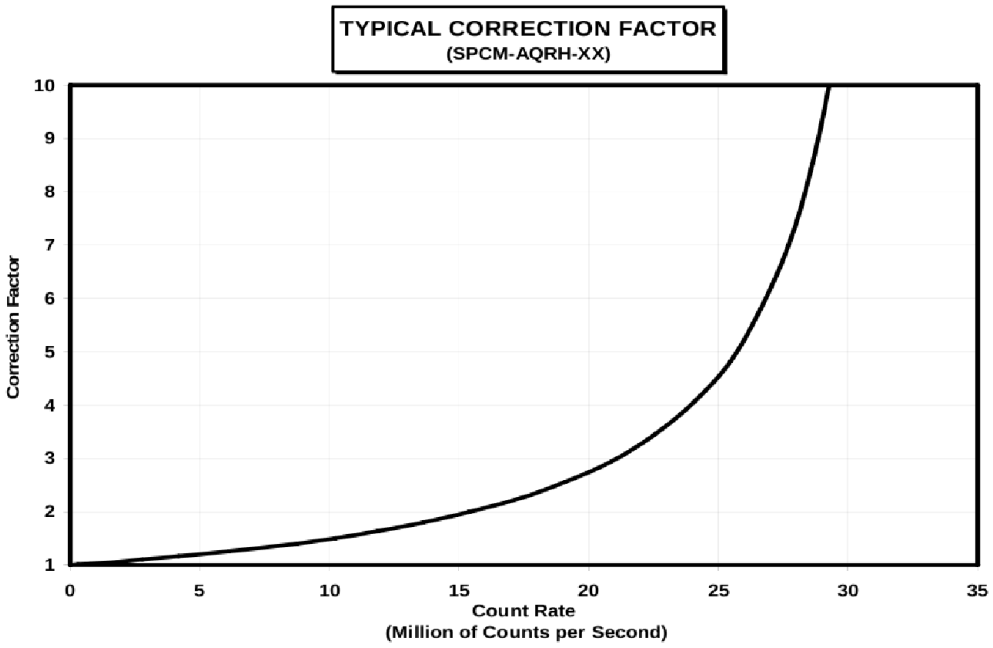

Figure 5.21: (a) Efficiency and (b) correction factor of photon count for SPCM-device. Figures from [36].

temporal resolution of one datapoint per 50 psec. The oscilloscope settings had to be chosen to fulfill the following criteria:

- To make sure the temporal resolution is high enought for all pulses to be detected, each pulse had to be at least two datapoints long
- The time span of one measurement should be as long as possible to obtain high statistics and even out possible fluctuation in the background and intensity of the beam
- The dataset should be of manageble size to minimize processing time

We found that for our use, a time span of 100 μsec and a total datalength of 10 Mega-samples was a good compromize. This gives a temporal resolution of 10 nsec per datapoint.

At the closing, let us mention one detail that may save a future user for frustration and waste of time. A bug in the software included in the oscilloscope causes the computer to crash if one tries to overwrite a file. All filenames must therefore be changed before saving.

5.4.5 Time-digitizer

Towards the finish of the experimental work, the laboratory was granted the economical means necessary to purchase a *time-digitizer*. The most important facet of a time-digitizer is that it may record the syncronized time of hits from different detectors. No selection of data needs to be made during measurements, and no trigger-mechanism between the two detectors are needed. In addition, only the time for registered hits are recorded. This significantly decreases the size of the data-sets that have to be saved and processed [53]. It is possible that the experiments described in this thesis could be done more easily and accurately with this new device.

Table 5.3: Reference data of experimental equipment.

Name	*Product code*	*Manufacturer*
HeNe-laser	HRR120	Thorlabs
Broadband dielectric mirror	BB1-E02	Thorlabs
Beam splitter	TWK 10	Bernhard Halle
Plano-convex lens	KPX100	Newport
Spectral calibration lamp	6030 Argon	Newport/Oriel
Spectral calibration lamp	6032 Neon	Newport/Oriel
Spectral calibration lamp	6035 Mercury (Argon)	Newport/Oriel
Bandpass filter (mercury)	546FS05-25	Andover
Bandpass filter (neon)	690FS10-25	Andover
Bandpass filter (argon)	694FS10-25	Andover
Single mode fiber (neon, argon)	P1-630A-FC-10	Thorlabs
Single mode polarizing maintaining fiber (mercury)	P1-488PM-FC-5	Thorlabs
Single mode fiber launch	MBT613/M	Thorlabs
Microscope objective	RMS20X	Thorlabs/Olympus
Travel stepper actuator	DRV001	Thorlabs
ATP stepper motor controller	BSC102	Thorlabs
Single Photon Counting Module	SPCM-AQRH-16	PerkinElmer
USBeamPro	PS-2323	Photon Inc.
Silicon photodetector	918D-SL-OD3	Newport
Power Meter	2931-C	Newport
LeCroy Digital Oscilloscope	WP7100A	LeCroy

Chapter 6

Experimental results for Ne692

We will now present the experimental results for Ne692. Some data was also obtained from Hg546. As we will see, an accurate measurement of the laser visibility was required to allow any conclusions from the measurements of the spectral lamps. Measurements of the laser visibility was only done during the experiments on Ne692. Attempts to use the same values for Hg546 were unsuccessful, and the results for this will therefore not be included in the chapter.

During the measurement on Ne692, it became clear that the limitations on the equipment did not allow us to obtain the results with the accuracy first expected, and we therefore chose not to spend time on repeating the measurements for Ar696.

The average background (including dark counts) was found to be about 110 counts per 100 μsec.

6.1 Measurements

We used the experimental setup depicted in figure 5.6. A SPCM was used as detection devise, and the intensity was assumed to be proportional to the pulse-density after the background had been subtracted. A simple Matlab-routine was used to count the number of pulses.

The total measurement consisted of several sets of sub-data, each data-set corresponding to intensity measurement over a distance of 2-3 wavelengths. To change the path length within one set of sub-data, a piezo-element was used. Linearity between the voltage applied and distance was assumed (cf. discussion of the piezo-element in chapter 5). Between each set of sub-data, the step-motor was moved 1 mm, corresponding to a total path difference of $\Delta l = 2$ mm.

Figure 6.1(a) shows the intensity of Ne692 as a function of path difference in the interferometer. In figure 6.1(b), we have zoomed in on the set of sub-data at $\Delta l = 0$. Note that the units of the x axis in the first case is in millimeters, in the

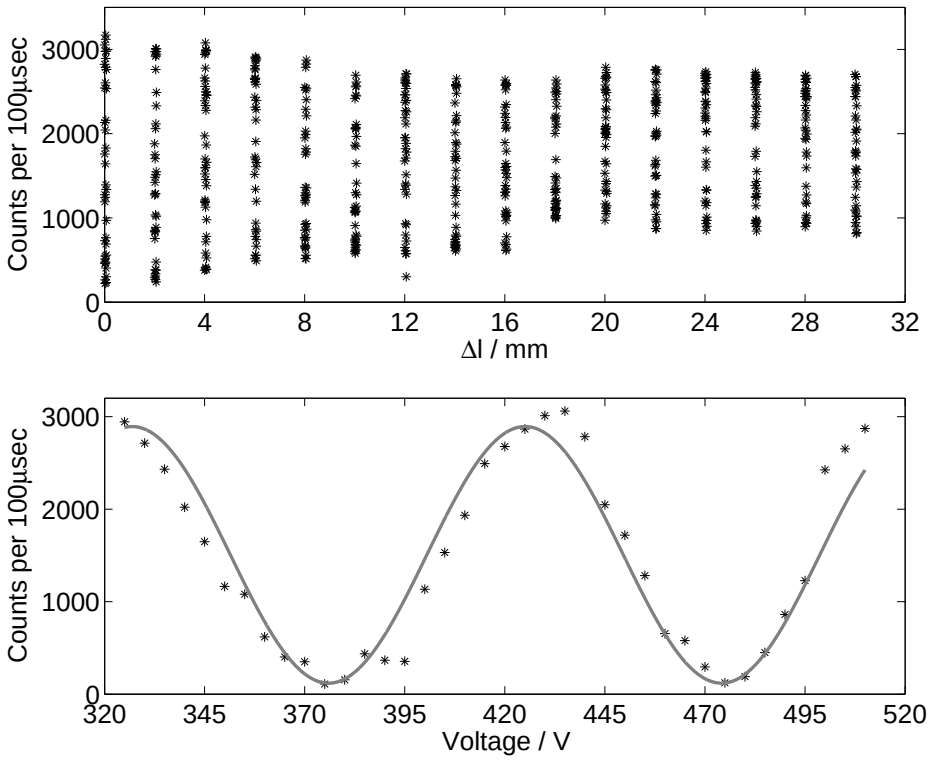

Figure 6.1: (a) The visibility of Ne692 as function of path difference, and (b) the intensity of Ne692 zoomed in on the sub-data at $\Delta l = 0$ mm (the far left line of data-points in the upper graph).

second case in volts to reflect the method used for moving the mirror.

For values of Δl from 0 mm to 18 mm, the measurements were made in order of increasing Δl (0 mm, 2 mm, 4 mm, ..., 16 mm). The μm-platform was then moved to give a total path-difference of 30 mm. As we will see below, moving the step-motor caused a large mechanical degrading of the visibility. The mirrors were therefore re-adjusted to obtain the highest possible visibility for the laser. Measurements were then made for decreasing values of Δl (30 mm, 28 mm, ..., 18 mm).

6.2 Discarding data

6.2.1 Discarding the data for $\Delta l = 30$ mm

In figure 6.1, the set of data for $\Delta l = 30$ mm does not seem to stand out among the other sets; its maximum and minimum values are about the same as for the previous data-sets, and the data-points seem to be evenly distributed as for the

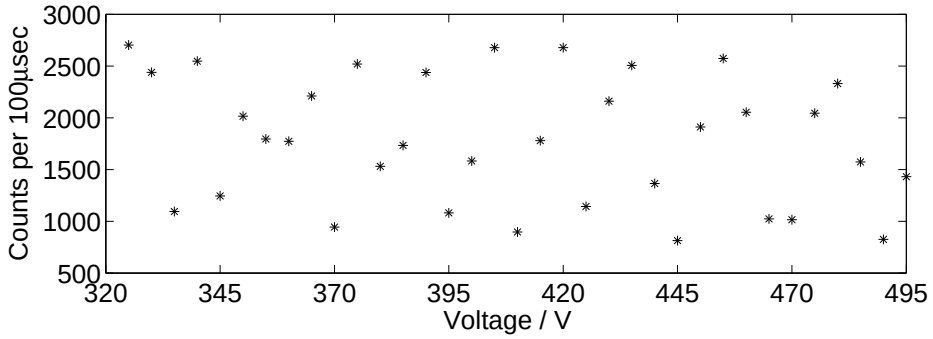

Figure 6.2: The data at $\Delta l = 30$ mm.

rest of the sets. When we zoom in on the set, the situation is another. As shown in figure 6.2, there is no indication of the data-points forming a function similar to the form of a sine.

We did not arrive at finding the reason for the strongly oscillating pattern in the figure. I *could* be an indication that we are past the coherence length, but as shown in figure 6.4 and in the data in appendix B, the visibility at $\Delta l = 28$ mm was about 0.6, and having *no* sign of an interference pattern at 30 mm therefore seems unlikely. In addition, an integration period of 100 μm is very long compared to the time it takes the light to move a distance of one wavelength. According to the theory discussed in chapter 2, with $\Delta l >> l_{\text{coh}}$ one would expect a constant intensity equal to half the incoming intensity of the light, something that is hardly the case in figure 6.2.

As mentioned in the beginning of the chapter, the data-set obtained for Hg546 is incomplete, and we do not have any data for Ar696. In the lack of a possible explanation or other measurements confirming the results presented in figure 6.2 we decided to discard the data-set in the determination of the visibility of Ne692.

6.2.2 Discarding of data due to hysteresis of piezo-element

Examine figure 6.3 showing the sets of sub-data for $\Delta l = 2$ mm and $\Delta l = 6$ mm. The right hand side of the figures resemble nicely periodic sines, while the left side of the figures do not. *All* sets of sub-data showed the same behaviour, *except* for the data for $\Delta l = 0$ mm (cf. figure 6.1(b)). Recall that this was the first set of data to be recorded. Starting from the second set of sub-data, the voltage over the piezo-element was turned from 520 V to 320 V immediately before beginning the measurements, and the left-most data point were the first to be recorded in each data-set. We therefore believe the unpredictability of the first part of the data-set to be due to hysteresis of the element.

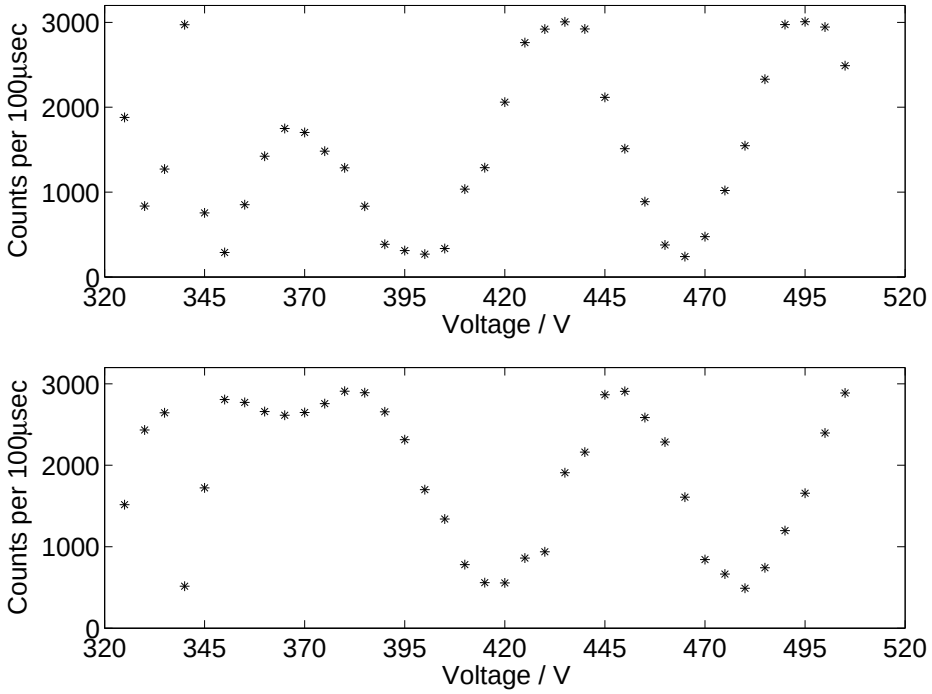

Figure 6.3: The data for (a) $\Delta l = 2$ mm and for (b) $\Delta l = 6$ mm.

Data-points that seemed to have been subject to this hysteresis were not included in the least-square fit described above.

6.3 Finding the visibility of the spectral lamps

To determine the coherence length, we needed to find the visibility of the data presented in figure 6.1. Since the measurements clearly show an interference pattern for path differences of more than one centimeter, the visibility within one set of sub-data may be taken to be constant. To find the visibility of each set of sub-data, we made a least-square fit to a sine as indicated in figure 6.1. The visibility of the data set was then defined as the visibility of the cosine. The sets of sub-data and the code used to find the least-square sine fit are included in appendix B.

Scaling factor from laser visibility

The visibility of the laser was measured to be[1]

$$V(0 \text{ mm}) = 0.921$$
$$V(16 \text{ mm}) = 0.744 \pm 0.002$$

After the path-difference had been changed to 30 mm and the mirrors re-adjusted, we measured a visibility of:

$$V(30 \text{ mm}) = 0.954 \pm 0.002$$
$$V(18 \text{ mm}) = 0.719 \pm 0.004$$

At $\Delta l = 16, 18$ and 30 mm, two measurements of the visibility of laser were made for each value of the path difference. The uncertainty of the numbers only reflect the spread of the two measurements. The uncertainty due to varying background is probably somewhat higher.

The fact that the visibility of the laser was ~ 0.2 larger for a path difference of 30 mm than at 16 mm is a clear sign that in moving the step motor, there is a significant *mechanical* degrading of visibility (cf. discussion on page 82). To account for this fact when finding the visibility of the spectral lamps, we scaled each of the measurements with the visibility of the laser. In lack of accurate measurements of the laser visibility at each data-point, we assumed linearity.

In our simple scaling, we implicitly assumed that the degrading of the laser visibility was solely due to the *mechanical degrading* of the system, not to the limited coherence length of the laser itself. For this assumption to be valid, the coherence length of the laser must be much longer than the maximum path-difference in the measurements. The coherence length of the HeNe-laser used in the adjustments were in the order of 18 cm [22].

Calculation of visibility for Ne692

In chapter 4, we showed that spectral lines dominated by homogeneous and inhomogeneous broadening produced an exponential and Gaussian visibility function respectively. In figure 6.4 we have plotted the measured and scaled data with both an exponential and a Gaussian fit. Both functions were found using the built in Matlab-routine *cftool* of the scaled data.

The Gaussian curve reaches the value e^{-1} when $\Delta l = 33.8$ mm, the exponential when $\Delta l = 27.1$ mm. Since a physical light source in general is somewhere between a pure Gaussian and a pure Lorentzian, it seems natural to conclude that the

[1]The laser visibility was actually not measured at $\Delta l = 0$ mm. The visibility mentioned below is the visibility found from the data of Ne692.

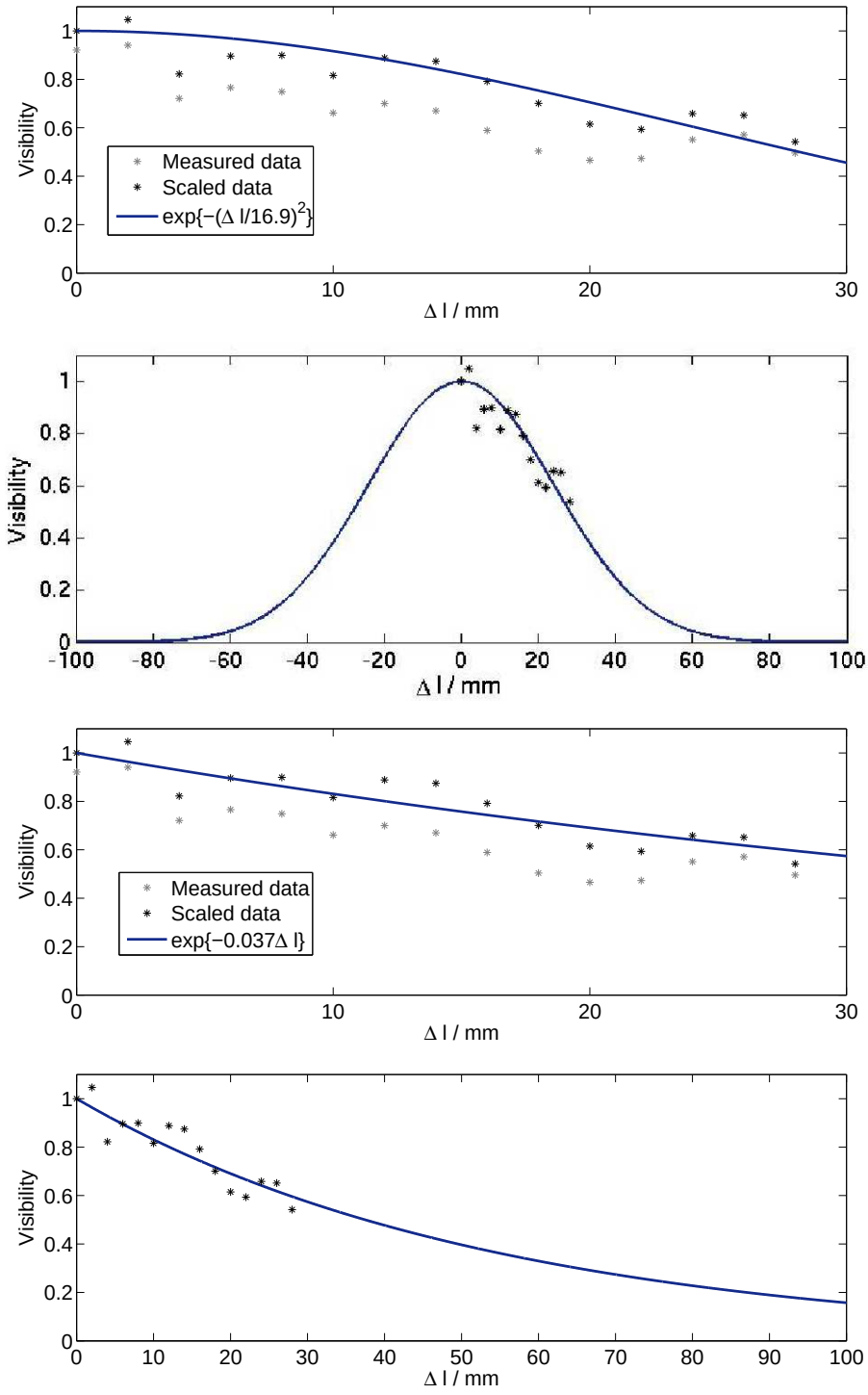

Figure 6.4: The visibility of Ne692 as function of path difference. (a) Measured and scaled visibility with a Gaussian fit. (b) Scaled visibility and Gaussian fit, showing the expected total visibility function. The figures (c) and (d) show exponential fit,

coherence length of Ne692 most likely lies in the interval:

$$27.1 \text{ mm} \ < \ l_{\text{coh}}(\text{Ne692}) \ < \ 33.8 \text{ mm}, \tag{6.1}$$

where the value $\Delta l = 27.1$ mm corresponds to a purely Lorenzian source, and $\Delta l = 33.8$ mm to one that is purely Gaussian.

6.4 Pulse number-density

The average distance between two pulses is given by the number of pulses per unit time divided by the speed of light. In our case, the maximum pulse number density n was about 3 200 per 100 μsec, which gives 32 000/sec. From figure 5.21, we find that the detection efficiency at wavelengths around 700 nm is about 65%, so the actual number density is in the order of 49 000/sec. The refracive index of air is very close to unity (see footnote on page 65), so the speed of light in air is very close to the speed of light in vacuum, about 3.0×10^8 m/sec. The average distance between two pulses is then:

$$\frac{3.0 \times 10^8 \text{ m/sec}}{4.9 \times 10^4 \text{ pulses/sec}} = 6 \times 10^3 \text{ m/pulse}.$$

The length of one arm of our interferometer was in the order of 10 cm, *much* shorter than the average distance of 6 000 meters between each pulse.

It should be mentioned that in our simple calculation above, we have not considered the statistical distribution of the light pulses. In general, for thermal light, this will be Poisson distributed. A distance of 6 000 meters between two pulses is nevertheless large enough to assume that two pulses were never present in the interferometer at the same time, and consequently our experiments may be said to have been carried out at the single-photon level. In addition to being simply a measurement of the coherence length of a spectral line, we have with the above described experiment and results made a demonstration of one of the puzzeling ascpects of the wave-particle duality mentioned in the introduction and at the beginning of chapter 1: Even though some experiments seem to require a description of light as an indivisible particle, light of intensities that indicate that we are working with only one particle at a time also show their wave-behavior through interference.

Chapter 7

Summary and outlook

As a finish, we will give a brief summary of our treatment of the concept of coherence and of our experimental work. We will then round off with some suggestions for future work, and some concluding remarks.

Coherence summarized

During the work, we have encountered several ways of representing or picturing temporal coherence of light. Coherence has been related to the size of a photon, to the average time between fluctuations in an electric field, and to the width of the auto-correlation function and of the power spectral density. The two former may be said to be of more phenomenological nature, the two latter more formal.

Temporal coherence length $l_{coh} = c\tau$ was defined in chapter 2 to be the length equivalent to the time-difference τ where the auto-correlation function has a value of e^{-1}. In the same chapter, we proved analytically that with this definition, the degree of first-order coherence may be found through sending light through a Michelson's interferometer, and finding the visibility as a function of path length. We also showed that defining the coherence length using the first-order auto-correlation function as above is equivalent to using the width of the power spectral density, as the two make up a Fourier-pair. The relations between the first-order correlation function, visibility, and power spectral density were illustrated using numerical simulations in chapter 3.

In defining coherence length using the auto-correlation function, we impute restrictions on the other suggested ways of perceiving coherence. The phenomenological pictures are only valid to the extend they correspond to the definition. By using a pulse-model, our simulations showed that coherence length may only correspond to photon size if one is willing to abandon the picture of a *photon* being the original pulse, and instead use the term to denote the wave packets that arise as a collective effect when one superposes several pulses.

The image of coherence length as equivalent to the average time between fluctu-

ations has not been expressly treated. In assembling bits and pieces from several of the chapters, we may, however, argue that though it may not *in itself* be identified as the coherence length, it may nevertheless be an important factor of limiting the coherence length of a given light source.

As mentioned above, we have shown that defining coherence length using the width of the auto-correlation function is equivalent to defining it using the power spectral density. The theory developed in chapter 2 says nothing explicitly about the fluctuations. Light made up of a large number of perfect lasers, each with infinite coherence length but slightly different wavelengths would, according to the theory, still have a finite coherence length since its spectrum would not be infinitely thin.

On the other hand, as we saw in chapter 2, power spectral density is equal to the absolute square of the frequency distribution of the electric field. A wide frequency distribution would cause the power spectral density to also be wide. Random fluctuations of the electric field may be defined as random deviations from the shape of a perfect cosine[1]. As it is shown in our presentation of the mathematics of Fourier transforms in appendix A, a large deviation from a cosine will result in more components in the Fourier spectrum[2]. Deviations, discrete or continuous, from a pure cosine, will therefore serve to broaden the spectrum and therefore also the power spectral density, and the coherence length will shorten.

In the description of broadening mechanisms in chapter 4, we argued that *"Each time an excited atom undergoes a collision, it may gain or lose energy. The total transition rate will therefore be higher than the rate one gets from Heisenberg uncertainty relation only"*. A collision may be imagined to cause an abrupt change in the electric field. Collision broadening may therefore be seen as one physical example of how the coherence length may be altered from deviations from the cosine-shaped electric field.

Albeit perhaps superfluous, we would like to again stress that a finite coherence length does not necessarily mean that those random fluctuations take place. To find a physical example of this, one needs only to again look at the discussion of Doppler broadening following that of collision broadening. It should also be pointed out that a collection of light sources (with infinite coherence length) of different velocity distributions is mathematically equivalent to the collection of perfect lasers mentioned above.

[1] Or sine.

[2] As implied from the discussion in appendix A, and from table A.1 in particular, the extreme example of deviation from a pure cosine is the δ-function. The Fourier transform of the δ-function is a constant line, so to write the δ-function as a sum of cosines, *all* frequencies are needed, the spectrum is infinitely broad, and the coherence length infinitely small.

Experimental work: Experience gained

The experiments proved to be technically harder and more time-consuming than expected, and some of the components of the setup offered negative surprises in their stability and resolution. As described in the previous chapter, we did manage to show interference of Ne962 at the single-photon level, and the visibility was decreasing more than what may be accounted for from a purely mechanical degrading. The coherence length of the spectral line seems to be in the order of a few centimeters.

The most important value of the experimental work that has been done, is perhaps the work described in chapter 5, where the experimental applications have been analysed. During the year that has passed since the work started, we have gained knowledge on the whims of the equipment, and methods passed on from the experiences of others have been tested and modified for our use.

Work *yet to be done*: Future perspectives

As the time reserved for the work approaches the end, the author has the strong impression that more questions have been posed than answered. Some of those questions could, perhaps, be explored in the work of another student:

1. Theory and numerical simulation
    - Is it possible to use statistical physics to analyse the features of the auto-correlation function? How does the auto-correlation function depend on the parameters of the emission model employed, and what may that teach us about nature?
    - What would the figures 3.9 and 3.10 look like if the original pulse did not have a Gaussian envelope, and especially if it were not symmetric?
2. Experiment
    - If the measurements on Ne692 are repeated, are the large fluctuations at $\Delta l = 30$ mm reproduced? If the fluctuations are found, do Hg546 and Ar696 show the same behavior? What about other light sources?
    - Do the coherence length and the shape of the auto-correlation function depend on the intensity of the beam, as our simulations suggest?
    - Is it possible to obtain more accurate data using a time-digitizer rather than an oscilloscope?

Concluding remarks

As defined in the introduction, the goal of this work was originally to obtain a greater understanding of the concept of coherence, through experimental measurements of the coherence length of atomic spectral lines. If judged by the experimental results alone, the work can hardly be said to have been as successful as

we were hoping for. It is the author's hope that the experimental work may be continued by another student. In that case, a year of struggling in the dark[3] is a year of experience gained, and may be said to have been a necessity.

If judged by the criteria of having increased our understanding of coherence, the picture seems to be quite different. We would especially like to mention again the numerical analysis in chapter 3. The simulations, which originally were planned to illustrate the theorems and relations found in chapter 2, showed some surprising details that *could* open the way for an experimental determination of the nature and shape of the light emitted from atoms.

[3] Literally!

Appendix A

Fourier transforms

Since Fourier transforms have been used in several places in the thesis, we here include a very brief introduction to the idea behind the mathematics. The focus has been on making the main idea conceptional clear. Mathematical proofs and theorems may be found in basically any book on mathematical methods for scientists, we used [4] and [41].

A.1 General introduction

Let us begin this section with an example taken from J. F. James' little book [24], which well describes the idea of Fourier transforms.

Imagine singing a steady note, where the air pressure F as a function of time can be described as a pure cosine[1] (the factor $2A$ is just a constant):

$$F(t) = 2A\cos(2\pi\nu_0 t). \tag{A.1}$$

Alternatively, this can be rewritten using Euler's formula[2]:

$$F(t) = A(e^{+i2\pi\nu_0 t} + e^{-i2\pi\nu_0 t}). \tag{A.2}$$

A note sung is rarely a pure cosine. If one is trying to sing the note *La*, the main contributor will be a pressure function of frequency 440 Hz, but other frequencies will play a part, giving the voice its particular flavor. The resulting signal may look like the graph in figure A.1. To better visualize the frequency contents of a signal, one may instead choose to plot the amplitude in front of each exponential, as a function of the frequency. The graph may then look like figure A.2. However,

[1] Although more common to define an $\omega = 2\pi\nu$, I am choosing to follow the convention of James [24] for two reasons: It avoids the somewhat awkward factors of $\frac{1}{\sqrt{2\pi}}$ in front of the Fourier integrals, and it avoids having to introduce -for our use- the more abstract idea of angular frequency, making the transition to frequency spectra of light very straight-forward.

[2] **Euler's formula** says that $e^{ix} = \cos x + i\sin x$. Using it with the identities of the trigonometric functions: $\sin(-x) = -\sin x$ and $\cos(-x) = \cos x$ one may deduce the formula for the cosine: $\cos x = (e^{ix} + e^{-ix})/2$.

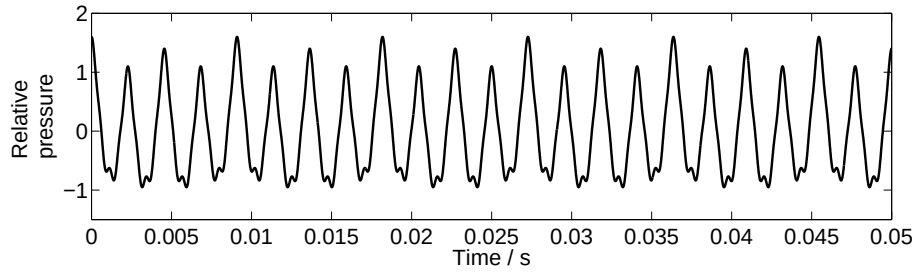

Figure A.1: The signal coming from a voice more flavorful than one that holds a pure cosine.

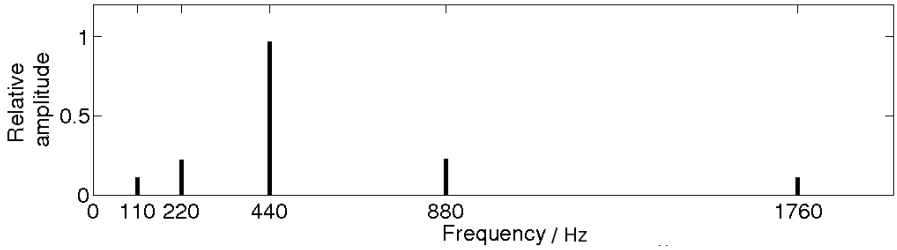

Figure A.2: The frequency spectrum of the pressure function of the flavorful voice in figure A.1 (We have omitted the negative frequencies since, according to equation (A.2) this would be the mirror-image of what we show).

in gaining information about the frequency content, we lose information of the time-aspect and phase of the original function.

In general, a signal that consists of a sum of cosines may be written using the form

$$\begin{aligned} F(t) &= A(\nu_0)e^{i2\pi\nu_0 t} + A(\nu_1)e^{i2\pi\nu_1 t} + A(\nu_2)e^{i2\pi\nu_2 t} + ... + A(\nu_n)e^{i2\pi\nu_n t} \\ &= \sum_{m=0}^{n} A(\nu_m)e^{i2\pi\nu_m t}. \end{aligned} \tag{A.3}$$

To describe a function very different from a cosine, one may need the entire continuous set of frequencies, and the sum in equation (A.3) becomes an integral[3]

$$F(t) = \int_{-\infty}^{\infty} A(\nu)e^{i2\pi\nu t}d\nu.$$

If we know the function $A(\nu_m)$, the function F(t) is unambiguously determined. $A(\nu)$ is called the Fourier transform of F(t). It can be shown that F(t) is also the Fourier-transform of $A(\nu)$, provided that one multiplies the exponent by a

[3]It may not be obvious that any function may be written as a sum of harmonic functions. It may however be shown that this is the case for most well-behaved functions [41].

minus-sign. We thus have

$$F(t) = \int_{-\infty}^{\infty} A(\nu) e^{i2\pi\nu t} d\nu \qquad \rightleftharpoons \qquad \int_{-\infty}^{\infty} F(t) e^{-i2\pi\nu t} dt = A(\nu). \tag{A.4}$$

We will call the set of functions $F(t)$ and $A(\nu)$ a Fourier pair. Symbolically, we will write $F \rightleftharpoons A$ to show that that A is the Fourier transform of F, or equivalently, that the two form a Fourier pair.

A list of Fourier transform of function that we will use in the continuation is included in table A.1. As an example, we have included a complete calculation of the Gaussian function in the following section.

Table A.1: Some useful Fourier pairs from [42].

$A(\nu)$	$F(t)$
1	$2\pi\delta(t)$
$e^{-\lambda(2\pi\nu)^2}$	$\sqrt{\frac{\pi}{\lambda}} e^{-\frac{t^2}{4\lambda}}$
$\frac{1}{(2\pi\nu)^2 + a^2}$	$\frac{\pi}{a} e^{a\lvert t\rvert}$
$e^{-2\pi\beta\nu} e^{i2\pi\lambda\nu}$	$\frac{i}{\lambda + t + i\beta}$

A.2 Fourier transform of a Gaussian function

A Gaussian function is a function on the form $F(t) = Ke^{-bt^2}$, where K and b are constants. Its Fourier transform is

$$\begin{aligned} A(\nu) &= K \int_{-\infty}^{\infty} e^{-bt^2} e^{-i2\pi\nu t} dt \\ &= K \int_{-\infty}^{\infty} e^{-(bt^2 + i2\pi\nu t - \frac{\pi^2\nu^2}{b}) - \frac{\pi^2\nu^2}{b}} dt \\ &= K e^{-\frac{\pi^2\nu^2}{b}} \int_{-\infty}^{\infty} e^{-\left(\sqrt{b}t + \frac{i\pi\nu}{\sqrt{b}}\right)^2} dt \\ &= K \sqrt{\frac{\pi}{b}} e^{-\frac{\pi^2\nu^2}{b}} \\ &= K' e^{-b'\nu^2} \end{aligned} \tag{A.5}$$

The easiest way to obtain the result in (A.5) is to simply put the original expression for $F(t)$ into equation (A.4) above, complete the square as we did in the third line, and solve as a normal Gaussian integral over $t' = \sqrt{b}t + \frac{i\pi\nu}{\sqrt{b}}$. The author, being a physicist, is inclined to claim that this *of course* has to be right. Although this is true in our case, changing the variable means at the same time adding a complex

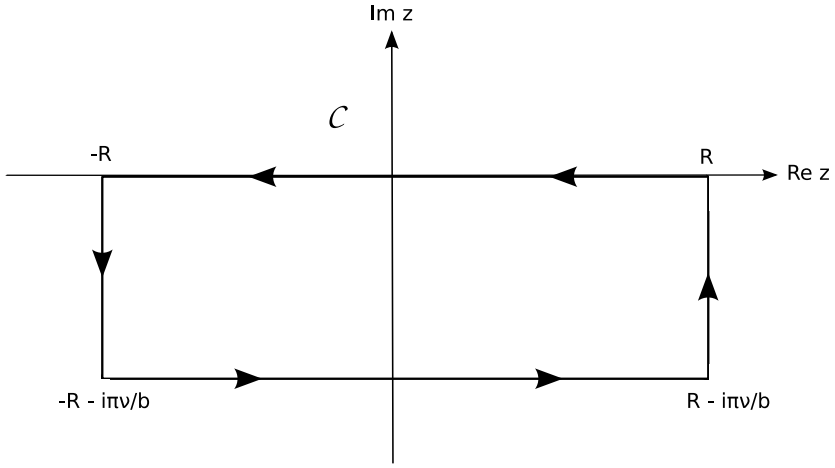

Figure A.3: The loop over which the integral is done.

factor to the integration limits, and it *is* in general a problem to have complex limits of an integral over a real variable. To make our claim more plausible, one can argue that in an integral on the form

$$\int_{-\infty}^{\infty} e^{-bt^2} e^{-i2\pi\nu t} dt \tag{A.6}$$

the function e^{bt^2} goes so fast to zero that the oscillations caused by the imaginary term don't contribute enough to make the infinities a problem. However, to be mathematically rigid one should use Cauchy's theorem[4] on the rectangle $\mathcal{C}$ in the complex plane that has its corners in the points $\pm R$ and $\pm R - i\pi\nu/b$. Se figure A.3.

Making the shift $z = t - i\pi\nu/b$, one has

$$A(\nu) = \int_{-\infty - \frac{i\pi\nu}{b}}^{\infty - \frac{i\pi\nu}{b}} e^{-bz^2} dz \tag{A.7}$$

Since e^{-bz^2} is analytic everywhere, we have

$$\oint_{\mathcal{C}} e^{-bz^2} dz = \int_{-R}^{R} e^{-bz^2} dz + \int_{R}^{R - \frac{i\pi\nu}{b}} e^{-bz^2} dz + \int_{R - \frac{i\pi\nu}{b}}^{-R - \frac{i\pi\nu}{b}} e^{-bz^2} dz + \int_{-R - \frac{i\pi\nu}{b}}^{-R} e^{-bz^2} dz = 0 \tag{A.8}$$

In the limit $R \to \infty$, the first integral in (A.8) is just the normal Gaussian integral that can be looked up anywhere (for example in [42]), and that equals $\sqrt{\pi/b}$. If the integration limits are interchanged, the third integral is the same as our integral for $A(\nu)$ in equation (A.7). Shifting the integration variable (and limits) of the

[4] **Cauchy's theorem**: The loop integral of an area in the complex plane, with no singularities, is equal to zero [4].

second integral to $z \to z + i\pi\nu/b$ and making the substitution $z' = -z$, it is fairly easy to see that this integral cancels the fourth, and we are left with

$$\left[\sqrt{\tfrac{\pi}{b}} - \int_{-R-\frac{i\pi\nu}{b}}^{R-\frac{i\pi\nu}{b}} e^{-bz^2} dz.\right]_{R\to\infty} = 0 \tag{A.9}$$

Taking the limit $R \to \infty$ should convince the reader that (A.5) is correct [4], [38].

In any case, $A(\nu)$ is also Gaussian, but with new constants $K' = K\sqrt{\pi/b}$ and $b' = \pi^2/b$. Therefore, the narrower the original Gaussian is, the broader its Fourier partner.

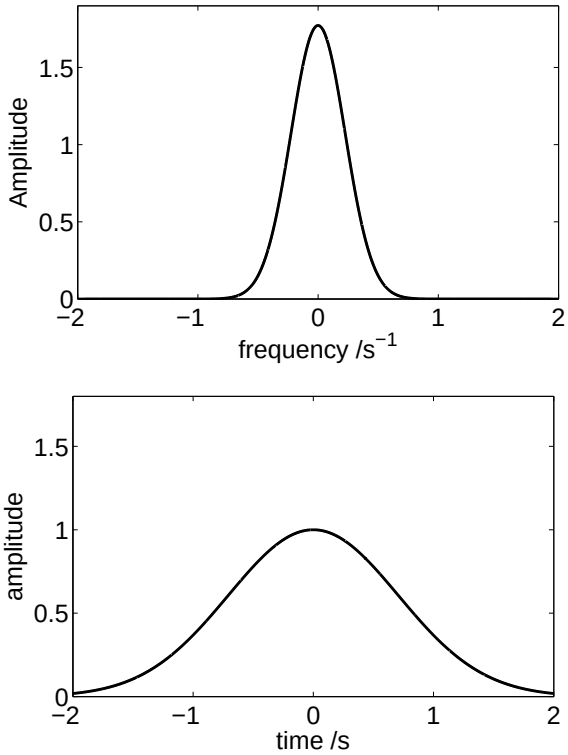

Figure A.4: The Fourier transform of a Gaussian function is also Gaussian. The lower and wider the original graph, the narrower and higher is its Fourier partner (In the above figures, $K = b = 1$).

Appendix B

Data

For reference we will here include the graphs of the original data of the intensity of of Ne692. The whole gray line is a least-square fit of a sine found using the code in section B.2.

B.1 Data

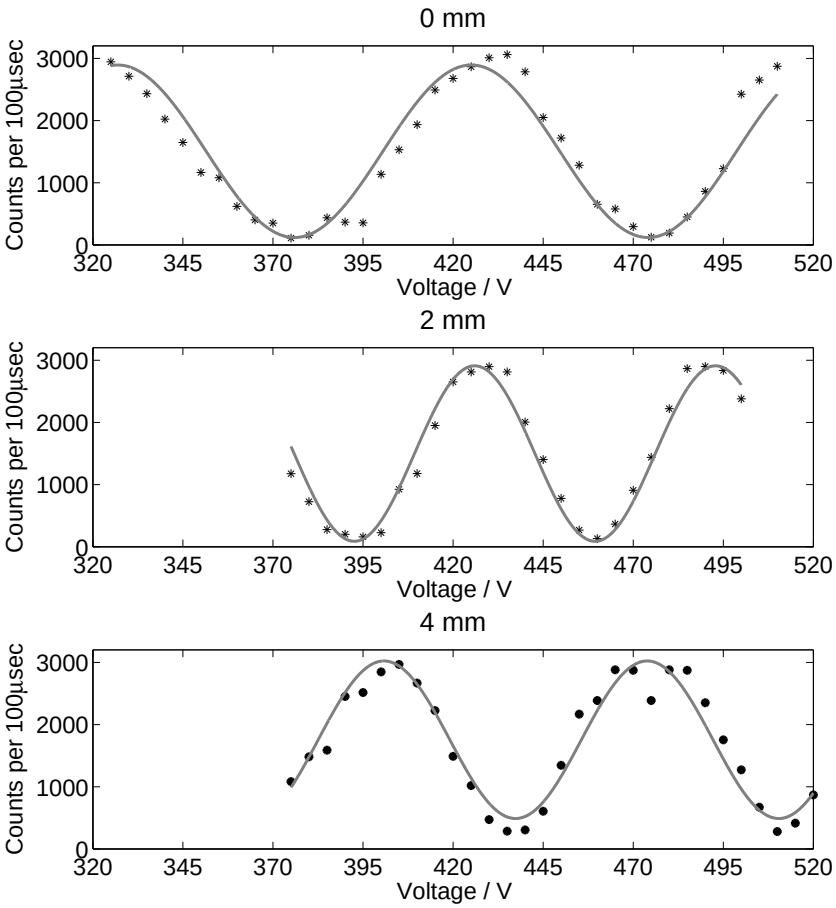

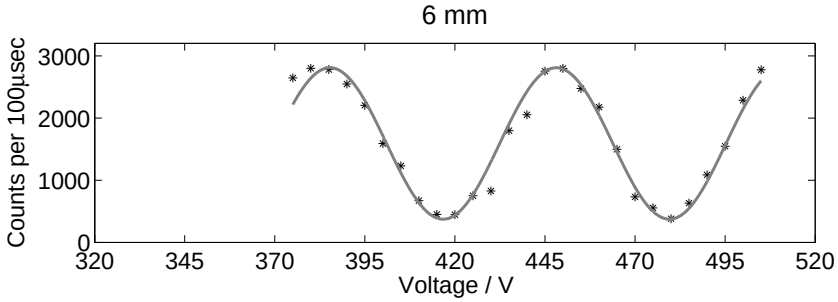
6 mm
Counts per 100µsec
3000
2000
1000
0
320
345
370
395
420
445
470
495
520
Voltage / V

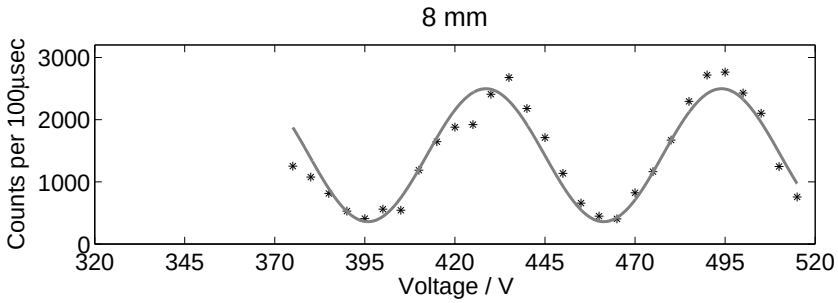
8 mm
Counts per 100µsec
3000
2000
1000
0
320
345
370
395
420
445
470
495
520
Voltage / V

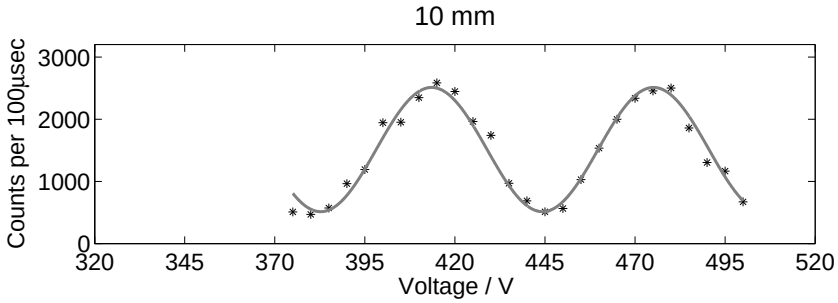
10 mm
Counts per 100µsec
3000
2000
1000
0
320
345
370
395
420
445
470
495
520
Voltage / V

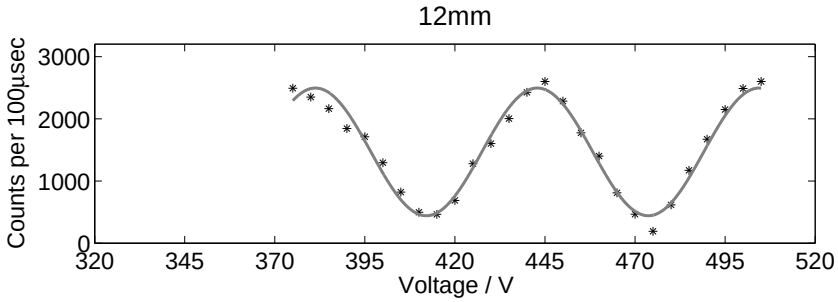
12mm
Counts per 100µsec
3000
2000
1000
0
320
345
370
395
420
445
470
495
520
Voltage / V

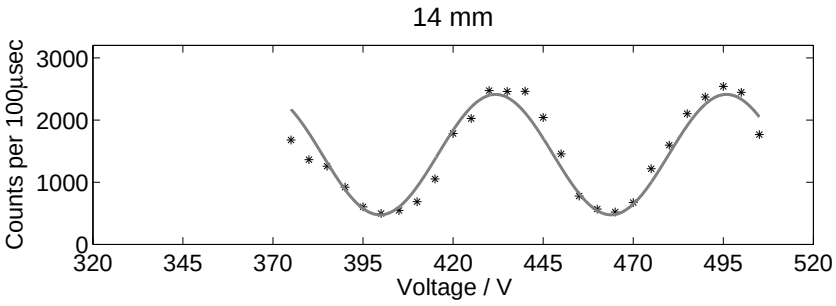
14 mm
Counts per 100µsec
3000
2000
1000
0
320
345
370
395
420
445
470
495
520
Voltage / V

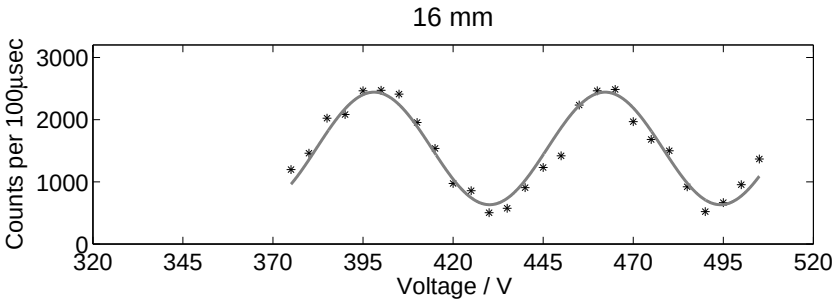
16 mm
Counts per 100µsec
3000
2000
1000
0
320
345
370
395
420
445
470
495
520
Voltage / V

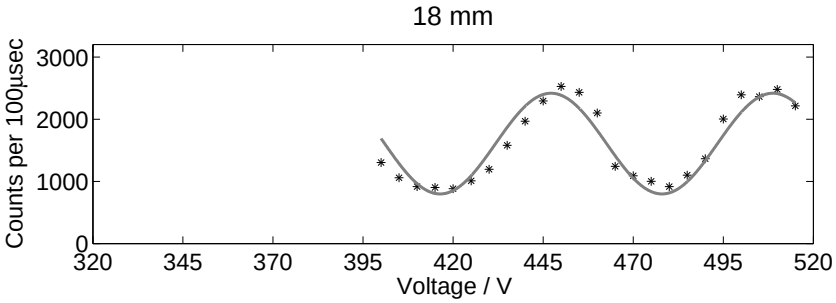
18 mm
Counts per 100µsec
3000
2000
1000
0
320
345
370
395
420
445
470
495
520
Voltage / V

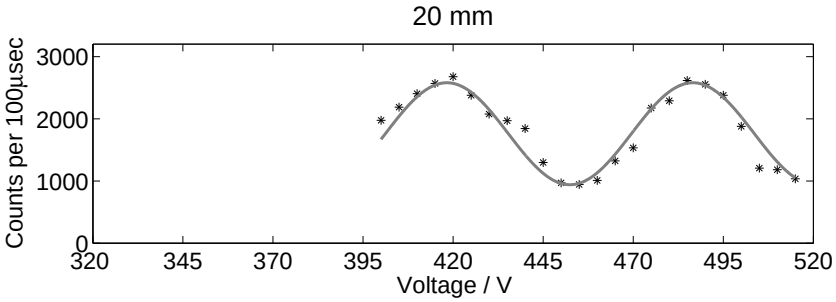
20 mm
Counts per 100µsec
3000
2000
1000
0
320
345
370
395
420
445
470
495
520
Voltage / V

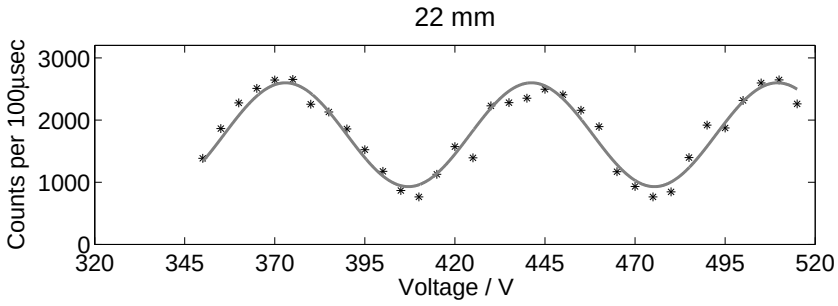
22 mm
Counts per 100µsec
0
1000
2000
3000
320
345
370
395
420
445
470
495
520
Voltage / V

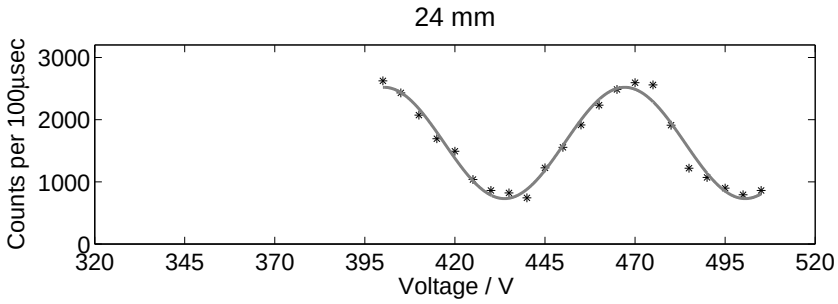
24 mm
Counts per 100µsec
0
1000
2000
3000
320
345
370
395
420
445
470
495
520
Voltage / V

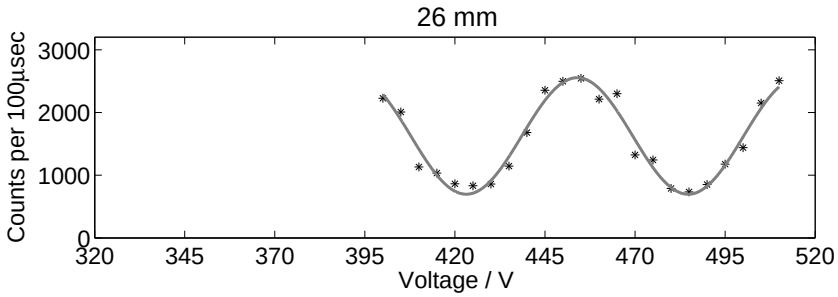
26 mm
Counts per 100µsec
0
1000
2000
3000
320
345
370
395
420
445
470
495
520
Voltage / V

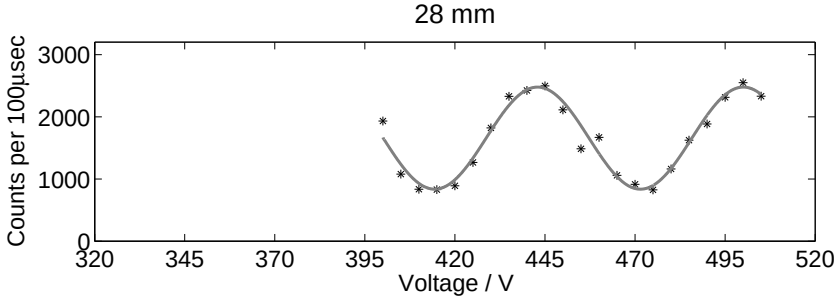
28 mm
Counts per 100µsec
0
1000
2000
3000
320
345
370
395
420
445
470
495
520
Voltage / V

B.2 Code for finding least square fit of sine to data

```
%Function makes a least square fit of data to a shifted sine.User has
%to state constants c1, c2, c3 and c4 to define size of loops finding
%amplitude and shift constant of sine.

function[visibilitet] = leastsquare(data, c1, c2, c3, c4)

data = data - 110;                              %Substracting noise
x = 1:length(data);

ymax = max(data); ymin = min(data);
ysnitt = floor((ymax+ymin)/2)
nullpkt = ymax - ysnitt

minstefeil = -1;
for a = nullpkt+c1:nullpkt+c2                   %a = amplitude
    for b = 0:0.01:3.15                         %b = weight of x-comp.
        for c =-3.15:0.01:3.15                  %c = phase
            for d = ysnitt+c3:ysnitt+c4;        %d = shift constant
                 y = a*sin(b*x +c) + d;         %least square function
                 feilvektor = data-y;           %difference to data
                 feilvektor = feilvektor.^2;
                 feil = sum(feilvektor);

                 if minstefeil == -1            %first loop only
                     minstefeil = feil;
                 elseif feil< minstefeil        %finding least square
                     A = a; B = b;
                     C = c; D = d;
                     minstefeil = feil;
end; end; end; end; end;

xriktig = 1:0.01:length(data);
yriktig = A*sin(B*xriktig + C) + D;

plot (x, data, '*r')
hold on
plot(xriktig, yriktig);

k1 = max(yriktig); k2 = min(yriktig);           %max and min of sine
visibilitet = (k1 - k2)/(k1+k2);                %visibility
```

Appendix C

Program used in simulations

```
%Koherens2 is made to make graphic simulation of the theory found in the
%thesis, especially to show examples of the Wiener-Khinchine theorem and
%simulate the intensity and calculate visibility from a michelsons
%interferometer. The input-data to any of the functions called by koherens2
%should be textfiles with columns separated by space.

%If user asks program to plot coloumn 2, it is assumed that coloumn 1 is
%x-axis. If user chooses to plot another column, program asks for
%delta_tau, the time between two datapoints. The program also asks the user
%for a cut-value to be given in numbers of datapoint. This cut-value serves
%to save time since function 2 and 3 will only run through calculation
%loops for time differences (or lengths c*tau) up to this value. The value
%for tau_cut should be larger than the expected coherence length of the
%signal, but be much smaller than the total length of the signal.

%Program calls on one of four functions to plot signal, fourier transformed
%or various methods to make analysis of coherence length or theorems
%described in the thesis. A tau_cut is introduced to shorten calculation
%time. tau_cut should be chosen to be larger than the expected coherence
%length, but much smaller than length of signal to ensure good statistics.

%The program offers to save to file all fourier transforms and enveloping
%functions for easy later manipulation of these to show theorems described
%in thesis. To more easily comparison of functions, most graphs are
%normalized to show functions relative to 1.

%User is asked to call one or more of four functions:
%1 - manipulere_signaler plots the original signal. It ask user to define a
%number of subsegments. The function finds the fourier transform of each
%subsegment, and superposes them to obtain the final total fourier
%transform of the signal. More subsegments then give a better picture of
%the actual fourier transform of the signal, but too short segments will
```

```
33 %increase unwanted edge-effects of the fourier spectrum. Note also that the
34 %subsegmenting must be used with care! -It requires signal of high
35 %ergodicity (do not use on single pulses and similar signals!!!).
36
37 %2 - autocorealtion2 plots the nth order autocorelation function of the
38 %original signal as defined in thesis, up to a timedifference of tau, and
39 %the fourier transform of this. If first order autocorrelation is chosen,
40 %the function caluclates and plots the absolute value of the
41 %autocorrelation function and the envelope of this.
42
43 %3 - michelson2 simulates sending the signal through a Michelsons
44 %interferometer with a 50-50 beam splitter for values of delta-l from zero
45 %to c*tau. It then calculates the visibility of the signal and gives choise
46 %to save the envelop of the visibility function to allow plotting with
47 %absolute value of correlation function.
48
49 %4 - spectral_power again splits signal into chosen number of subsegments,
50 %but this time finds the fourier transform of the sqare of each and
51 %superposes them. The warnings given under the description of #1 on the use
52 %of subsegment apply.
```

C.1 Main program

```
53 clear all
54 %Reading data from file
55 innfil = input('please enter name of datafile: ', 's');
56 x = load(innfil);
57 full_lengde = length(x);
58
59 %Choosing coloumn of file.
60 kolonne = input('please enter which coloumn to plot [2] : ');
61 if isempty(kolonne)
62     kolonne = 2;
63 end
64 a = x(:,kolonne);
65
66 %Full length of signal (datapoints).
67 display('full lengde: ');
68 full_lengde
69
70 %chosing at what value to cut tau. NB: datapoints, not time. Must be smaller
71 than 'full_length'.
72 tau_cut = input('Please enter cut value for tau in number of datapoints: ');
73
74 %delta_tau is time between two datapoints
```

```
75  if kolonne == 2
76     tidskolonne = x(:, 1);
77     delta_tau = (tidskolonne(full_lengde)-tidskolonne(1))/full_lengde;
78  else
79      samples_per_second = input('please enter sample rate in samples per seconds
80  [1]: ');
81      if isempty(samples_per_second)
82          samples_per_second = 1;
83      end
84      delta_tau = 1/samples_per_second;
85  end
86
87  %Choosing what to do.
88  valg1 = -1;
89  while valg1 ~= 0
90      valg1 = input('Enter 0 to end program, 1-Signal, 2-Autocoherence,
91  3-Michelsons simulation, 4-spectral power density: ');
92      switch valg1
93          case 0 %Ends program
94              return
95          case 1 %plots signal and its fourier transformed
96              manipulere_signaler(a, tidskolonne, delta_tau);
97          case 2 %plots autocoherence function of chosen order and its fourier
98  transformed.
99              autocorelation2(a, tidskolonne, delta_tau, tau_cut);
100         case 3 %Simulating signal from michelsons interferometer
101             michelson2(tidskolonne, a, delta_tau, tau_cut)
102         case 4 %Plot intenisty and spectral power density
103             spectral_power(a, delta_tau);
104         otherwise
105     end
106 end
```

C.2 Plotting the original signal and its Fourier transform

```
107 function[q] = manipulere_signaler(a, t, delta_tau)
108
109 l = length(a);
110
111 %Plotting orignial signal
112 figure
113 plot(t, a, 'k');
114 xlim([0 l*delta_tau]);
```

```
115 title('Original signal','FontSize',16);
116 xlabel('Time / s', 'FontSize', 16);
117 ylabel('Electric field, relative units', 'FontSize', 16);
118 set(gca, 'FontSize', 16);
119
120 %Choosing number of subsegments
121 antall_deler = input('Number of subsegments: ');
122
123 %tau_lengde = length of each subsegment
124 tau_lengde = floor(l/antall_deler);
125
126 %NFFT = length of frequency axis of fourier-plot
127 NFFT = 2^nextpow2(tau_lengde-1);
128 total_Y = zeros(NFFT/2, 1);
129
130 %Calculating fourier transform of each subsegment, adding to those allready
131 %calculated
132 for n = 1:antall_deler
133     fil = a(n:n-1+tau_lengde);
134
135     Y = fft(fil,NFFT)/tau_lengde;
136     Y = 2*abs(Y(1:NFFT/2));
137
138     total_Y = total_Y + Y;
139     n = n + tau_lengde;
140 end
141
142 %Giving right values to x-axis
143 f = (1/delta_tau)/2*linspace(0,1,NFFT/2);
144
145 %normalizing fourier graph
146 normering = input('Press 1 if you wish to normalize fourier funtion: ');
147 if normering == 1
148     total_Y = total_Y/max(total_Y);
149 end
150
151 %Plotting superposed fourier transform of subsegments
152 figure
153 plot(f, total_Y, 'k');
154 title('Fourier transform of original signal','FontSize', 16);
155 xlabel('Frequency / Hz', 'FontSize', 16);
156 ylabel('Relative amplitude', 'FontSize', 16);
157 set(gca, 'FontSize', 16);
158
159 %Gives choise of saving datafile with fourier transform
```

```
160 lagre_fourier = input('Press 1 if you wish to save fourier transform: ');
161 if lagre_fourier == 1;
162     fourier_fil = zeros(length(f), 2);
163     fourier_fil(:,1) = f;
164     fourier_fil(:,2) = total_Y;
165     navn_fil = input('Choose name of file: ', 's');
166 
167     dlmwrite(navn_fil, fourier_fil, 'delimiter', ' ');
168 end
```

C.3 Plotting the auto-correlation function

```
169 function[q] = autocorelation2(a, t, delta_tau, tau_cut)
170 
171 full_lengde = length(t);
172 
173 %chosing order of coherence
174 degree = input('please enter order of coherence [1]: ');
175 if isempty(degree)
176     degree = 1;
177 end
178 a = a.^degree;
179 
180 startpkt = tau_cut+1;
181 sluttpkt = full_lengde-tau_cut;
182 signal_lengde = sluttpkt - startpkt;
183 
184 %Making vector to become x- and y- axis. N is the normalizing factor N=<a(t)a(t)>
185 tau = (-tau_cut:tau_cut);
186 tau = tau*delta_tau;
187 tau_lengde = length(tau);
188 
189 A = zeros(tau_lengde, 1);
190 N_vektor = a(startpkt:sluttpkt);
191 N = mean(N_vektor.*N_vektor);
192 
193 %gives values to tau and A
194 for n = 1:tau_cut
195     ampl = 0;
196     for k = startpkt:sluttpkt
197         ampl = ampl + a(k)*a(k-n);
198     end
199     ampl = ampl/(N*signal_lengde);
200     A(tau_cut+1-n) = ampl;
201 end
```

```
202
203 A(tau_cut+1) = 1;
204
205 for n = tau_cut+2 : 2*tau_cut+1
206     ampl = 0;
207     for k = startpkt:sluttpkt
208         ampl = ampl + a(k)*a(k+n-tau_cut-1);
209     end
210     ampl = ampl/(N*signal_lengde);
211     A(n) = ampl;
212 end
213
214 %q = vanlig_signal2(A, tau, delta_tau, 'Autocorrelation function', 'Fourier
215 transform of autocorrelation function');
216 %full_lengde = length(t);
217
218 %Plotting signal
219 figure
220 plot(tau, A, 'k');
221 title('Autocorrelation function','FontSize',16);
222 xlim([-tau_cut*delta_tau tau_cut*delta_tau])
223 xlabel('\tau / s', 'FontSize',16);
224 ylabel('g^1(\tau)','FontSize',16 );
225 set(gca, 'FontSize', 16);
226
227 %Calculating fourier transformed
228 NFFT = 2^nextpow2(full_lengde);
229 Y = fft(A,NFFT)/full_lengde;
230 Y = 2*abs(Y(1:NFFT/2));
231 f = (1/delta_tau)/2*linspace(0,1,NFFT/2);
232 tittel = 'Amplitude';
233
234 normering = input('Press 1 if you wish to normalize fourier funtion: ');
235 if normering == 1
236     Y = Y/max(Y);
237     tittel = 'Relative amplitude';
238 end
239
240 %Plotting fourier transformed
241 figure
242 plot(f, Y, 'k');
243 title('Fourier transform of g(\tau)','FontSize',16);
244 xlabel('Frequency/Hz','FontSize',16);
245 ylabel(tittel,'FontSize',16);
246 set(gca, 'FontSize', 16);
```

```
247
248 %Saving fourier transform
249 lagre_fourier = input('Press 1 if you wish to save fourier transform: ');
250 if lagre_fourier == 1;
251     fourier_fil = zeros(length(f), 2);
252     fourier_fil(:,1) = f;
253     fourier_fil(:,2) = Y;
254     navn_fil = input('Choose name of file: ', 's');
255
256     dlmwrite(navn_fil, fourier_fil, 'delimiter', ' ');
257 end
258
259 if degree == 1
260     abs_autocor = abs(A);
261     [pks,locs] = findpeaks(abs_autocor);
262
263     locs = locs*delta_tau;
264     locs = locs + tau(1);
265
266     figure
267     plot(tau, abs_autocor, 'color', [.5 .5 .5]);
268     xlim([-tau_cut*delta_tau tau_cut*delta_tau])
269     hold on
270     plot(locs, pks, 'k');
271     xlabel('tau','FontSize',16);
272     ylabel('|g^1(\tau)|','FontSize',16);
273     title('Absolute value of the first order autocorrelation function',
274 'FontSize',16);
275     set(gca, 'FontSize', 16);
276
277     lagre_kant = input('Press 1 if you wish to save enveloping function: ');
278     if lagre_kant == 1;
279         kant_fil = zeros(length(locs), 2);
280         kant_fil(:,1) = locs;
281         kant_fil(:,2) = pks;
282         navn_fil = input('Choose name of file: ', 's');
283
284         dlmwrite(navn_fil, kant_fil, 'delimiter', ' ');
285     end
286 end
```

C.4 Simulating a Michelson's interferometer

```
287 function[q] = michelson2(tid, ampl, delta_tau, tau_cut)
288
```

```
289 %Lengden til opprinnelig signal
290 lengde = length(tid);
291
292 tau_teller = (-tau_cut:tau_cut);
293 tau = delta_tau*tau_teller;
294 tau_lengde = length(tau);
295
296 %Makes vecotor for e-field and intensity
297 e_lengde = lengde-tau_lengde;
298 e_felt = zeros(e_lengde, 1);
299 intensitet = zeros(tau_lengde, 1);
300
301 %Loop running through signal, sums up e-fields, find
302 %intensity.
303 for k = -tau_cut:tau_cut
304     for l = tau_cut+1:lengde-tau_cut
305         e_felt(l) = ampl(l)+ampl(l+k);
306     end
307     e_kvadrat = e_felt.^2;
308     intensitet(k+tau_cut+1) = mean(e_kvadrat);
309 end
310 intensitet = intensitet/intensitet(tau_cut+1);
311
312 figure
313 plot(tau, intensitet, 'k');
314 xlim([-tau_cut*delta_tau tau_cut*delta_tau])
315 title('Intensity after Michelsons interferometer','FontSize',16);
316 xlabel('tau / s','FontSize',16);
317 ylabel('Relative intensity','FontSize',16);
318 set(gca, 'FontSize', 16);
319
320 %abs_int_p = abs(intensitet);
321 [pks_p,locs_p] = findpeaks(intensitet);
322 [pks_n,locs_n] = findpeaks(-intensitet);
323 pks_n = -pks_n;
324
325 ln = length(locs_n);
326 lp = length(locs_p);
327 if ln ~= lp
328     ln = min(ln, lp);
329     pks_n = pks_n(1:ln);
330     pks_p = pks_p(1:ln);
331     locs_n = locs_n(1:ln);
332     locs_p = locs_p(1:ln);
333 end
```

```
334
335 locs = floor((locs_p + locs_n)/2);
336 locs = (locs*delta_tau)+tau(1);
337 visibility = (pks_p-pks_n)./(pks_p+pks_n);
338
339 figure
340 plot(locs, visibility, 'k');
341 xlim([-tau_cut*delta_tau tau_cut*delta_tau])
342 title('Visibility after Michelsons interferometer','FontSize',16);
343 xlabel('tau / s','FontSize',16);
344 ylabel('Visibility','FontSize',16);
345 set(gca, 'FontSize', 16);
346
347 lagre_kant = input('Press 1 if you wish to save visibility function: ');
348 if lagre_kant == 1;
349     kant_fil = zeros(length(locs), 2);
350     kant_fil(:,1) = locs;
351     kant_fil(:,2) = visibility;
352     navn_fil = input('Choose name of file: ', 's');
353
354     dlmwrite(navn_fil, kant_fil, 'delimiter', ' ');
355 end
```

C.5 Power spectral density

```
356 function[q] = spectral_power(a, delta_tau)
357
358 %Choosing number of subsegments
359 antall_deler = input('Number of subsegments: ');
360
361 %finding the length of the signal and defining length of each subsegment
362 l = length(a);
363 tau_lengde = floor(l/antall_deler);
364
365 %Making fourier transform of  each subsegmeng and superposing them
366 NFFT = 2^nextpow2(tau_lengde-1);
367 total_sp = zeros(NFFT/2, 1);
368
369 n = 1;
370 while n <= l-tau_lengde+1;
371     fil = a(n:n-1+tau_lengde);
372
373     Y = fft(fil,NFFT)/tau_lengde;
374     Y = 2*abs(Y(1:NFFT/2));
375     sp = Y.^2;
```

```
376         sp = 2*abs(sp(1:NFFT/2));
377         total_sp = total_sp + sp;
378         n = n + tau_lengde;
379     end
380     f = (1/delta_tau)/2*linspace(0,1,NFFT/2);
381
382     %normalizing power spectrum, defining the highest peak to have value = 1
383     normering = input('Press 1 if you wish to normalize fourier funtion: ');
384     if normering == 1
385         total_sp = total_sp/max(total_sp);
386     end
387
388     %plotting spectral power denstiy
389     figure
390     plot(f, total_sp, 'k');
391     title('spectral power density','FontSize',16);
392     xlabel('Frequency / Hz','FontSize',16);
393     ylabel('Amplitude','FontSize',16);
394     set(gca, 'FontSize', 16);
395
396     %choise to save spectrum for later plotting and smooting (to compare with
397     %fourier transformed of auto correlation function)
398     lagre_fourier = input('Press 1 if you wish to save fourier transform: ');
399     if lagre_fourier == 1;
400         fourier_fil = zeros(length(f), 2);
401         fourier_fil(:,1) = f;
402         fourier_fil(:,2) = total_sp;
403         navn_fil = input('Choose name of file: ', 's');
404
405         dlmwrite(navn_fil, fourier_fil, 'delimiter', ' ');
406     end
```

Bibliography

[1] S. Aerts, P. Kwiat, J. Åke Larsson, and M. Zukowski, *Two-photon franson-type experiments and local realism*, Physical Review Letters, 83 (1999), pp. 2872–2875.

[2] S. S. Afshar, E. Flores, K. McDonald, and E. Knoesel, *Paradox in wave-particle duality*, Foundations of Physics, 37 (2007), pp. 295–305.

[3] Andover Corporation, *General/technical information: Bandpass filters*. `http://www.andovercorp.com/Web_store/General_info/Technical.php#Bandpas%s\%20filters`, 13 January 2010.

[4] M. L. Boas, *Mathematical methods in the physical science*, Wiley, third ed., 2006.

[5] M. Born and E. Wolf, *Principles of optics*, Cambridge University Press, seventh ed., 1999.

[6] B. H. Bransden and C. J. Joachain, *Physics of atoms and molecules*, Longman Scientific & Technical, 1983.

[7] ——, *Physics of atoms and molecules*, Prentice Hall, second ed., 2003.

[8] H. Brox. Presentation of the detection problem, Private seminar, 2010.

[9] P. Busch, *On the energy-time uncertainty relation*, Foundations of physics, 20 (1990), pp. 1–43.

[10] P. A. Bélanger, *Beam propagation and the ABCD ray matrices*, Optics Letters, 16 (1991), pp. 196–198.

[11] C&L Instruments Inc., *Interference filters: The key to it all*. `http://www.fluorescence.com/tutorial/int-filt.htm`, 13 January 2010.

[12] J. Daintith, ed., *Oxford dictionary of physics*, Oxford University Press, fifth ed., 2005.

[13] *Dalsa: CCD vs. CMOS*. `http://www.dalsa.com/corp/markets/ccd_vs_cmos.aspx`, 31 May 2010.

[14] E. Flores, *Reply to comments of steuernagel on the afshar's experiment*, Foundations of Physics, 38 (2008), pp. 778–781.

[15] M. Françon, *Thèmes actuels en optique*, Masson, 1986.

[16] P. Grangier, G. Roger, and A. Aspect, *Experimental evidence for a photon anticorrelation effect on a beam splitter: A new light on single-photon interference*, Europhysics Letters, 1 (1986), pp. 173–179.

[17] W. Greiner, *Quantum mechanics, an introduction*, Springer-Verlag, second corrected ed., 1989.

[18] D. J. Griffiths, *Introduction to quantum mechanics*, Pearson, second ed., 2005.

[19] R. Haag, *Local quantum physics, fields, particles, algebras*, Springer Verlag, 1996. p. 309.

[20] E. Hecht, *Optics*, Addison Wesley, fourth ed., 2002.

[21] W. Heisenberg, *Encounters with Einstein and other essays on people, places and particles*, Princeton Science Library, 1989.

[22] B. Jagielski, *Elements of the wave-particle duality of light.* Master thesis, University of Oslo, May 2009.

[23] B. Jagielski and J. Lein, *Koherens_gui: Matlab-code for generation and analysis of coherence length of signals*, 2010.

[24] J. F. James, *A student's guide to Fourier transforms*, Cambridge, second ed., 2002.

[25] P. Kwiat, *Hyper-entangled states*, Journal of modern optics, 44 (1997), pp. 2173–2184.

[26] D. R. Lide, ed., *CRC handbook of chemistry and physics*, CRC Press, 2008.

[27] L. Mandel and E. Wolf, *Optical coherence and quantum optics*, Cambridge University Press, 1995.

[28] National Aeronautics and Space Administration, *Dr. Nicholas Short's remote sensing tutorial.* `http://rst.gsfc.nasa.gov/Sect20/09_Double-Slit-05.jpg`, 27 January 2010.

[29] Newport, *Product description: Pencil style calibration lamps.* `http://www.newport.com/Pencil-Style-Calibration-Lamps/377846/1033/catal%og.aspx`, 15 January 2010.

[30] *Newport: Silicon Photodetector.* `http://search.newport.com/?q=918D-SL-OD3`, 27 May 2010.

[31] I. Newton. *Letter to Robert Hooke.* May 5, 1675.

[32] ——, *Opticks*, Dover Publications INC, 1979.

[33] *Nikon digital SLR camera D200 specifications.* `http://www.nikonusa.com/Find-Your-Nikon/Product-Archive/Digital-SLR/252%35/D200.html`, 26 May 2010.

[34] National Institute of Standards and Technology, *NIST atomic spectra database lines form.* `http://physics.nist.gov/PhysRefData/ASD/lines_form.html`, 20 August 2009.

[35] F. L. Pedrotti, L. M. Pedrotti, and L. S. Pedrotti, *Introduction to optics*, Pearson Prentice Hall, third ed., 2007.

[36] PerkinElmer *Single Photon Counting Modul - SPCM.* `http://www.perkinelmer.com`, March 24, 2010.

[37] *USBeamPro camera beam profiler.* `http://www.photon-inc.com/products/usbeampro/usbeampro.html`, 27 May 2010.

[38] N. Prakash, *Mathematical perspectives on theoretical physics*, Imperial College Press, 2000.

[39] A. P. Prudnikov, Y. A. Brychkov, and O. I. Marichev, *Integrals and series, volume 1: Elementary functions*, Gordon and Breach Science Publishers, 1986.

[40] F. Reif, *Fundamentals of statistical and thermal physics*, McGraw-Hill, 1985.

[41] K. F. Riley, M. P. Hobson, and S. J. Bence, *Mathematical methods for physics and engineering*, Cambridge, second ed., 2002.

[42] K. Rottmann, *Matematisk formelsamling*, Spektrum forlag, 2003.

[43] T. Salamon, *Michelson and fabry-perot interferometers with light sources of gaussian and lorentzian spectral destribution*, Acta Physica Academiae Scientiarum Hungaricae, 36 (1974), pp. 269–286.

[44] B. E. A. Saleh and M. C. Teich, *Fundamentals of photonics*, Wiley, second ed., 2007.

[45] D. V. Schroeder, *An introduction to thermal physics*, Addison Wesley Longman, 2000.

[46] O. Steuernagel, *Afshar's experiment does not show a violation of complementarity*, Foundations of physics, 37 (2007), pp. 1370–1385.

[47] A. Sudbø, *Nobelprisen i fysikk 2009*, Fra fysikkens verden, (2009), pp. 105–107.

[48] Thorlabs http://www.thorlabs.de, October 2010.

[49] Thorlabs *Travel stepper actuator.* http://www.thorlabs.com/NewGroupPage9.cfm?ObjectGroup_ID=1881&pn=DRV001%&RiLink=5, May 19, 2010.

[50] *Thorlabs: FiberPort Collimators, operating manual.* http://www.thorlabs.de/NewGroupPage9.cfm?ObjectGroup_ID=2940, June 1 2010.

[51] R. Tilley, *Understanding solids*, Wiley, 2004.

[52] S. Viefers, T. Engeland, and M. Hjort-Jensen, *Forelesningsnotater i FYS2140 Kvantefysikk*, Department of Physics, University of Oslo, 2005.

[53] A. I. Vistnes. Dr. Scient. Private conversations.

[54] A. Yariv, *Quantum electronics*, John Wiley & Sons, third ed., 1989.

[55] H. D. Young and R. A. Freedman, *University physics*, Pearson, eleventh ed., 2004.

[56] T. Young, *The bakerian lecture: Experiments and calculations relative to physical optics*, Philosophical Transactions of the Royal Society of London, 94 (1804), pp. 1–16.

[57] E. Østreng. MSc. Science of Materials. Private conversations.